N73-32277

THE PENNSYLVANIA
STATE UNIVERSITY

IONOSPHERIC RESEARCH

Scientific Report 416

AN EXPERIMENTAL INVESTIGATION OF MESOSPHERIC IONIZATION
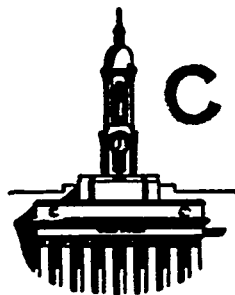
by

John D. Mitchell

June 29, 1973

IONOSPHERE RESEARCH LABORATORY

University Park, Pennsylvania

PSU-IRL-SCI-416
Classification Numbers 1.5.1 and 3.2.2

Scientific Report 416

An Experimental Investigation of Mesospheric Ionization

by

John D. Mitchell

June 29, 1973

Submitted by: _L. C. Hale_

L. C. Hale, Professor of
Electrical Engineering
Project Supervisor

Approved by: _B R F Kendall_

B. R. F. Kendall, Acting Director
Ionosphere Research Laboratory

Ionosphere Research Laboratory

The Pennsylvania State University

University Park, Pennsylvania 16802

ACKNOWLEDGEMENTS

TABLE OF CONTENTS

LIST OF TABLES

LIST OF FIGURES

ABSTRACT

Mesospheric ionization and its variability are the subject of this research. Data for this study were obtained primarily by the parachute-borne blunt probe technique conducted in coordinated rocket experiments at White Sands Missile Range, New Mexico and Wallops Island, Virginia. Electrical conductivity measurements and deduced charge density values from ten rocket launches are presented and discussed. Positive ion conductivity and electron density were found to be relatively invariant with height between 45 and 60 km. Variations in positive conductivity of a factor of two and enhancements in negative conductivity by as much as a factor of four were measured by the blunt probe.

A simple lumped parameter ion chemistry model is shown to satisfactorily explain the charge density values for the undisturbed lower D-region. Implications of the data in terms of this model are considered. The principal loss mechanism for positive ions in the 45 to 60 km. region is concluded to be dissociative recombination. Electron densities deduced from the conductivity data are explained by detachment involving a minor neutral constituent which is mixed between 65 and 45 km. and then cuts off sharply below 45 km.

A correlation study involving blunt probe measurements shows relatively good agreement between variations in positive conductivity and temperature. The good

correlation between variations in negative conductivity in the 55 to 65 km. region and noontime A3 radio wave absorption, which primarily indicates changes in electron density for heights above the blunt probe measurements, suggests that variations in both regions are caused by a similar process.

CHAPTER I

INTRODUCTION

1.1 Background

The day-to-day variability in mesospheric ionization has recently become a popular subject of aeronomic investigation. The "winter anomaly" represents one example of this variability which sporadically occurs for periods of usually one to three days in the midlatitude D-region of the ionosphere. This phenomenon was first reported by Appleton in 1937. Enhancements in electron density of an order of magnitude have been observed on such "anomalous" winter days (Bowhill, Mechtly, Sechrist and Smith, 1967). Since the variability in ionization is more dynamic during the winter, this season is ideally suited for conducting experiments to study this particular problem.

Prior to the mid-1960's, most investigations of D-region ionization variability were conducted using some form of ground-based radio wave propagation experiment. This remote sensing technique is particularly useful for providing information of a statistical nature concerning variations in electron number density. From such studies, Appleton and Piggott (1954) demonstrated that the "winter anomaly" could not be correlated with changes in magnetic activity or solar radiation. Some evidence has been presented for suggesting a possible relationship between the

variability in ionization and atmospheric temperature (Bossolosco and Elena, 1963; Shapley and Beyon, 1965; Sechrist, 1967).

The first rocket experiment for studying the ionization variability was conducted at Wallops Island, Virginia during the winter of 1966-67 (Bowhill, et al. 1967). Electron density measurements deduced from a nose tip current-measuring probe and temperature data from a rocket grenade experiment indicated a warm temperature layer occurring in the altitude region of enhanced electron density, thus suggesting a possible correlation between the two variables (Sechrist, Mechtly, Shirke and Theon, 1969).

Several explanations related either to the production or loss processes for electrons have been proposed for this observed variability in ionization. Sechrist (1967) and Manson (1971) have suggested that enhancements in D-region electron number density during the winter are caused by an increase in nitric oxide concentration, presumably induced by atmospheric motion or heating. Gnanalingam (1972) has speculated that the variability in ionization results from changes in solar radiation which in turn would influence the production of electrons. A third possible explanation for this ionization variability involves a change in some minor constituent, presumably by transport, which would affect the electron loss process in the D-region (Geller and Sechrist, 1971; Mitchell and Hale, 1972).

An interest in better understanding the variations in
D-region ionization led to a coordinated rocket experiment
being conducted at White Sands Missile Range (WSMR),
New Mexico during the winter of 1970-71 by members of The
Ionosphere Research Laboratory of The Pennsylvania State
University and The Atmospheric Sciences Laboratory of White
Sands Missile Range (Mitchell, Hale, Olsen, Randhawa and
Rubio, 1972). Variations in electron density during this
period were monitored on the ground by Al and A3 radio wave
absorption experiments. Payloads for measuring electrical
conductivity, temperature, wind, ozone, and neutral air
density were flown on three different days, two of high
absorption and one a low absorption control day. During the
summer of 1971, two additional conductivity probes were
flown in coordinated experiments at WSMR, New Mexico. These
rocket shots provided much needed summer data which could
be compared with the results from the three previous winter
launches. Other participants in the summer series were
The Atmospheric Sciences Laboratory of WSMR, Utah State
University, and Air Force Cambridge Research Laboratories.
These groups launched payloads for measuring electron and
neutral number densities, temperature, ozone, nitric oxide,
and Lyman-α radiation. The one other 1971 rocket launch
occurred in October when a joint experiment was conducted
at WSMR, New Mexico with NASA Goddard Space Flight Center
to measure positive ion density and composition.

The success and interest generated by the 1971 rocket

experiments and the need for additional data resulted in two
rocket programs to study variations in D-region ionization
during the winter of 1971-72. A coordinated rocket series
at Wallops Island (WI), Virginia was conducted jointly by
members of The Ionosphere Research Laboratory, the Aeronomy
Laboratory of the University of Illinois, and Air Force
Cambridge Research Laboratories to measure electrical
conductivity, electron number density, positive ion number
density and composition, and atmospheric temperature. The
instruments flown in the winter studies program at WSMR,
New Mexico were similar to those of the previous winter. In
addition, ground-based partial reflection experiments at
both launch sites provided further information about the
variations in D-region electron density.

Unfortunately, conditions for high absorption days did
not occur during the periods available for rocket launches
and thus the two rocket shots conducted by Penn State at
each site were on days of low and moderate absorption. For
this reason, an emphasis will be placed in the future on
obtaining conductivity measurements on days of high radio
wave absorption.

1.2 Scope of This Work

The subject of this research will be the analysis of
ionospheric conductivity measurements and their deduced
charge number densities obtained by the parachute-borne
blunt probe (Hale and Hoult, 1965). This is a subsonic
metallic probe technique utilizing continuum principles

(Hoult, 1965; Sonin, 1967). Parameters for the rocket launches are given in Table 1.1. The last column in this table classifies the launch dates according to their relative amount of high-frequency radio wave absorption, which is the subject of Chapter II. The electronic instrumentation of the blunt probe is discussed in Chapter III. Subsonic probe theory for charged particle collection and the measured conductivity and deduced density values are presented in Chapter IV. Chapters V and VI consider implications of the data in terms of simple ionospheric models and possible correlations with concurrently measured atmospheric parameters. Conclusions from this study are given in the final chapter.

Table 1.1   Parameters for WSMR and WI Rocket Launches

Date	Time (Hours)	Solar Zenith Angle	Location	Absorption
January 22, 1971	1300 MST	54°	WSMR	High
January 26, 1971	1430 MST	62°	WSMR	High
February 1, 1971	1215 MST	50°	WSMR	Low
June 9, 1971	0809 MST	53°	WSMR	Moderate
July 28, 1971	0705 MST	68°	WSMR	Moderate
October 13, 1971	1050 MST	44°	WSMR	Moderate
January 6, 1972	1337 EST	64°	WI	Low
January 19, 1972	1230 MST	53°	WSMR	Low
January 31, 1972	1305 EST	58°	WI	Moderate
February 1, 1972	1200 MST	51°	WSMR	Moderate

CHAPTER II

D-REGION RADIO WAVE ABSORPTION

2.1 Introduction

As discussed briefly in the introductory section, the days on which rockets were launched at White Sands Missile Range (WSMR) and Wallops Island (WI) are classified according to their relative amount of noontime radio wave absorption. Three methods for measuring ionospheric radio wave absorption are (Davies, 1969):

   (1) Measurement of the field strength of radio waves reflected from the ionosphere

   (2) Measurement of the minimum frequency vertically reflected from the ionosphere

   (3) Measurement of the absorption of extra-terrestrial noise (often referred to as the A2 method).

There are actually two variations to the first method given above. The A1 method measures the field strength of a fixed-frequency pulse train vertically reflected from the E-region of the ionosphere. The A3 method monitors the signal strength of a CW signal obliquely reflected from the E-region of the ionosphere.

The A3 method was used extensively for measuring the relative amount of radio wave absorption on the days of the WSMR and WI rocket launches. A general schematic of this measurement with a corresponding electron density profile for the ionosphere is given in Figure 2.1. For the purpose of clarity, only the single hop E-layer and F-layer
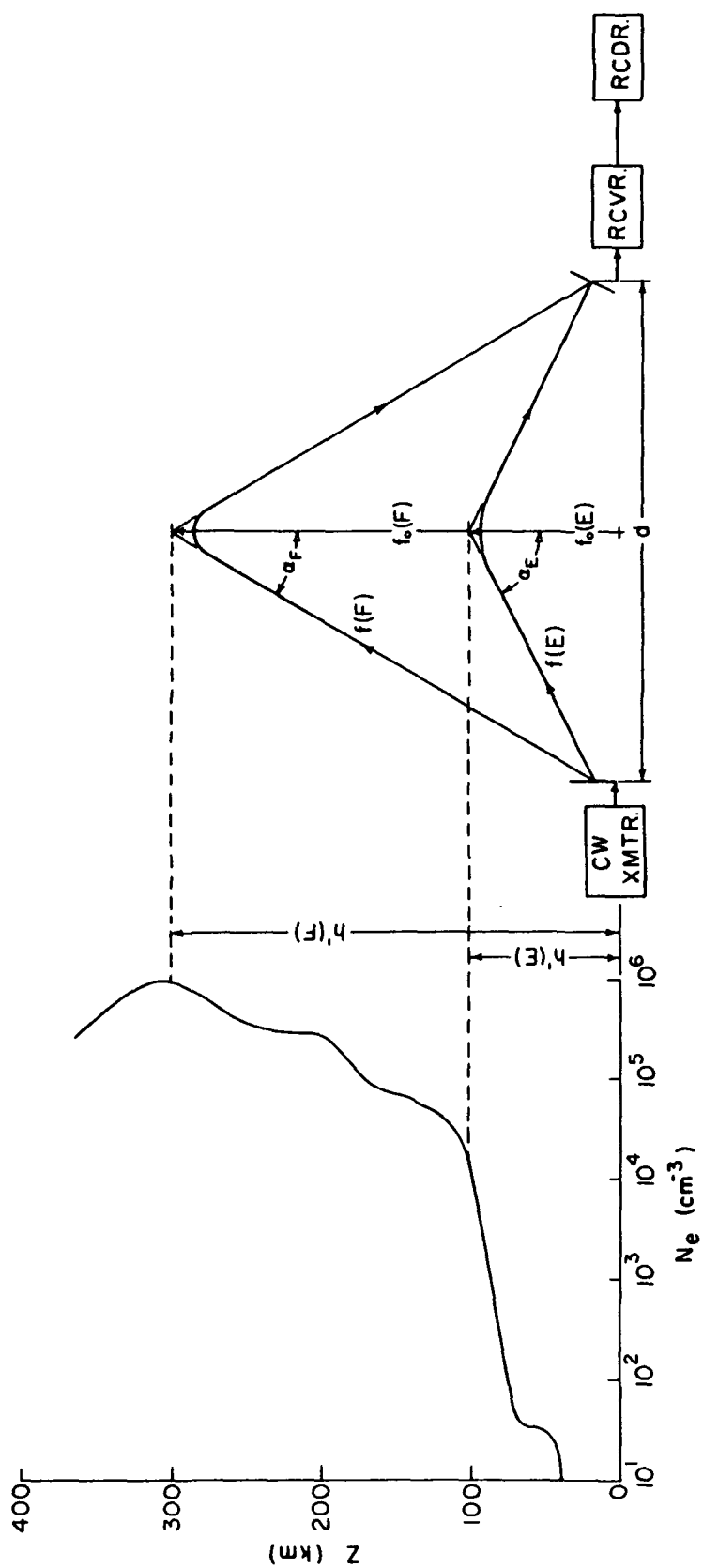
Figure 2.1. Schematic of an A3 Radio Wave Absorption Experiment.

reflections are shown. The wave mode suitable for A3 absorption measurements is the single hop E-layer reflection.

2.2 Theory

For the simplified case of a cold, weakly ionized plasma with no external magnetic field, the absorption per unit length for an electromagnetic wave is represented by the imaginary part of the complex propagation constant as follows (Davies, 1969):

$$K = \frac{e^2}{2\epsilon_o mc\mu} \frac{N_e \nu}{\nu^2 + \omega^2} \tag{2.1}$$

where e is the charge of an electron; N_e is the electron number density; ν is the electron-neutral collision frequency for momentum transfer; ϵ_o is the free space dielectric permittivity; m is the mass of an electron; c is the free space speed of light; μ is the real part of the index of refraction; and ω is the angular frequency of propagation. The real part of the index of refraction for this particular case is expressed by the equation

$$\mu = \frac{1}{\sqrt{2}} \left[1 - \frac{\omega_p^2}{\nu^2 + \omega^2} + \sqrt{\left(1 - \frac{\omega_p^2}{\nu^2 + \omega^2}\right)^2 + \frac{\omega_p^2 \nu^2}{(\nu^2 + \omega^2)^2}} \right]^{\frac{1}{2}} \tag{2.2}$$

where $\omega_p = \sqrt{N_e e^2 / m\epsilon_o}$ is the electron plasma frequency.

Although the above expression for K is an over-simplification of the actual situation, it is useful for approximating the dependence of radio wave absorption

on electron number density, collision frequency, and frequency of propagation. There are two interesting limits relating frequency of propagation to plasma frequency which will now be considered.

2.2.1 Nondeviative Absorption

When the propagation frequency is much larger than the plasma frequency i.e., $\omega >> _p$, $\omega\mu$ is essentially unity. This approximation is valid for an E-region reflected wave over most of its path (see Figure 2.1) since electron densities are relatively small at altitudes below 80 km. Since the direction of propagation is dependent on the real part of the index of refraction, the wave in this region experiences essentially no change in direction. Thus, the absorption is termed nondeviative and the absorption coefficient may be expressed as follows:

$$K \simeq \frac{1}{2c} \frac{\omega_p^2 \nu}{\nu^2 + \omega^2} \qquad (2.3)$$

Physically, radio wave absorption represents an energy loss from the wave to the electrons which in turn lose their kinetic energy in the form of heat by colliding with more massive neutrals. For a plasma slab of uniform electron density, the above expression suggests that nondeviative absorption is strongest in a region where the collision frequency is equal to the frequency of propagation.

2.2.2 Deviative Absorption

Electron density in the lower ionosphere is generally an increasing function with altitude, having a relatively large gradient in the 90 to 100 km. region (see Figure 2.1). For radio waves applicable to A3 absorption experiments, the plasma frequency for this altitude region becomes comparable in value to the frequency of propagation. When the collision frequency can be neglected, the real part of the refractive index is

$$\mu \simeq 1 - \frac{\omega_p^2}{\omega^2} \qquad (2.4)$$

Thus, μ is dependent on electron density and the wave is refracted as it travels through a region of varying electron density. Absorption in a region where the direction of the ray is changing is termed deviative absorption. Using the above equation for   in equation (2.1), the absorption coefficient is

$$K \simeq \frac{1}{2c} \frac{\omega_p^2 \nu}{(\nu^2 + \omega^2)\sqrt{1 - (\omega_p/\omega)^2}} \qquad (2.5)$$

An upward propagating wave is essentially reflected at an altitude where $\omega = \omega_p$ and then proceeds back to the ground. Actually, in the region where $\omega \simeq \omega_p$, the expression for K derived from simple ray theory is invalie and it is

necessary to use a full wave solution for calculating radio wave absorption (Budden, 1961).

2.3 A3 Absorption Measurements

There are two parameters which should be considered in conducting an A3 absorption experiment. They are distance (d) between the transmitter and receiver and the frequency (f) of propagation (ICSU, 1963). The minimum allowable distance between the transmitter and receiver is dependent on the signal strength of the ground wave which should be no larger than the background noise level. Also, if the distance is too short, E- and F-layer single hop and multi-hop reflections arrive at about the same angle making it very difficult to separate them. Criteria for establishing a maximum distance are that the signal should be strong enough to make local noon absorption measurements feasible and that the single hop E-layer relfection should be separable from any F-layer or multi-hop reflections.

In considering the frequency to be used in an A3 absorption experiment, it should be large enough to propagate through the D-region and be reflected from the E-layer. IQSY Manual No. 4 Ionosphere (ICSU, 1963) suggests that this condition is met if the propagation frequency satisfies the inequality

$$f \cos \alpha < 1.5 \text{ MHz} \tag{2.6}$$

where α is the angle formed by the ray path and a line normal to the surface of the earth. The maximum allowable frequency for a possible E-layer reflection is the screening frequency which is defined as follows:

$$f_s = f_{oE} \sec \alpha_F \qquad (2.7)$$

where f_{oE} is the E-layer critical frequency for a vertically propagating wave and α_F is the angle formed by the ray path of a wave reflected from the F-layer and a line normal to the earth's surface (see Figure 2.1).

2.3.1 Absorption Measurements for WSMR

The A3 absorption experiment conducted at WSMR used the 5.0 MHz north-south path from Fort Collins, Colorado to WSMR, New Mexico. Absorption calculations using a ray-tracing method developed by M. K. Lee (1972) have shown that most of the absorption along this path does occur in the D-region, thus providing a good indication of relative variations in D-region electron concentration (see Figure 2.2). Although the frequency of propagation is somewhat larger than those typically used for such an experiment, the relatively large distance (940 km.) between the transmitter and receiver compensates for this in such a way that the restrictions on propagation frequency discussed earlier are satisfied.

Hourly values for daytime absorption relative to their average nighttime level for the eight launch dates at WSMR

APRIL 1971
12.00 L.T.
$S_{10.7} = 140$
5.0 MHz
FORT COLLINS - WSMR
(940 km)

HEIGHT (km)

dB/(km ALTITUDE)
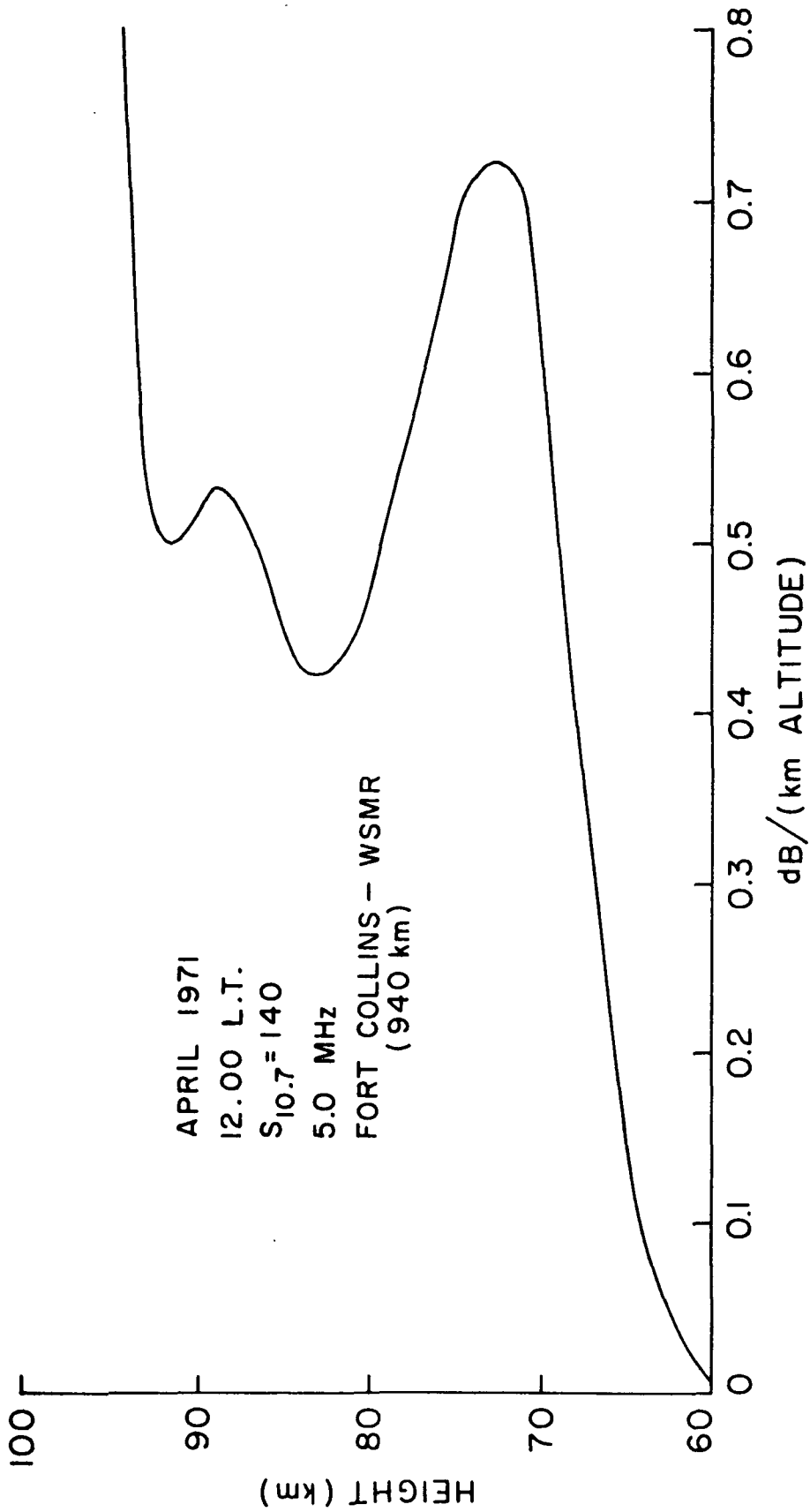
Figure 2.2. A3 Absorption Distribution for the 5.0 MHz
Fort Collins-WSMR Path.

are given in Figure 2.3. The arrows in the figure identify the curves and indicate the launch times. As can be seen from the data, January 22 and 26, 1971 were days of relatively high radio wave absorption. The radio wave absorption on June 9, 1971, July 28, 1971, October 13, 1971, and February 1, 1972 would be termed moderate while February 1, 1971 and January 19, 1972 were days of relatively low absorption.

2.3.2 Absorption Measurements for WI

A 3.36 MHz A3 absorption experiment from Annapolis, Maryland to University Park, Pennsylvania was used by Rowe, Ferraro, and H. S. Lee (1972) to provide absorption data concurrent with the rocket launches at WI. The distribution of absorption with respect to height, as calculated by M. K. Lee (1972), is shown in Figure 2.4. Qualitatively, the absorption measurements recorded on the WI launch dates indicate that January 6, 1972 was a relatively low absorption day and January 31, 1972 was a day having a moderate amount of radio wave absorption.
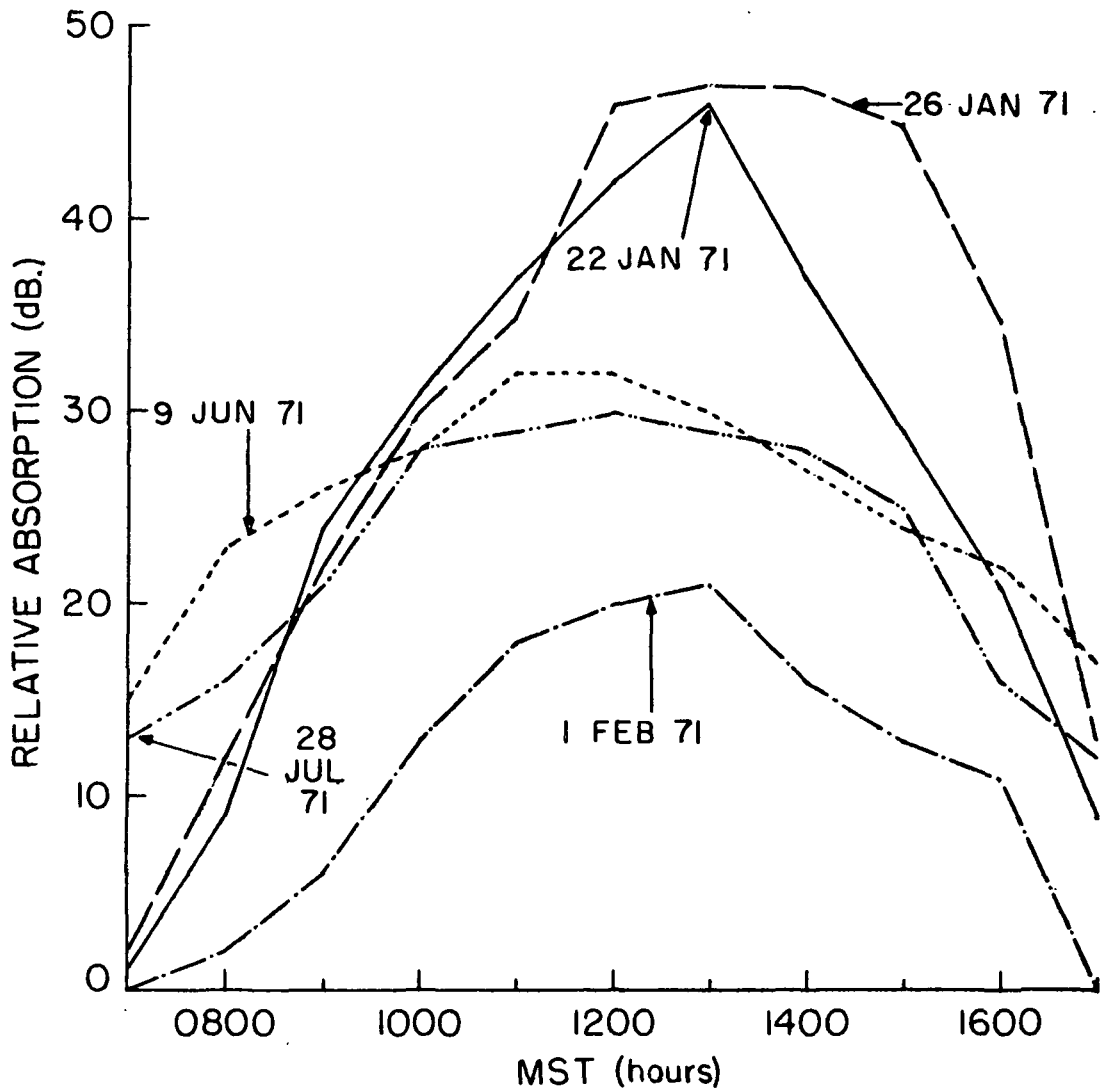
Figure 2.3a.   Hourly Values of A3 Relative Absorption for
the 5.0 MHz Fort Collins-WSMR Path.
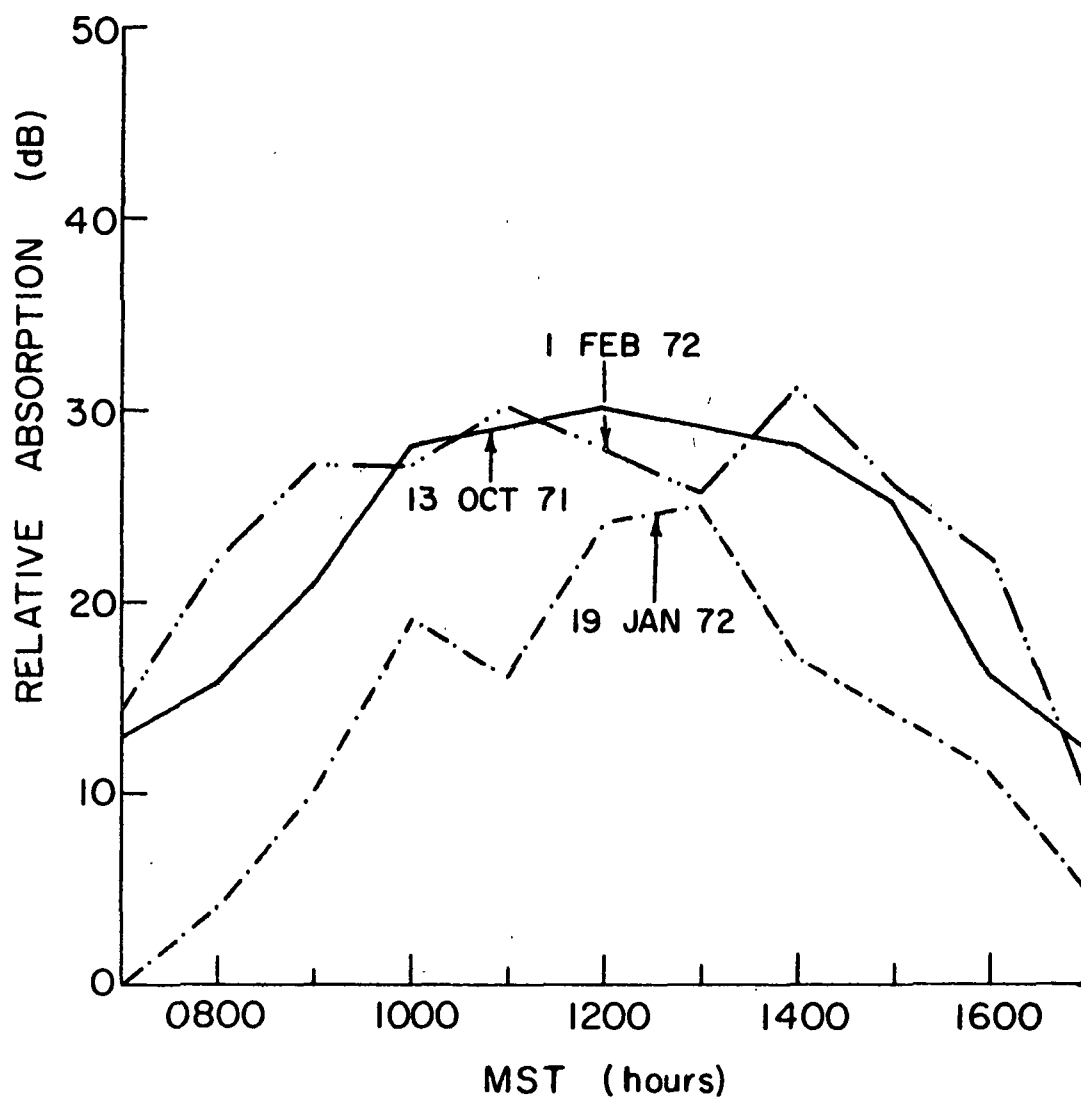
Figure 2.3b.   Hourly Values of A3 Relative Absorption for the 5.0 MHz Fort Collins-WSMR Path.
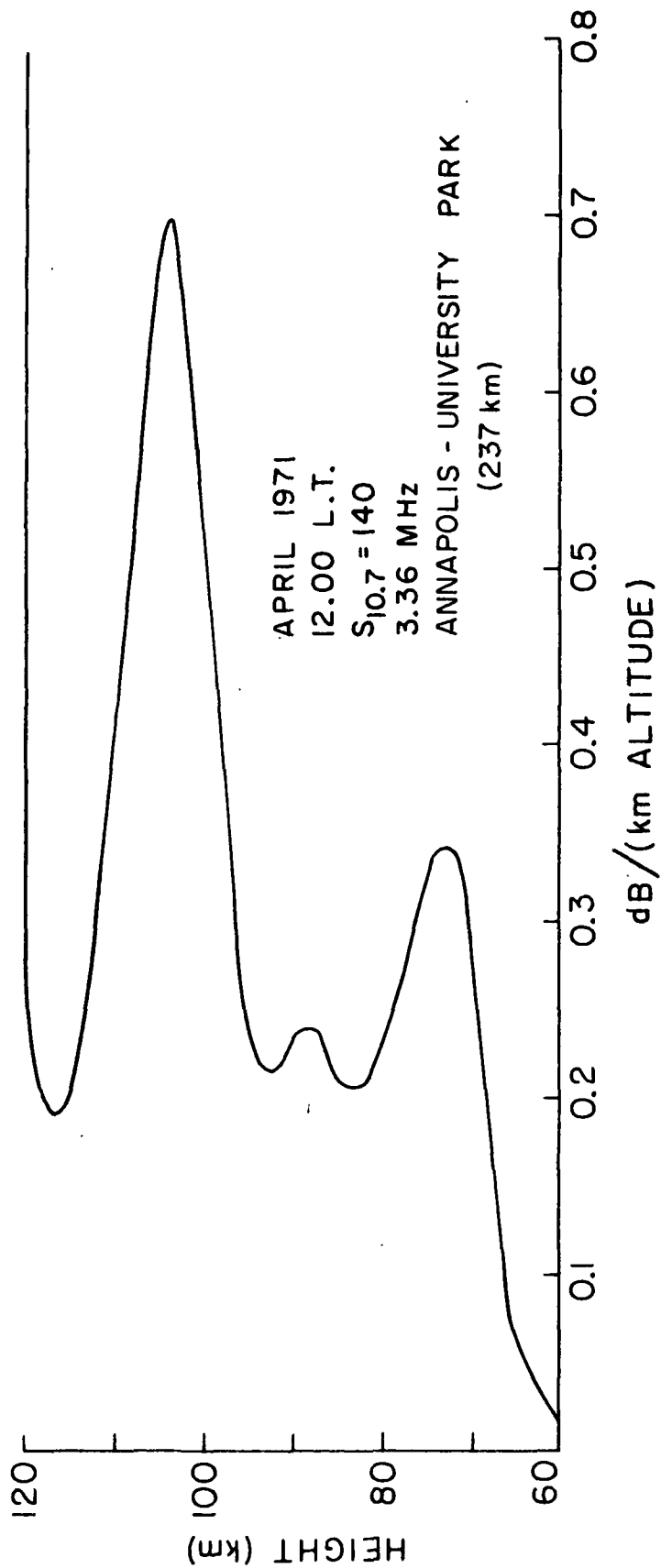
Figure 2.4. A3 Absorption Distribution for the 3.36 MHz
Annapolis-University Park Path.

CHAPTER III

THE BLUNT PROBE

3.1 Introduction

The blunt probe (Figure 3.1) is a two electrode instrument for measuring the bipolar conductivity of a weakly ionized plasma, namely the lower ionosphere. The original instrument was designed in 1964 by L. C. Hale, D. P. Hoult, and associated graduate students of The Ionosphere Research Laboratory (Hale and Hoult, 1965). In addition to studying the so-called "normal" daytime and nighttime D-region (Hale, Hoult and Willis, 1966; Hale, 1967; Hale, Hoult and Baker, 1968; Hale, Nickell, Kennedy and Powell, 1972), such ionospheric phenomena as a solar eclipse (Baker and Hale, 1970; Hale, 1970), a polar cap absorption (PCA) event (Hale, Mentzer and Nickell, 1971), and the "winter anomaly" (Mitchell, Hale, Olsen, Rubio and Randhawa, 1972; Mitchell and Hale, 1972) have been investigated using these probes.

Most of the useful data obtained from this instrument occurs after expulsion from the rocket when it is descending subsonically to the earth on a parachute. Although the theory for charged particle collection has been extended to consider supersonic flow (Sonin, 1967), the probe has been designed for subsonic flow which reduces uncertainities in the operation.

The aluminum disc and circular guard ring (Figure 3.1) form the collecting electrode for the instrument and are
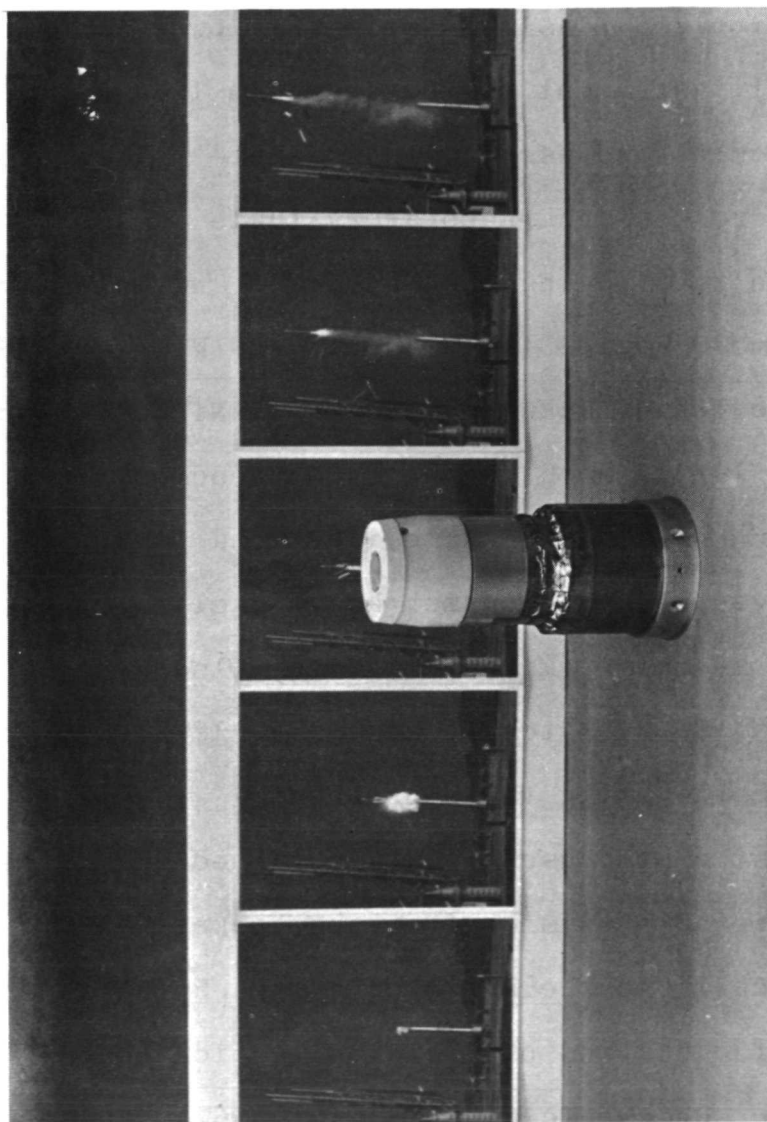
Figure 3.1. The Blunt Probe

electrically separated from the return electrode by a nylon
spacer. For daytime measurements, it is necessary to shield
the collecting surface from the sun. This is accomplished
by using a flat collector plate geometry which, despite
swinging of the parachute, stays out of the sunlight for
sufficient time to make the desired measurements. The
larger return electrode consists of the antenna can and the
power supply which are wrapped with copper foil. During
the daytime, photoelectric currents provide a very low
impedance path between the return electrode and the
surrounding plasma. Thus, when the collecting surface is
biased negatively with respect to the return electrode,
positive ions form the current drawn into the collector.
Similarly, when the collector is positively biased,
electrons and negative ions are collected. In actual
operation, a linear voltage waveform having both polarities
is swept between the electrodes of the probe.

3.2   Instrumentation

A block diagram describing the operation of the blunt
probe is given in Figure 3.2. Circuit diagrams for the
different subsystems are given in Figures 3.3 to 3.6 and
will be briefly discussed in this section.

3.2.1   Sweep Voltage Generator

By applying a known voltage waveform between the two
electrodes of the payload and measuring the corresponding
current collected, it is possible to calculate the
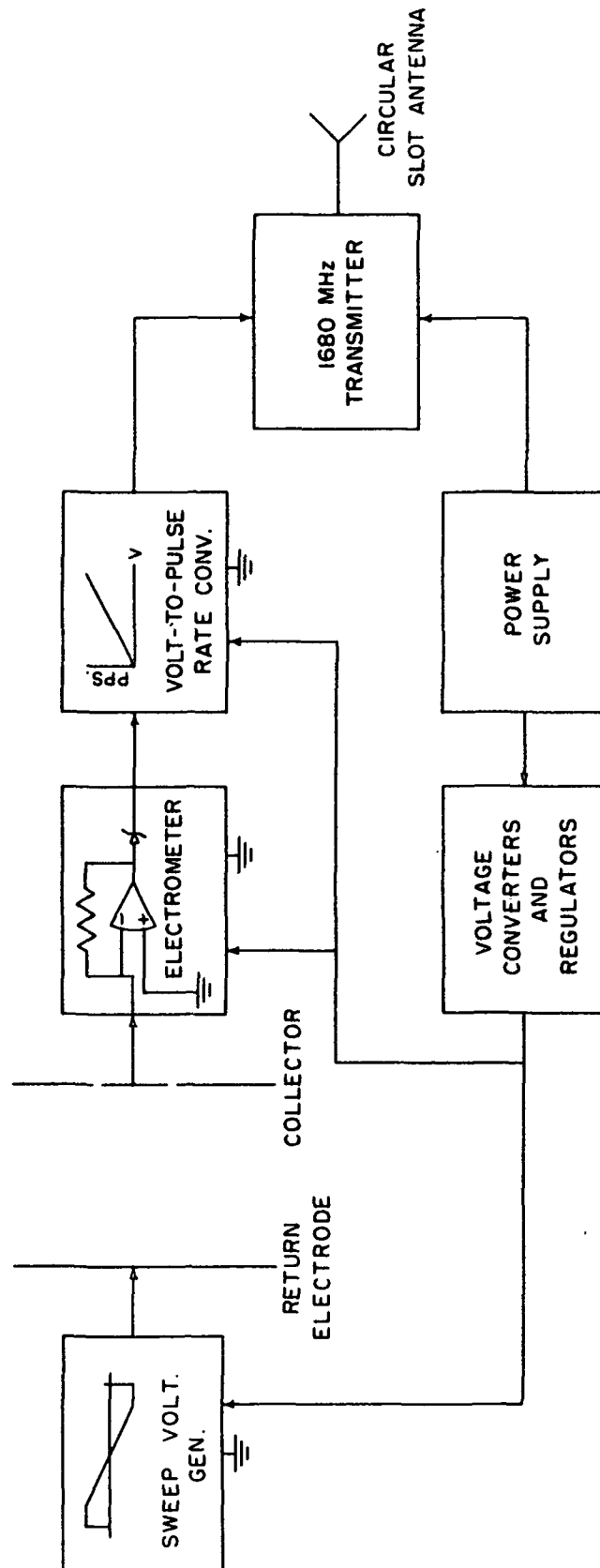
Figure 3.2. Schematic of Blunt Probe Instrumentation
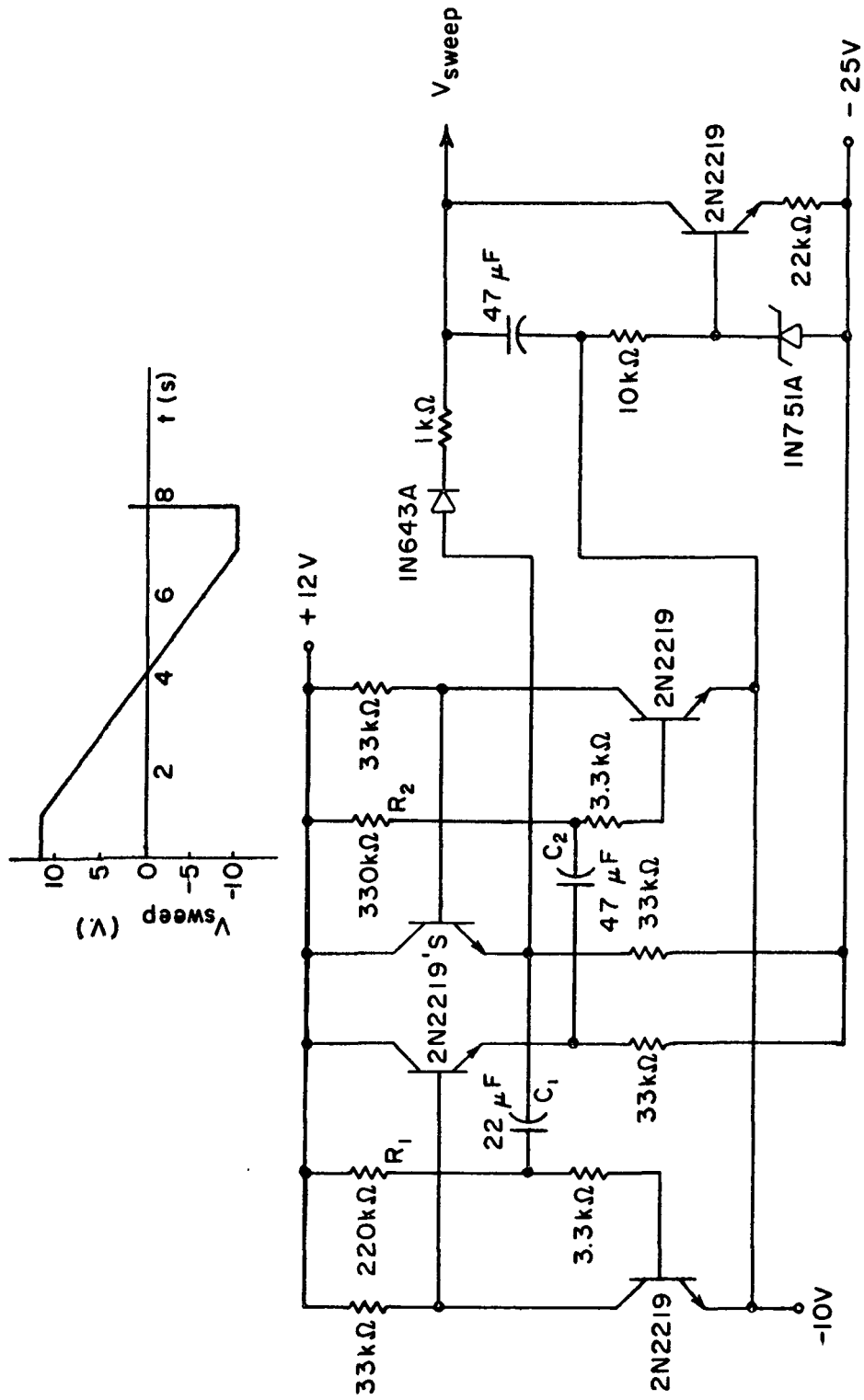
Figure 3.3. Sweep Voltage Generator Circuit.
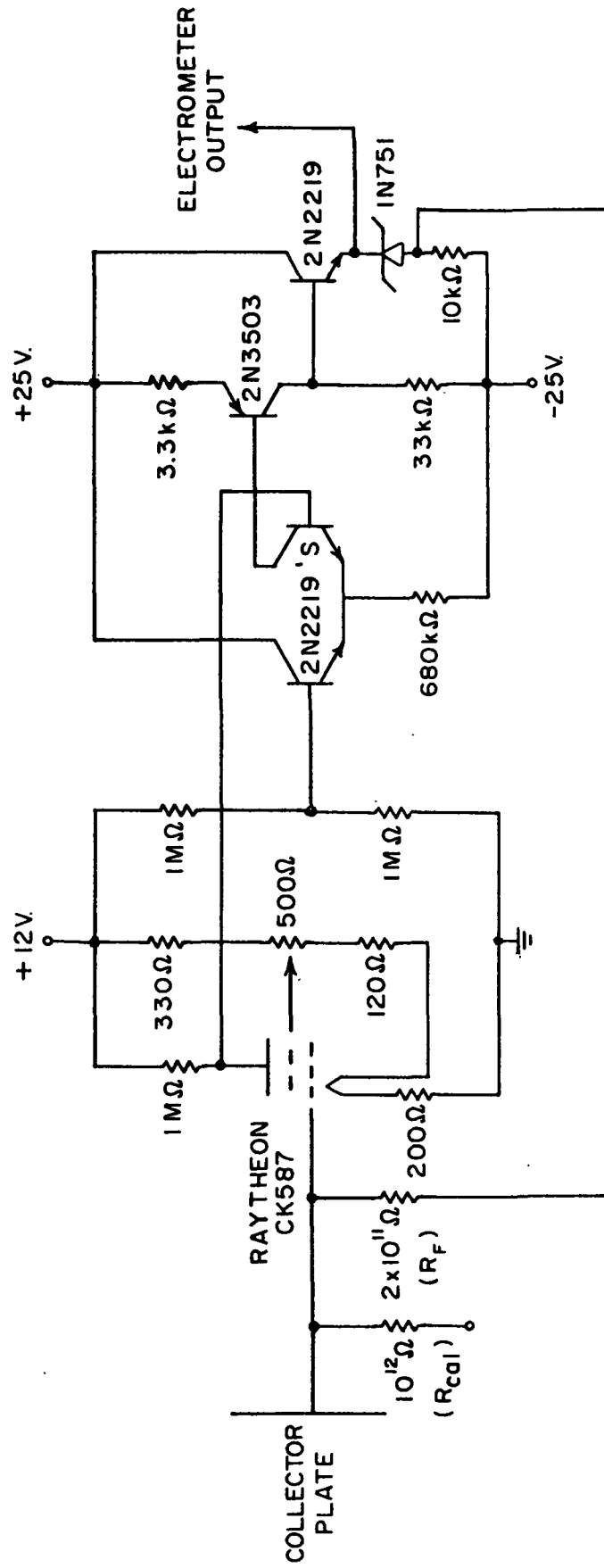
Figure 3.4. Electrometer Circuit.
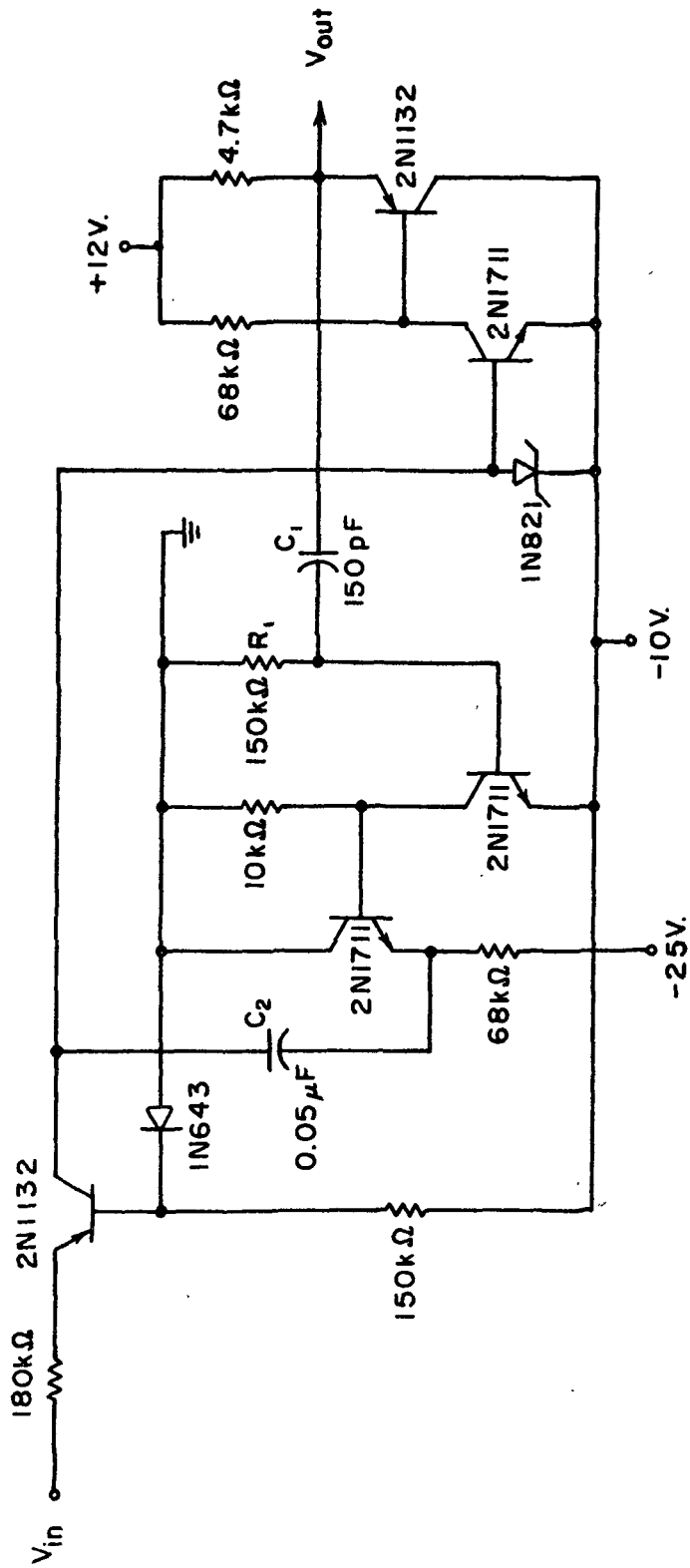
Figure 3.5.   Voltage-to-Pulse Rate Converter Circuit.
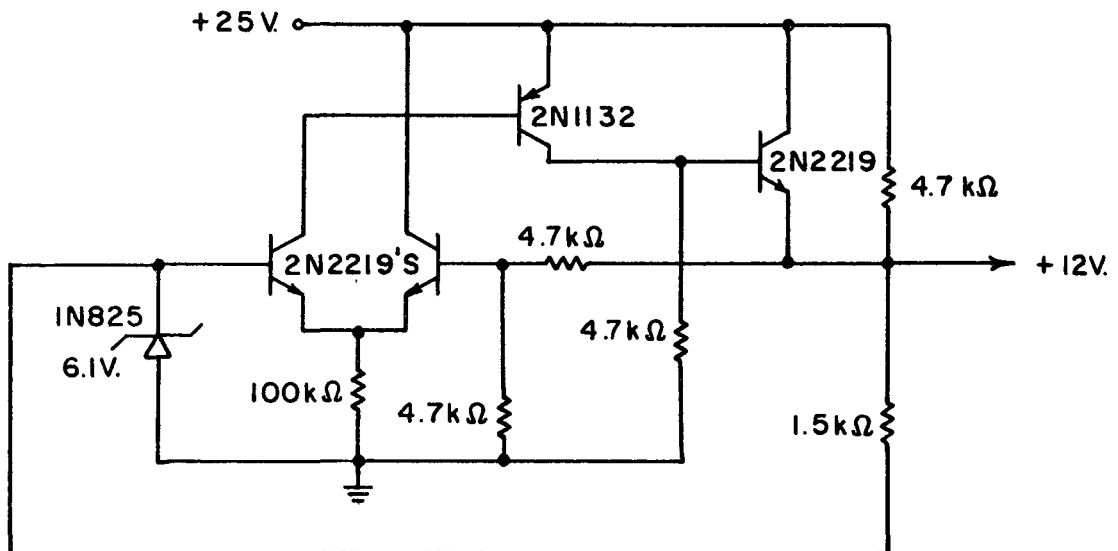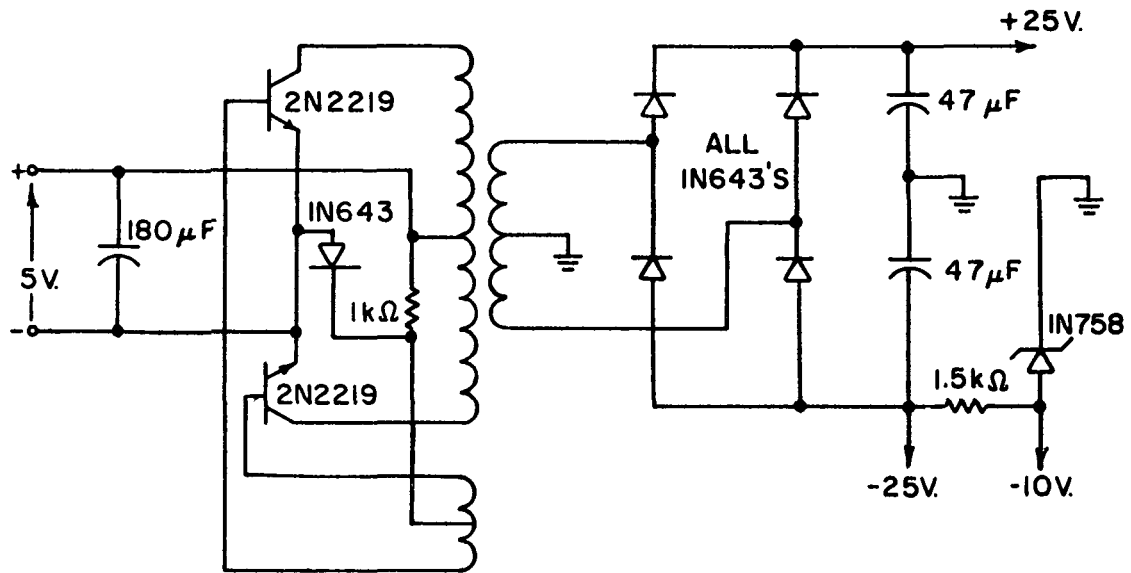
Figure 3.6.   Voltage Converter and Regulator Circuits

conductivity of the surrounding plasma. The particular
waveform used for the blunt probes in this experiment and
the electronics necessary for generating it are given in
Figure 3.3.

The sweep voltage generator is essentially an astable
multivibrator followed by a constant current run-down
circuit which provides a negative-going ramp function for
the output voltage when the multivibrator's output is
negative. The rectangular waveform of the multivibrator
has a positive on-time determined by R_1C_1 with an amplitude
of +12 volts followed by a negative pulse of amplitude
-10 volts whose time duration is controlled by R_2C_2. The
emitter follower in the multivibrator output shortens the
switching times and provides a low impedance output for
charging the run-down capacitor.

3.2.2 Electrometer

The core of the blunt probe is the electrometer which
is a highly sensitive ammeter used to measure the very small
current of charged particles drawn into the collector. A
circuit diagram for the electrometer is given in Figure 3.4.

The input stage of the electrometer is a Raytheon
CK587 tetrode which has a very high input resistance. The
output resistance ($\simeq 10^6$ ohms) of the electrometer tube is
dependent on the input voltage and forms one branch of a
balanced bridge network. Variations in voltage across the
bridge network, caused by changes in the tetrode's output
resistance, are fed into a differential amplifier whose

output is amplified by a cascaded transistor pair. The
output voltage of the final transistor stage, which is
proportional to the electrometer's input current, provides
negative feedback to the overall circuit, thus:

(1)   keeping the potentials of the collector disc and
       exterior guard ring approximately the same;

(2)   improving the overall frequency response; and

(3)   stabilizing the gain of the system to be
       essentially the feedback transresistance.

A Zener diode at the output of the electrometer shifts the
voltage level to keep the input to the voltage-to-pulse
rate converter nonnegative.

3.2.3   Voltage-to-Pulse Rate Converter

The voltage-to-pulse rate converter transforms the
output voltage of the electrometer into a waveform suitable
for modulating the 1680 MHz transmitter tube. The modulation
scheme used in telemetering the data back to ground is a
very simple PPM-AM system in which the transmitter is pulsed
off for a fixed time duration, the rate being proportional
to the output voltage of the electrometer. The voltage-to-
pulse rate converter network is shown in Figure 3.5.

This circuit consists basically of an astable collector-
coupled multivibrator. The on-time for the -25 volt pulses
is determined by R_1C_1 and remains constant. The off-time
is dependent on the charging rate of C_2 which is linearly
proportional to the input voltage. An emitter follower is

used at the output to minimize the turn-off time and to
provide a low impedance output.

3.2.4 Telemetry System

The telemetry system consists of an RCA integral tube
and cavity transmitter typically tuned to 1680 MHz which
directly feeds a 0.925 λ circular slot antenna. The input
grid of the triode is pulsed off by the voltage-to-pulse
rate converter at a typical rate of 0-200 pps. This form
of modulation is compatible with the GMD/TMQ-5 receiving
and recording equipment, which is a telemetry system
presently used by the Meteorological Rocket Network (MRN).
A discussion of the antenna characteristics for this
particular probe configuration is given in Ionosphere
Research Laboratory Scientific Report No. 249 (Cuffin, 1965).

3.2.5 Power Supply, Voltage Converters and Regulators

The necessary voltages for operating the previously
mentioned blunt probe electronics are unregulated values
of +110, +5, and ±25 volts and regulated values of +12 and
-10 volts. Four 1.25 volt series-connected nickel cadmium
batteries and two converters form the power supply for the
blunt probe. The power supply, built by Schellenger Research
Laboratory of The University of Texas at El Paso, provides
potentials of +110 and +5 volts for operating the transmitter
tube. The +5 volt potential is also converted to voltages
suitable for operating the other electronics.

The converter used for obtaining an isolated and

unregulated ±25 volts from the +5 volt power supply is drawn in Figure 3.6. Also included are the voltage regulator circuits which provide positive and negative regulated voltages from the ±25 volts. A dc feedback voltage amplifier is used to provide a regulated voltage value of +12 volts with a 0.01% regulation. A Zener diode is used to obtain a regulated -10 volts.

3.3 The Probe's Physical Structure

The blunt probe, which has a height from base plate to collector (see Figure 3.1) of 9.15 inches and weighs four pounds, is compatible for flying on the Arcas rocket, a vehicle commonly used by the MRN. The collector is comprised of an interior collecting disc with a radius (r) of 1.075 inches and an exterior circular guard ring having an outer radius (R) of 2.875 inches.

The electronics for the electrometer are seated directly behind the collector and are shielded in a small aluminum cup. This keeps wiring at a minimum and avoids r-f pickup. Erie 003 r-f feed-thru filters are used to provide electrical connections through the can into the electrometer. The electronics are embedded in polystyrene wax which has very high resistivity and provides good mechanical damping to reduce microphonic response.

A nylon spacer electrically separates the collector from the larger return electrode, which is comprised of the aluminum antenna can and power supply wrapped with copper tape (Figure 3.1). The remaining electronic subsystems,

excluding the power supply, are contained inside the antenna can. The voltage sweep generator, voltage-to-pulse rate converter, and voltage converters and regulators are all mounted on one printed circuit board. The transmitter is on a separate board which is secured to the side of the can by two screws that directly feed the transmitter output to the slot antenna. The printed circuit boards are potted with Eccofoam which serves as insulation and provides mechanical strength.

The antenna can is mounted to the power supply by three cylindrical spacers. The base plate, which is attached to the opposite side of the power supply, is necessary for connecting the parachute to the payload and mating the payload with the nose cone and rocket motor.

CHAPTER IV

DATA

4.1   The Blunt Probe Launch

The launch and telemetry requirements for the

parachute-borne blunt probe are compatible with those for

the temperature-measuring Arcasonde (Ballard and Rofe,

1969) used by the Meteorological Rocket Network (MRN),

thus somewhat simplifying launch operations at any MRN

range.   Prior to launch, the preflight calibration

procedure involves inserting a precision resistor between

the collecting and return electrodes and recording the

telemetered probe response on magnetic tape.   A good

quarter-inch stereo tape recorder is sufficient for

recording either the video or demodulated signal from the

GMD receiving equipment.   Electrically, this calibration

procedure is represented by the schematic in Figure 4.1a.

The sweep voltage waveform and the demodulated probe

response for the preflight calibration mode are drawn in

Figures 4.2a and 4.2b, respectively.

While the payload is in flight, the impedance of the

surrounding medium (or for this case, electrical

conductivity) is the unknown quantity which is measured.

The in-flight mode is schematically represented in

Figure 4.1b.   A demodulated waveform depicting typical

in-flight data is drawn in Figure 4.2c.   A timing code

recorded concurrently with the in-flight measurements and

a radar plot showing the position of the payload as a
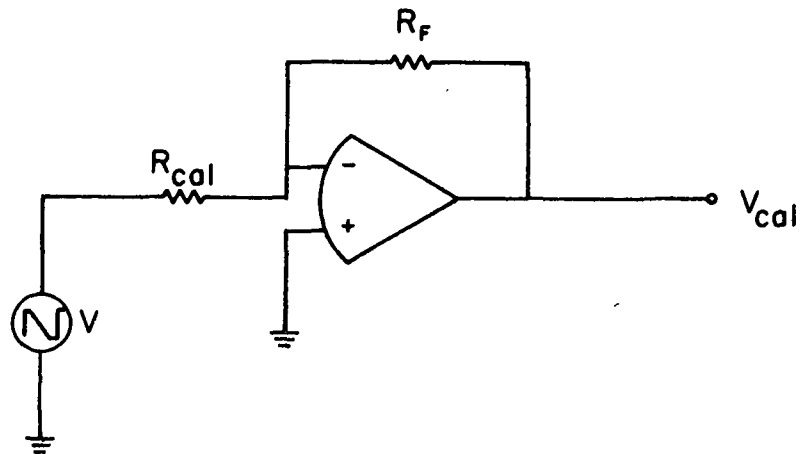
PREFLIGHT CALIBRATION MODE
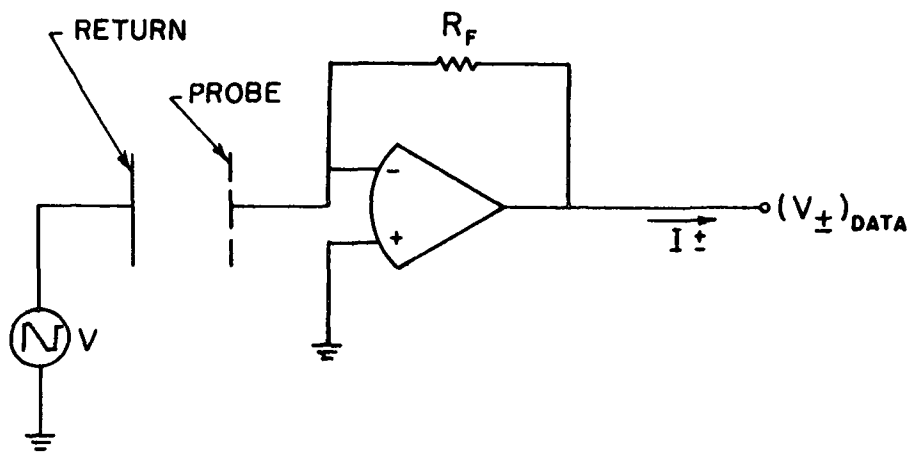
IN-FLIGHT CALIBRATION MODE

Figure 4.1. Schematic of Blunt Probe Operation
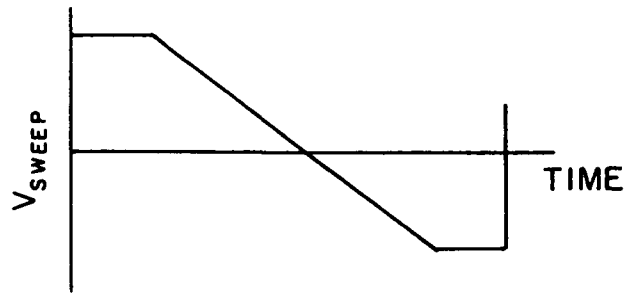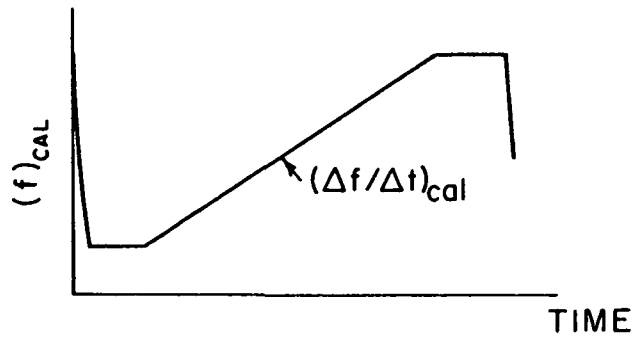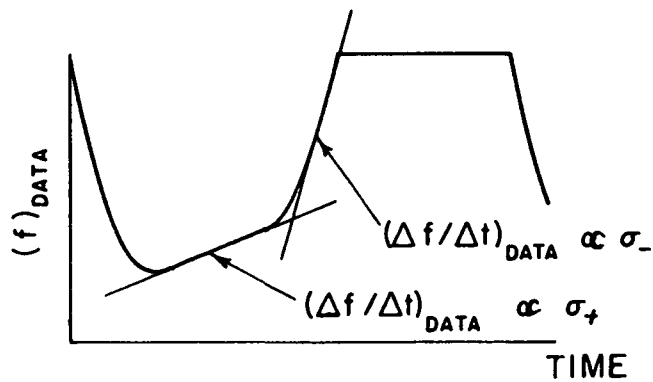
Figure 4.2.   Representative Blunt Probe Waveforms.

function of time provide the information necessary for determining the altitude at the time of the measurement. The preflight calibration and in-flight data are transmitted and received using the same system, whose parameters as a result cancel in the final equations used for data reduction.

4.2 Blunt Probe Theory

The theory describing the collection of charged particle species by a subsonic blunt probe was originally constructed by Hoult (1965). A more complete theory treating both subsonic and supersonic flow was developed later by Sonin (1967). Sonin's theory for charged particle collection is applicable if:

    (1)   the flow Reynold's number $\gg 1$;

    (2)   the ion reaction times $\gg R/v_\infty$;

    (3) $(\lambda_D/R)^2 \gg kT/eV$; and

    (4)   the plasma is weakly ionized.

In (2) and (3) above, R represents a characteristic length such as the radius of the collecting surface; v_∞ is the speed of the probe; λ_D is the Debye length; and V is the potential of the collecting surface.

The blunt probe system generally satisfies conditions (1), (3), and (4) above. The questionable assumption is (2) relating to chemically frozen flow. In this case, the most serious problems are charge transfer and dissociation of ions induced by collisions (Keller, 1968). Dissociation of ions would certainly be more serious for supersonic

operation, thus justifying the use of subsonic probes. For the subsonic case, the most serious problem is probably charge transfer which would affect the mobility of the ions but not their number density. The use of a properly chosen average mobility is an appropriate approach to this problem.

One additional problem is possible contamination from the probe itself in the form of outgassed water vapor. This would hydrate the ions, thus decreasing their apparent mobility and lowering the measured conductivity (York, 1972). An indication that this is not happening is that ion conductivity measurements on geophysically similar days are similar, and it is doubtful that contamination effects would be so reproducible.

Using Sonin's theory, the expression for probe current is

$$I_{\pm} = \int_{s} \sigma_{\pm} |E| \, dS \qquad (4.1)$$

where the surface of integration is the collecting surface and $|E|$ represents the magnitude of the electric field at the surface of the collector necessary to draw in either a current I_{+} of positively charged particles or a current I_{-} of negatively charged particles. For this particular probe geometry, the electric field at the surface of the collector is (Jeans, 1925)

$$E = \frac{2}{\pi} \frac{V}{R} \qquad (4.2)$$

where V is the potential of the collector and R is the
exterior radius of the guard ring. Thus, the equation for
collector current is

$$I_{\pm} = \int_{s} \sigma_{\pm} \frac{2}{\pi R} |V| \, dS$$

$$= \frac{2r^2}{R} \sigma_{\pm} |V| \qquad\qquad (4.3)$$

where r is the radius of the inner collector disc. In
order to avoid the problem of estimating the probe's
potential, conductivity is actually determined from the
derivative $|dI_{\pm}/dV|$ as follows:

$$\sigma_{\pm} = \frac{R}{2r^2} \left| \frac{dI_{\pm}}{dV} \right| \qquad\qquad (4.4)$$

Referring to the waveforms in Figure 4.2, the recorded
signals actually represent frequency as a function of time.
The slope of the straight line drawn through the preflight
calibration ramp will be designated $(\Delta f/\Delta t)_{CAL}$ and the
corresponding slopes of the in-flight data waveform, which
are proportional to σ_{+} and σ_{-}, will be labeled $(\Delta f_{+}/\Delta t)_{DATA}$
and $(\Delta f_{-}/\Delta t)_{DATA}$, respectively. The steeper slope for
$(\Delta f_{-}/\Delta t)_{DATA}$ in Figure 4.2 suggests the presence of
electrons which have a much greater mobility than positive
ions.

Referring to the electrical schematic of the blunt
probe (Figure 4.1), the equation for $(dI_{\pm}/dV)$ is

$$\frac{dI_{\pm}}{dV} = \frac{1}{R_{CAL}} \frac{(\Delta V_{\pm})_{DATA}}{(\Delta V)_{CAL}} = \frac{1}{R_{CAL}} \frac{(\Delta V_{\pm}/\Delta t)_{DATA}}{(\Delta V/\Delta t)_{CAL}} \qquad (4.5)$$

Since the output voltage of the electrometer is converted linearly to frequency, the following expression may be written for $(dI_{\pm}/dV)$:

$$\frac{dI_{\pm}}{dV} = \frac{1}{R_{CAL}} \frac{(\Delta f_{\pm}/\Delta t)_{DATA}}{(\Delta f/\Delta t)_{CAL}} \qquad (4.6)$$

Substituting equation (4.6) into equation (4.4) gives the following equation which is applicable for reducing the data:

$$\sigma_{\pm} = \frac{R}{2r^2} \frac{1}{R_{CAL}} \frac{(\Delta f_{\pm}/\Delta t)_{DATA}}{(\Delta f/\Delta t)_{CAL}} \qquad (4.7)$$

4.3 Positive and Negative Conductivities

Figures 4.3-4.8 show measured positive and negative conductivity values for six of the rocket launches listed in Table 1.1. Smoothed curves were constructed to best fit the measured values. When considering electrons, the concept of negative conductivity is rather arbitrary since electron mobility is a nonlinear function of E/P, the ratio of electric field to atmospheric pressure. The curves shown represent data measured for particular E/P values in a consistent manner on all experiments and thus form the basis for making comparisons of negative conductivities.
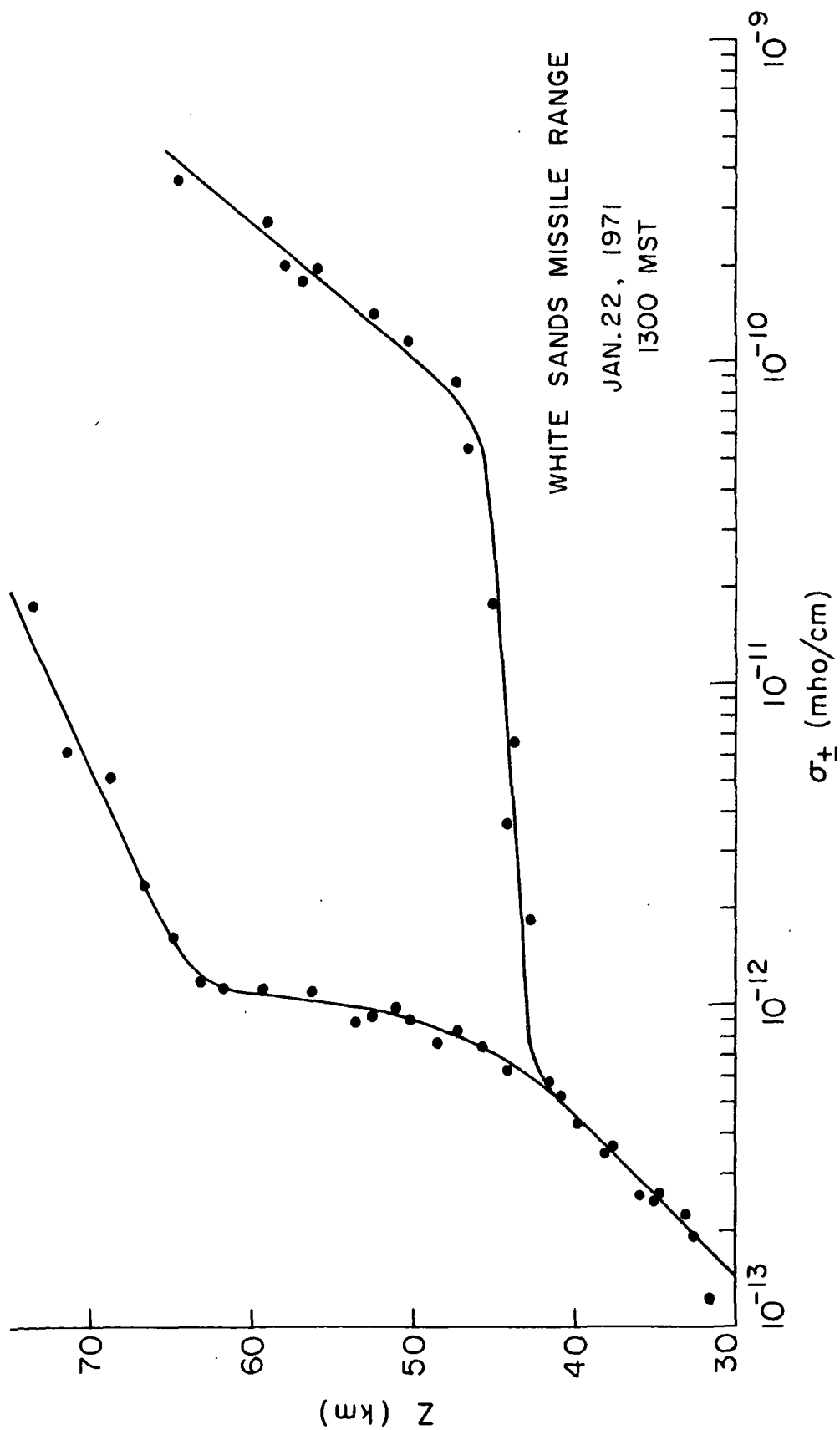
Figure 4.3. Conductivity Data for January 22, 1971 at WSMR.
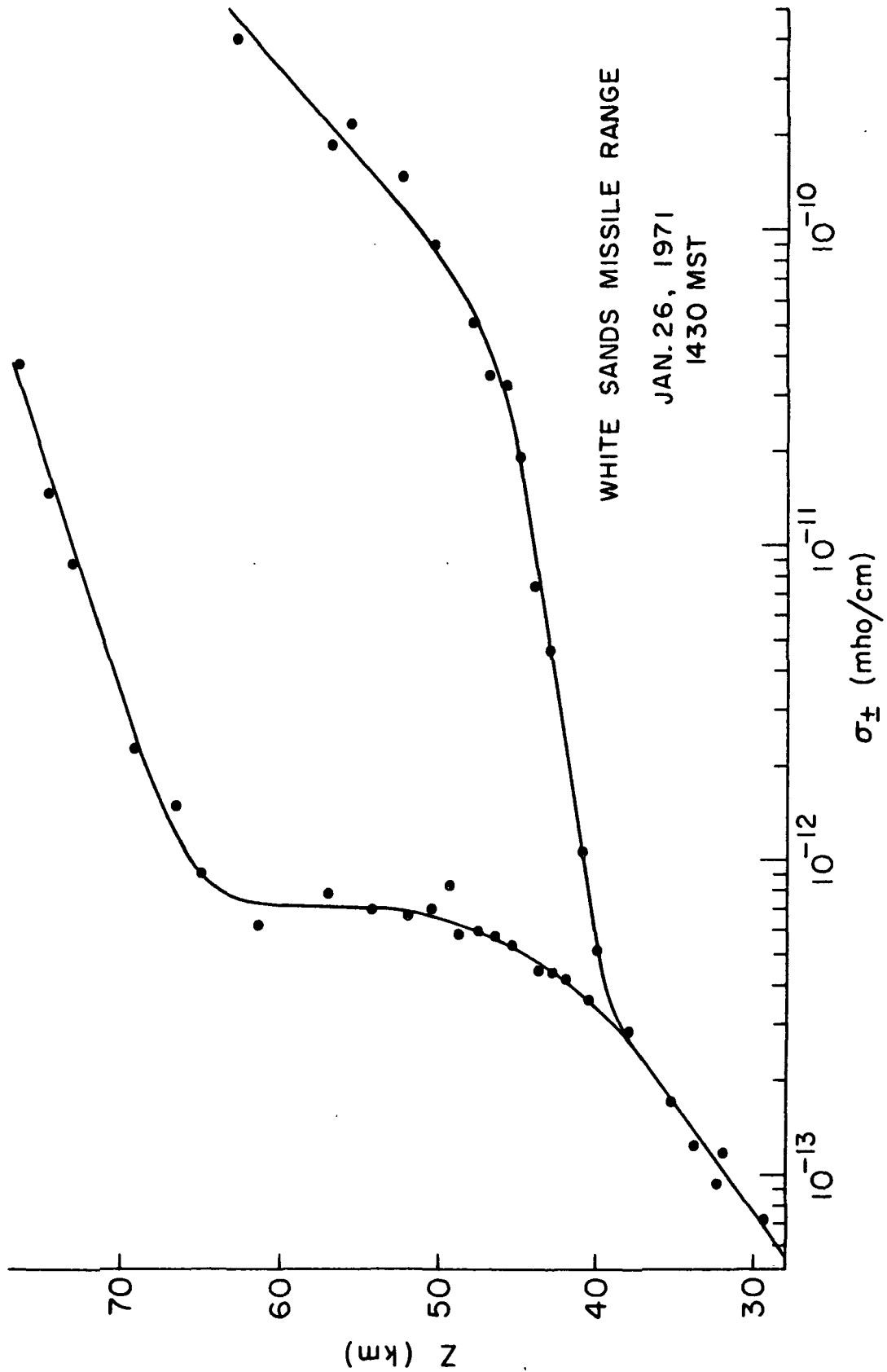
Figure 4.4. Conductivity Data for January 26, 1971 at WSMR.
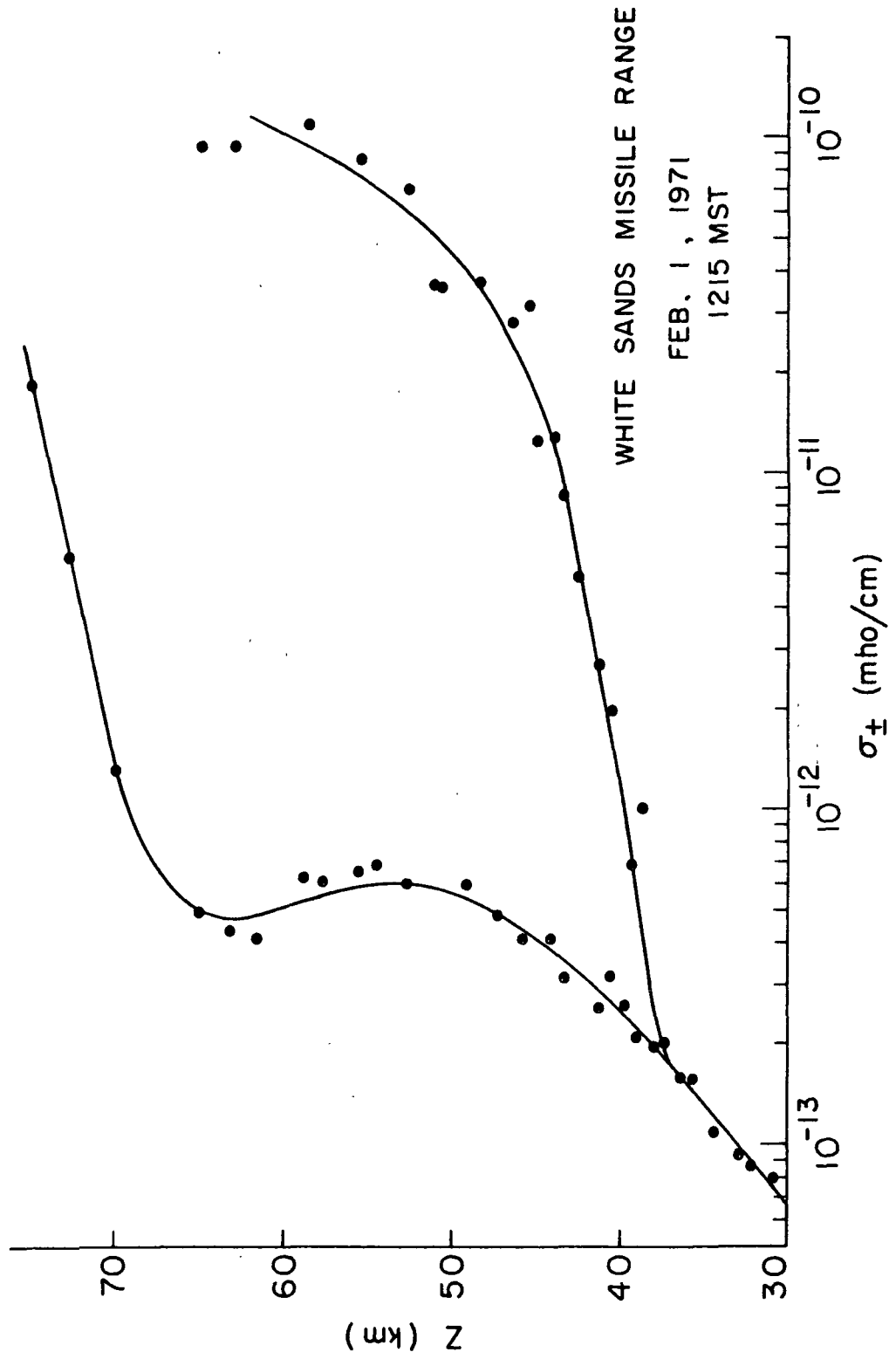
Figure 4.5. Conductivity Data for February 1, 1971 at WSMR.
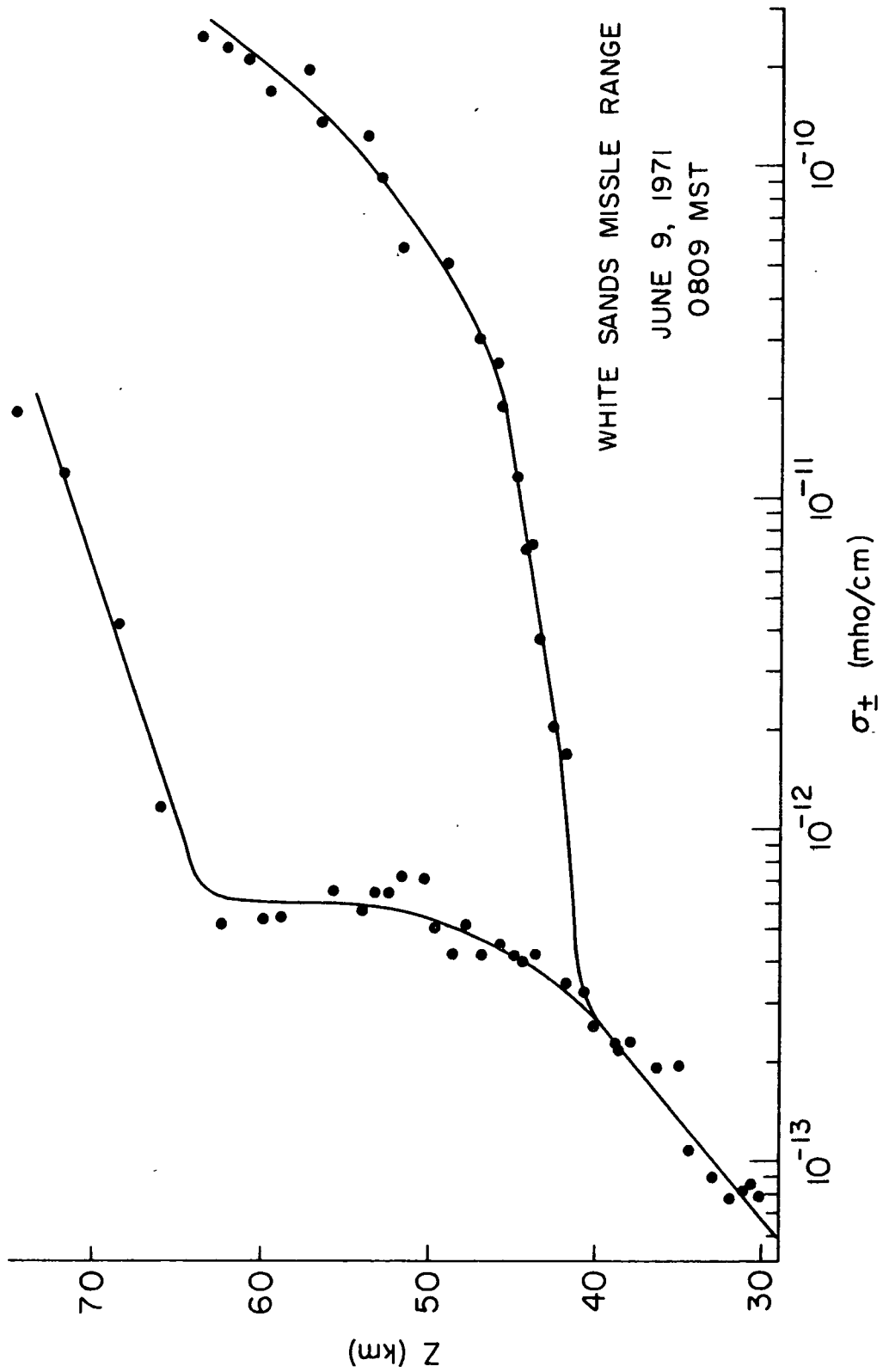
Figure 3.6. Conductivity Data for June 9, 1971 at WSMR.
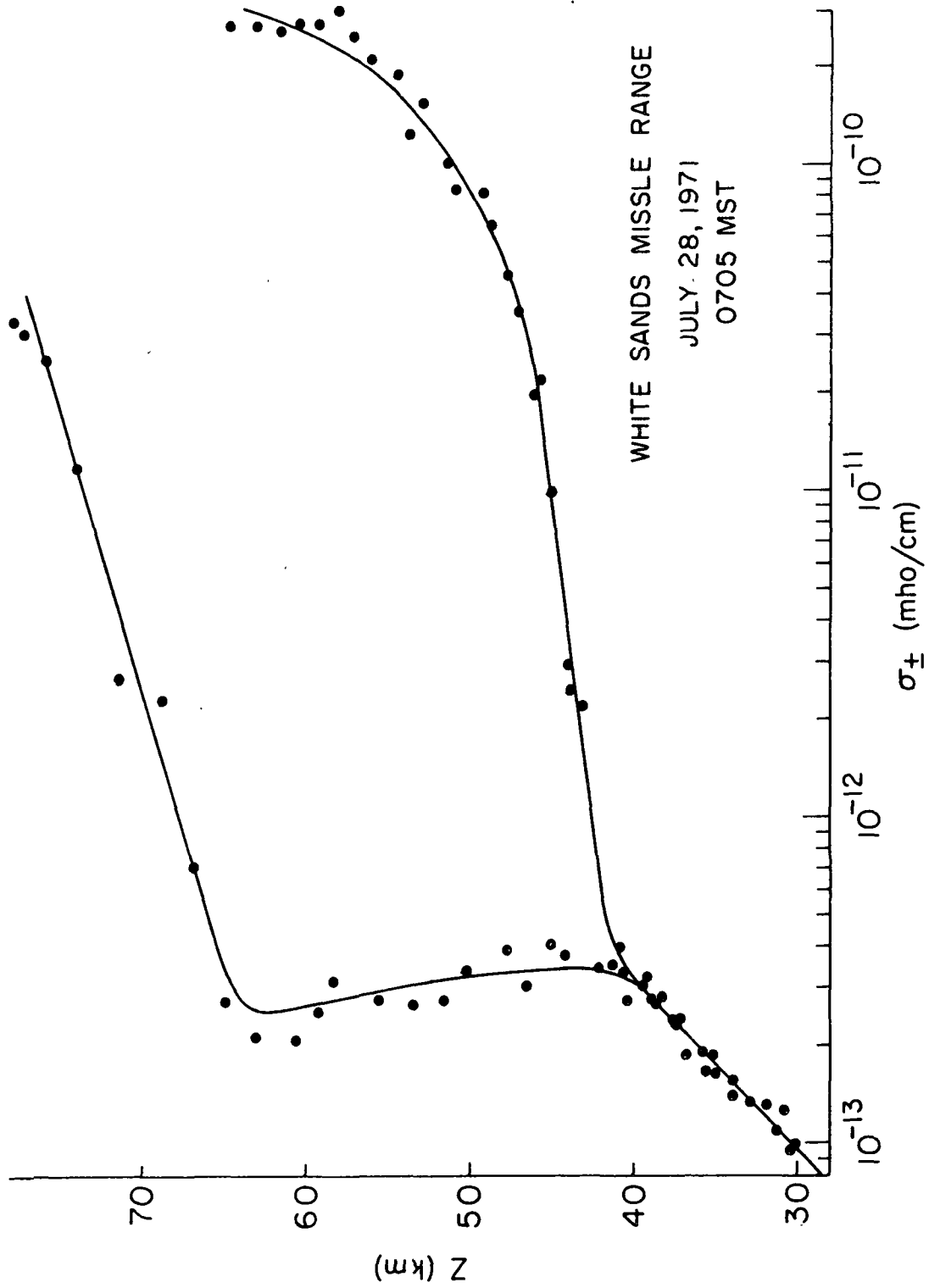
Figure 4.7. Conductivity Data for July 28, 1971 at WSMR.
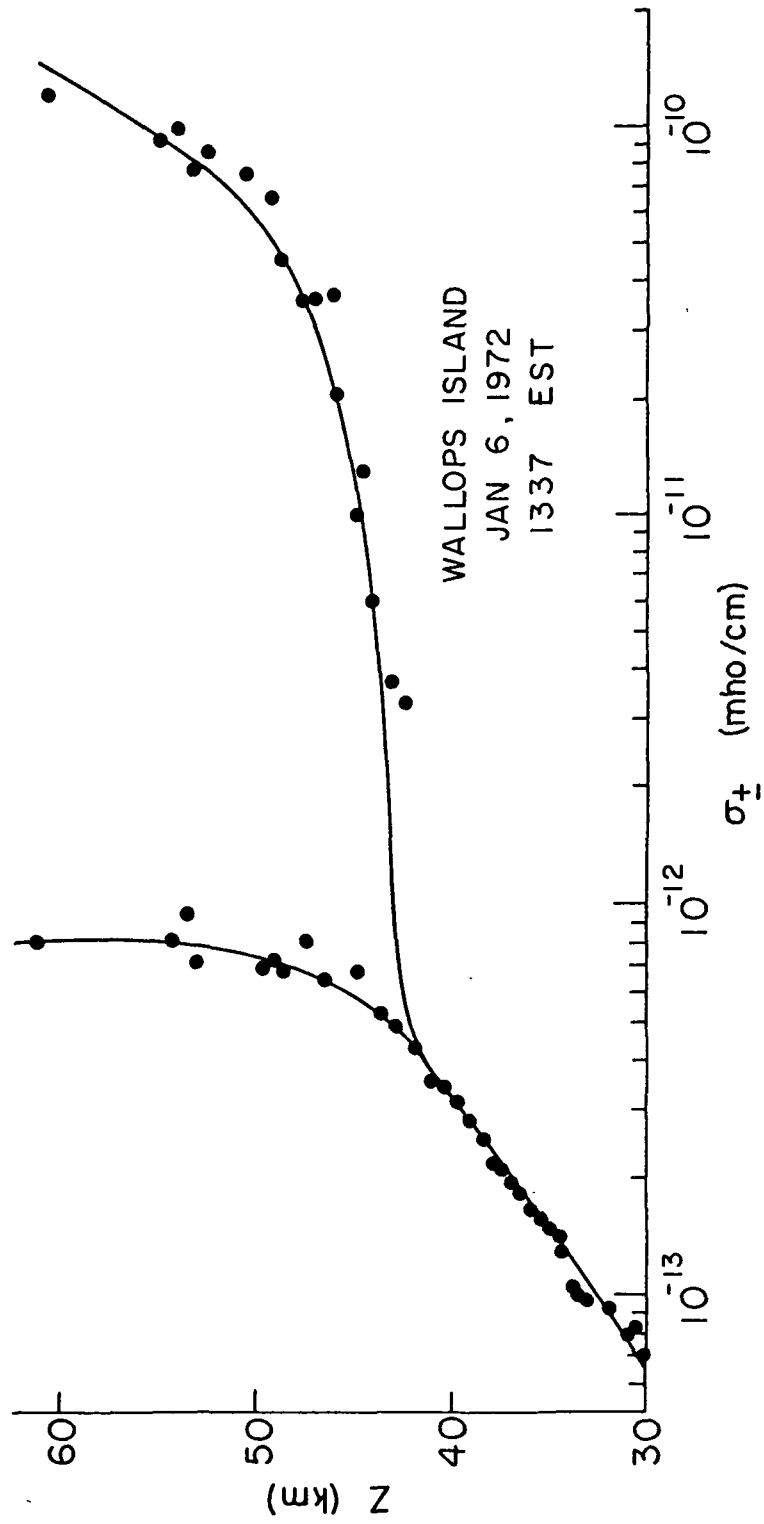
Figure 4.8. Conductivity Data for January 6, 1972 at WI.

A composite of the six positive and negative conductivity profiles is drawn in Figure 4.9.

The same data reduction procedure was followed by Cipriano (1973), a graduate student of The Ionosphere Research Laboratory, for the four remaining rocket launches listed in Table 1.1. The smoothed conductivity profiles for these four rocket shots are given in Figure 4.10.

4.4 Positive Ion Densities

For a multi-species plasma, positive conductivity is related to positive ion number density by the equation

$$\sigma_+ = e \sum_i N_{i+} u_{i+} \qquad (4.8)$$

where N_{i+} and u_{i+} are the positive ion number density and mobility of the ith species, respectively, and e is the charge of an electron. Assuming that the mobilities of the different positive ions are comparable in value and may be represented by an effective small ion reduced mobility model (Dalgarno, 1962), equation (4.8) simplifies to the following expressions:

$$\sigma_+ = N_+ e u_+ = N_+ e u_{0+} \frac{T}{T_0} \frac{P_0}{P} \qquad (4.9)$$

$$N_+ = \frac{\sigma_+}{e u_{0+}} \frac{T_0}{T} \frac{P}{P_0} \qquad (4.10)$$
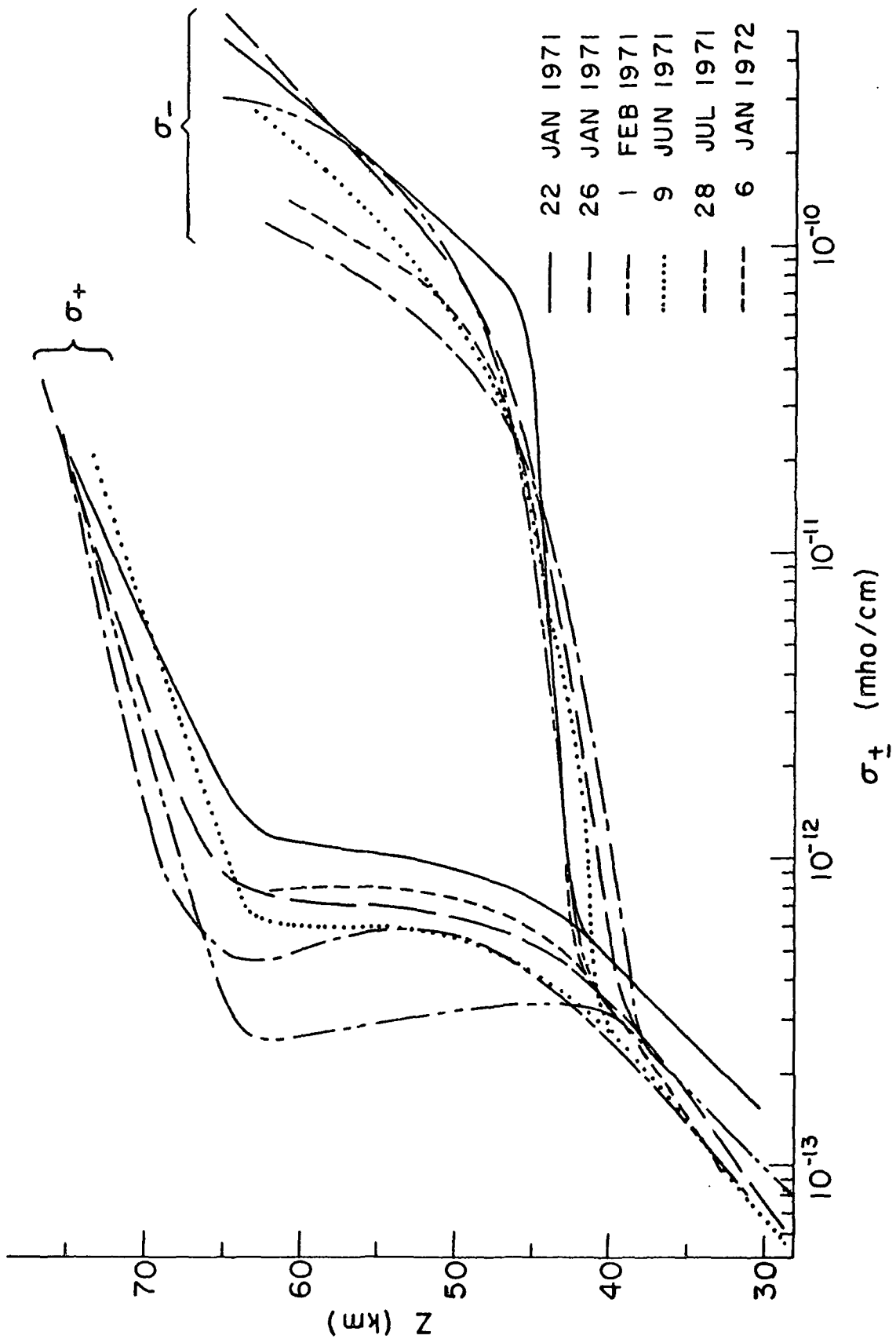
Figure 4.9. Smoothed Conductivity Profiles for WSMR and WI.
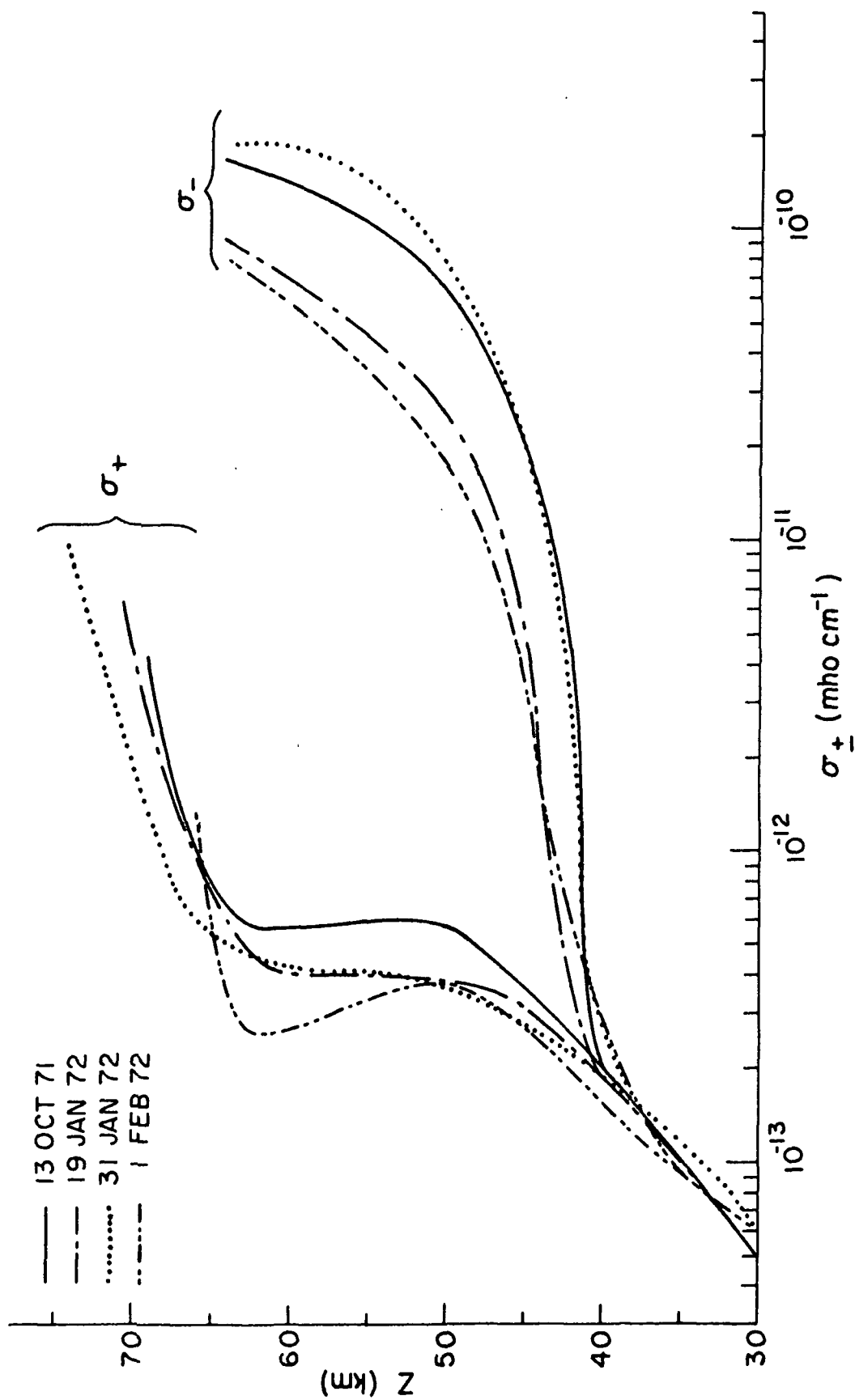
Figure 4.10. Smoothed Conductivity Profiles for WSMR and WI.

In determining N_+, the reduced mobility u_{o+} was assumed to be 1.8 $cm^2/v.s.$ (Cole and Pierce, 1965), a value used previously by Hale (1967). Values for T and P were obtained from CIRA 1965 and T_o and P_o represent the standard temperature and pressure values.

The positive ion density values deduced from the σ_+ data (Figures 4.3-4.8) and the corresponding smoothed profiles are drawn in Figures 4.11-4.16. A composite of the six profiles is drawn in Figure 4.17. Smoothed curves for positive ion density from the blunt probe conductivity data of Cipriano (1973) are given in Figure 4.18.

4.5   Electron Densities

Electron density (N_e) may be determined from negative conductivity by using a procedure analogous to the one used for deducing positive ion density. Assuming an effective small ion reduced mobility for negative ions and the following expression for negative conductivity:

$$\sigma_- = N_e eu_e + N_- eu_- \qquad (4.11)$$

the solution for electron number density is

$$N_e = \frac{1}{u_e} \left[\frac{\sigma_-}{e} - N_- u_- \right] \qquad (4.12)$$

The equation for conservation of charge and the assumption that $u_e \gg u_-$ simplifies equation (4.11) to the following expression:
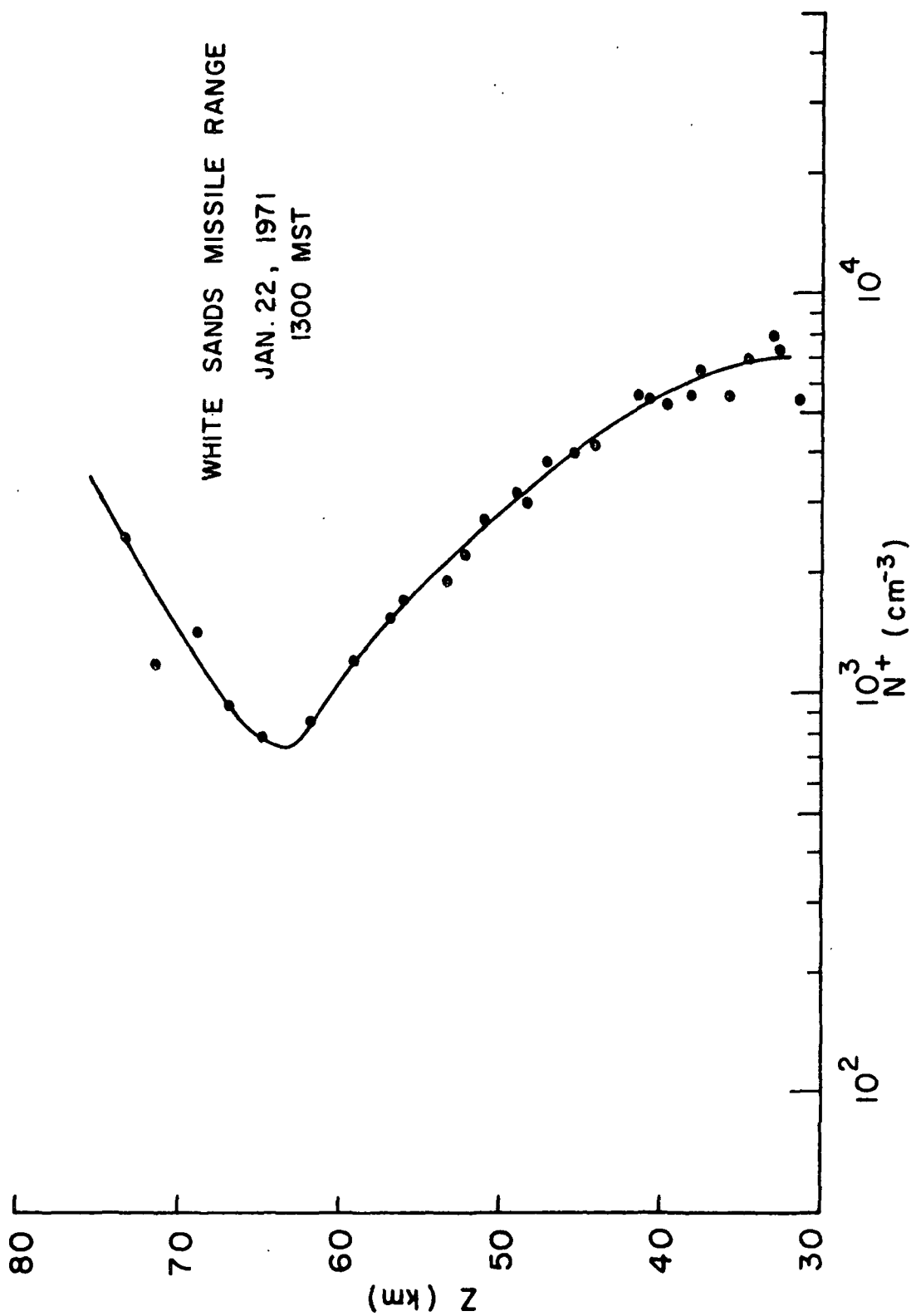
Figure 4.11. Positive Ion Density Data for January 22, 1971 at WSMR.
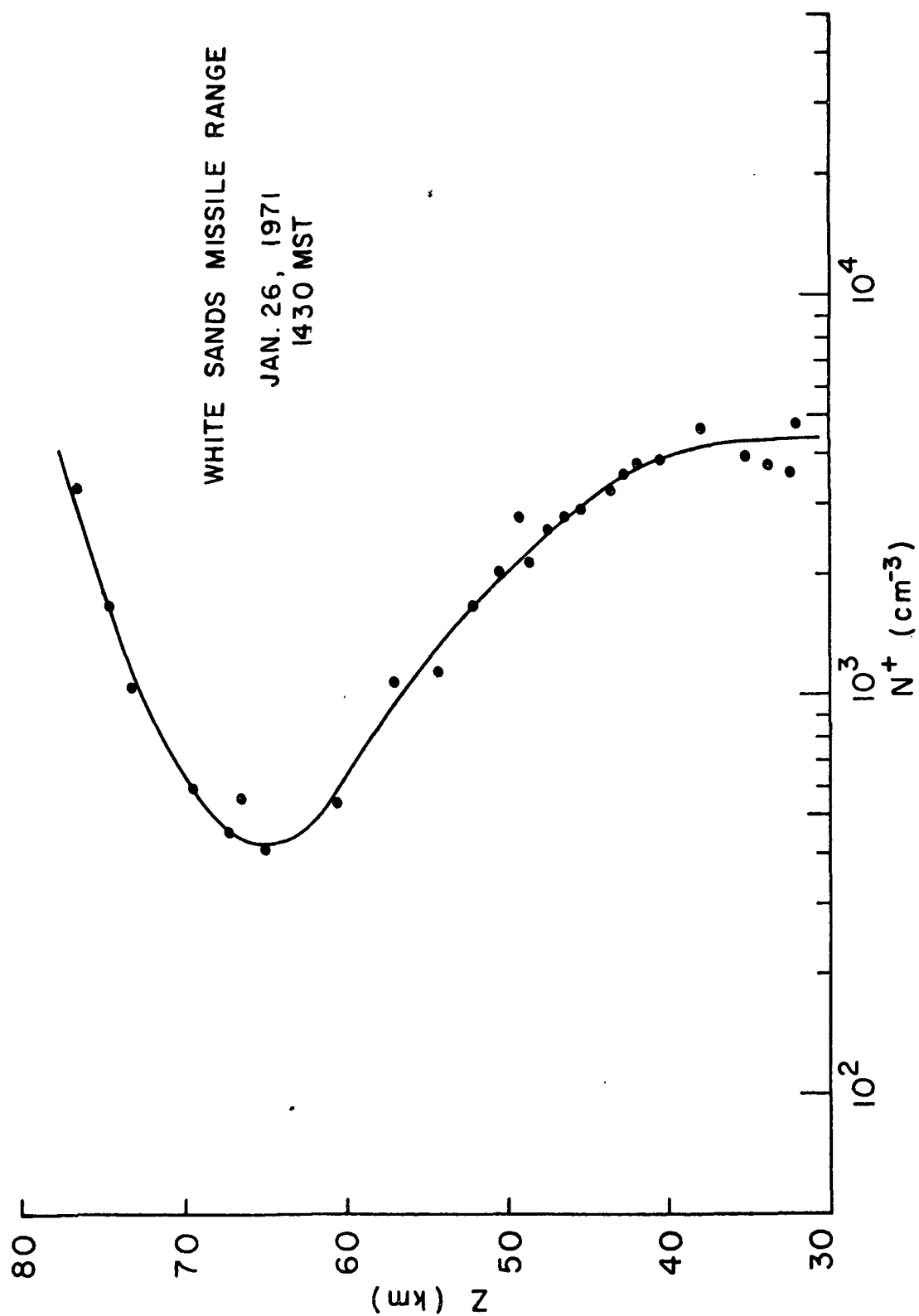
Figure 4.12. Positive Ion Density Data for January 26, 1971 at WSMR.
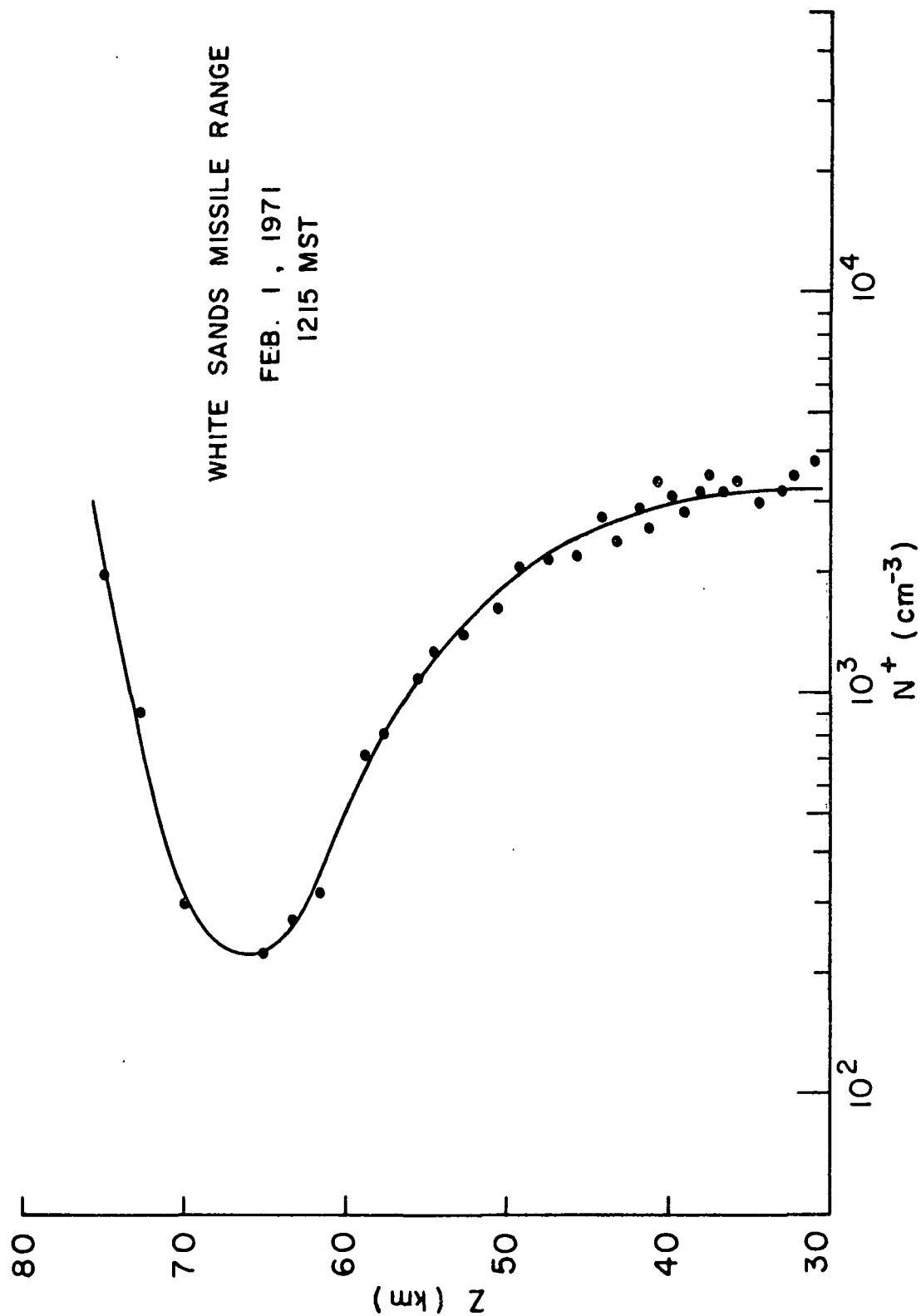
Figure 4.13. Positive Ion Density Data for February 1, 1971 at WSMR.
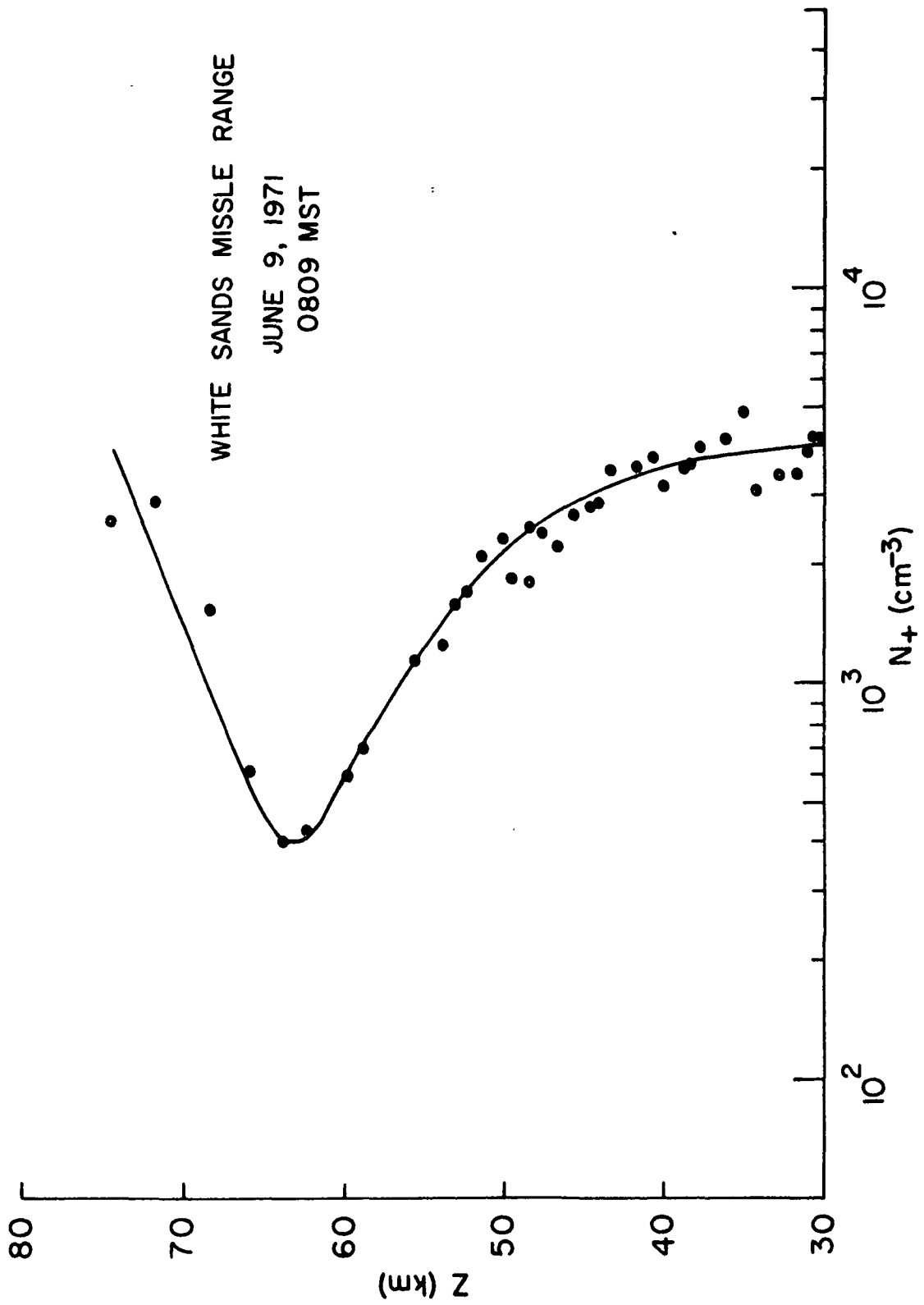
Figure 4.14. Positive Ion Density Data for June 9, 1971 at WSMR.
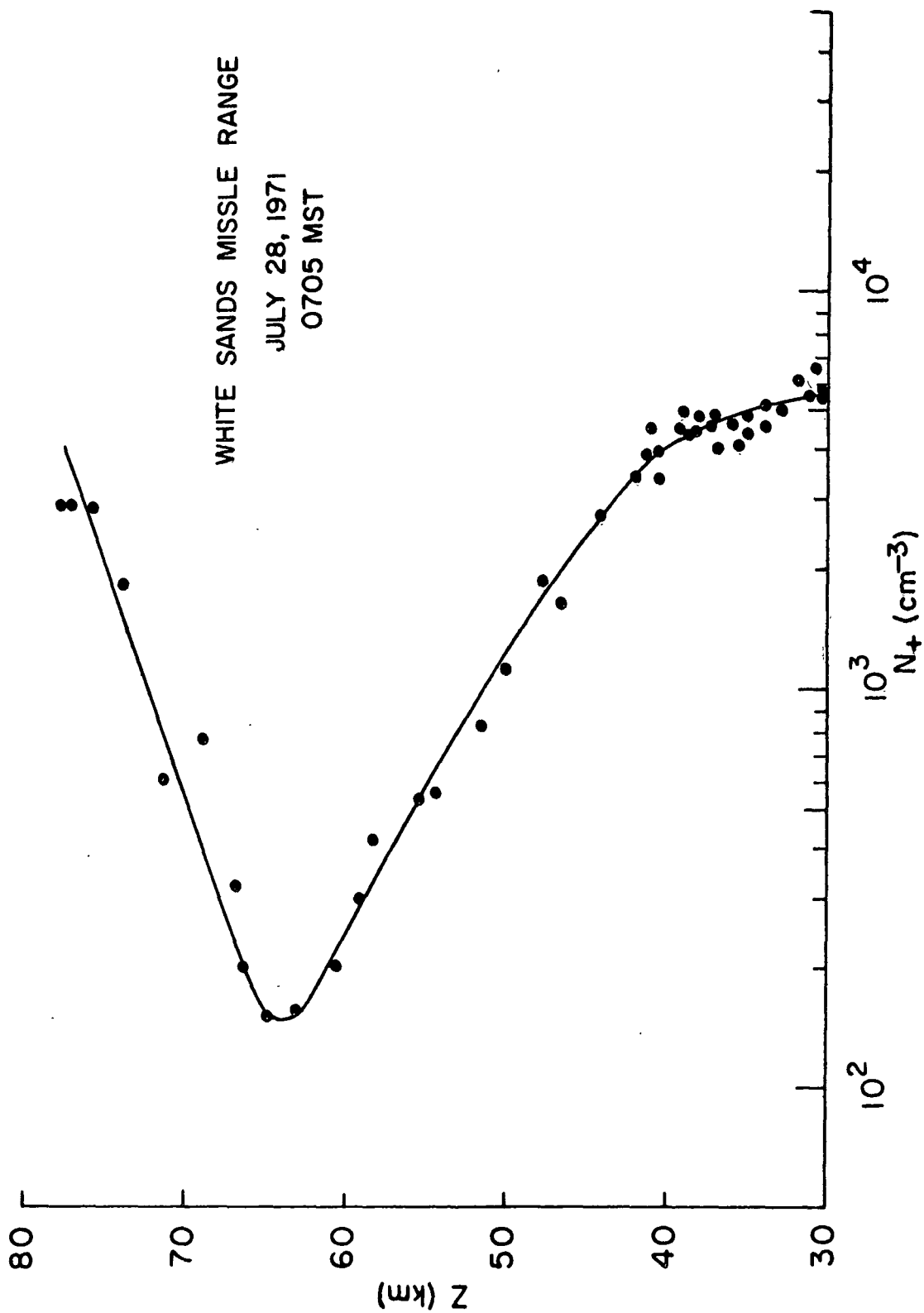
Figure 4.15. Positive Ion Density Data for July 28, 1971 at WSMR.
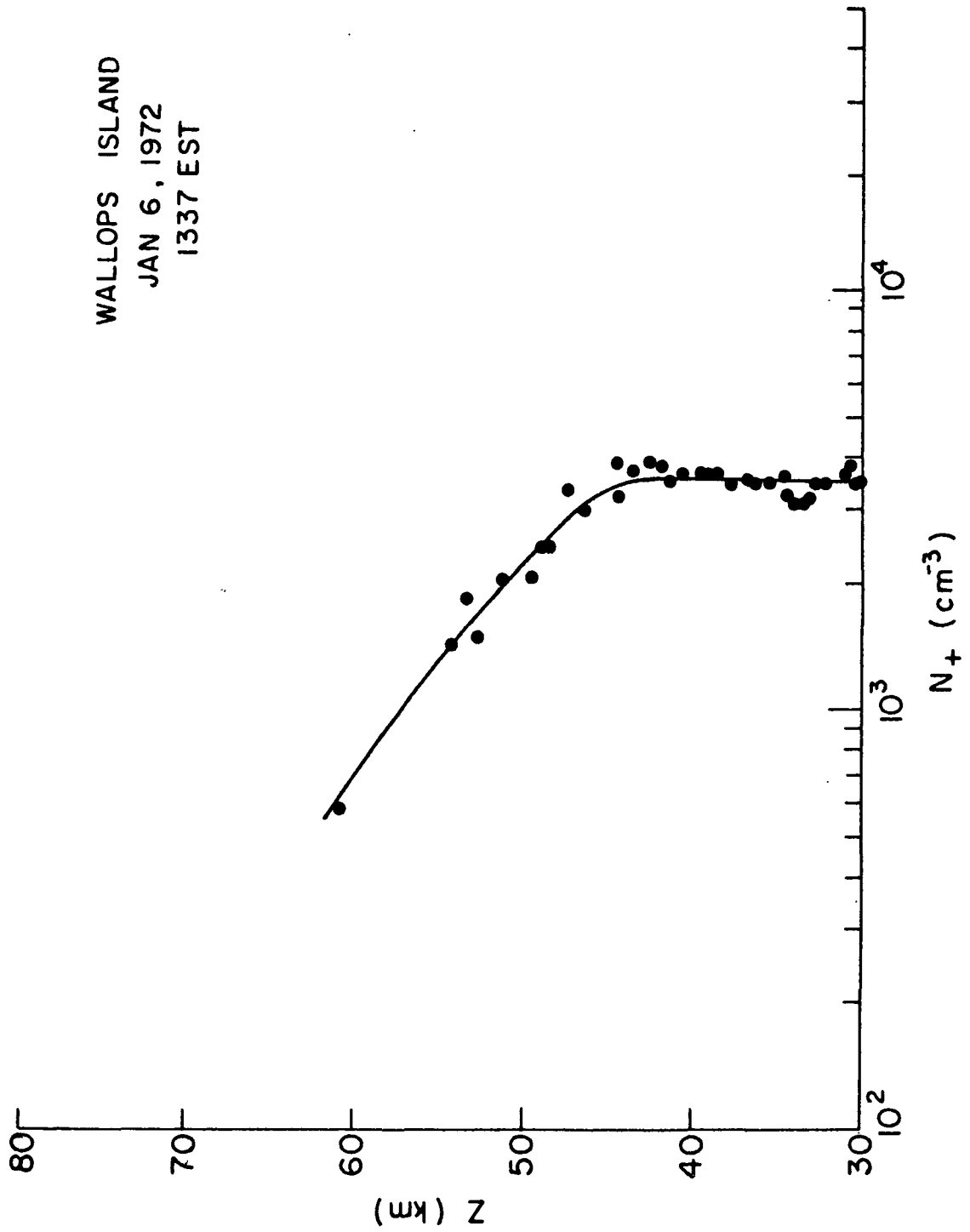
Figure 4.16. Positive Ion Density Data for January 6, 1972 at WI.
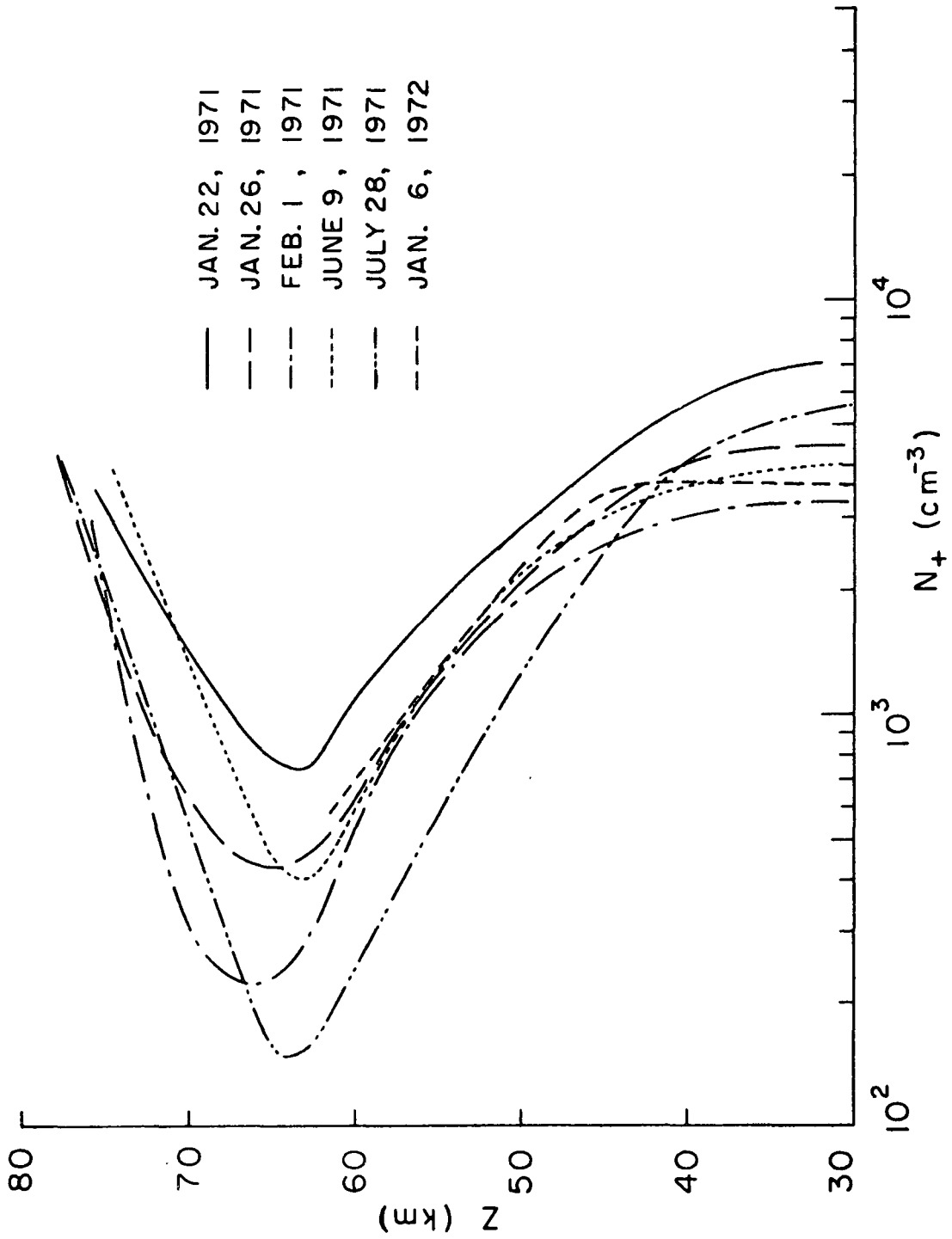
Figure 4.17. Positive Ion Density Profiles for WSMR and WI.
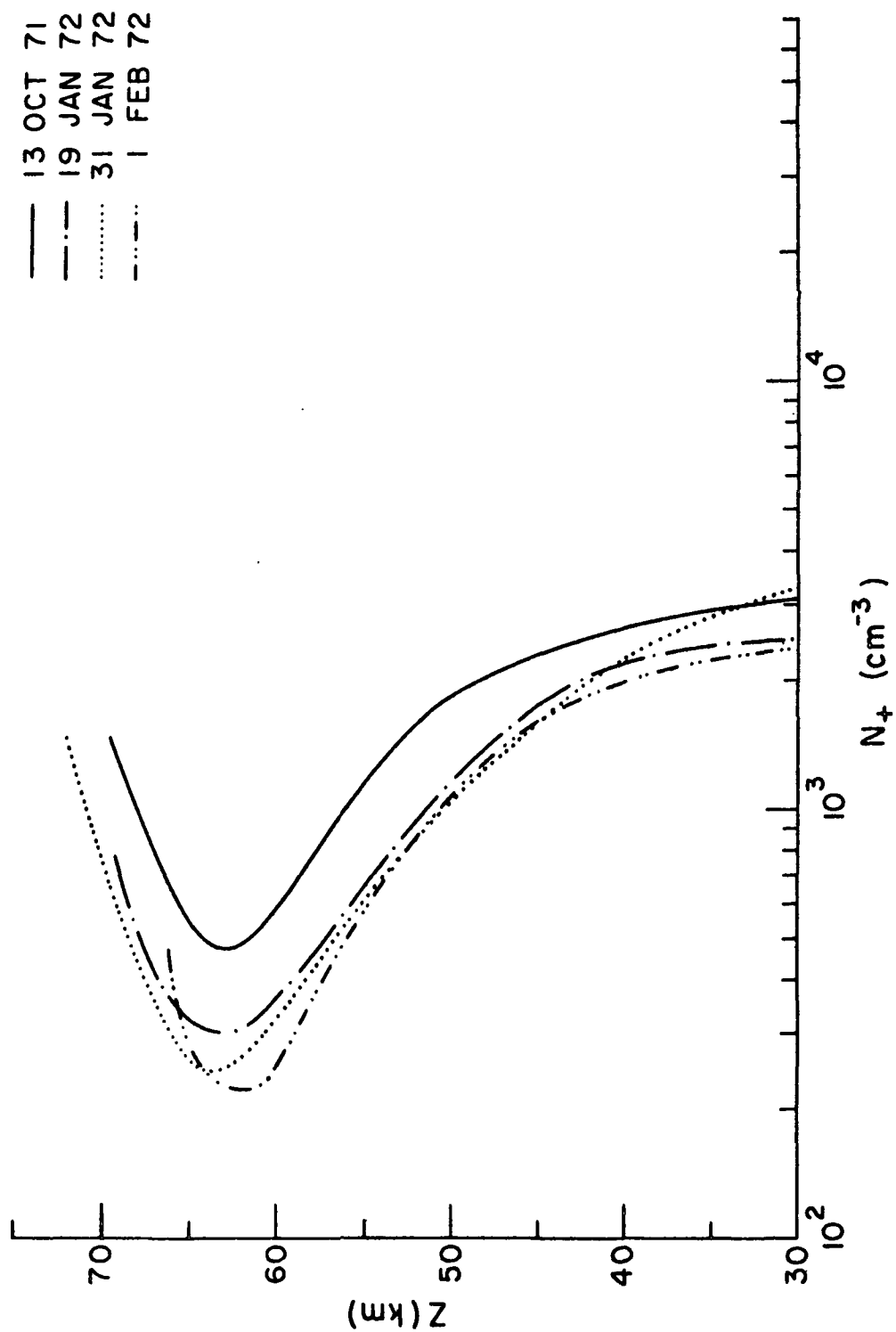
Figure 4.18. Positive Ion Density Profiles for WSMR and WI.

$$N_e \simeq \frac{1}{u_e} \left[\frac{\sigma_-}{e} - N_+ u_- \right] \qquad (4.13)$$

The electron density profiles in Figures 4.19 and 4.20 were determined by using: a negative ion reduced mobility value of 2.3 cm^2/v.s. (Cole and Pierce, 1965); Nielson and Bradbury's electron drift velocity data for air (McDaniel, 1964) to determine u_e; and the positive ion density profiles in Figures 4.17 and 4.18. The four curves for electron density in Figure 4.20 are from the data of Cipriano (1973).

4.6   Experimental Measurement Errors

For an experiment of this nature, it is very difficult to realistically discuss absolute errors concerning the conductivity measurements. A higher level of confidence is placed on the positive conductivity and deduced ion density values than on their respective counterparts, negative conductivity and electron number density. This arises primarily from the difficulty involved in interpreting the blunt probe theory for the collection of electrons and the implications of defining negative conductivity measurements in such a manner as to deduce electron density. However, all of the curves for σ_- (Figures 4.9-4.10) and N_e (Figures 4.19-4.20) represent data measured and reduced in a consistent manner, thus placing a higher level of confidence on these values when using them for comparative analyses.
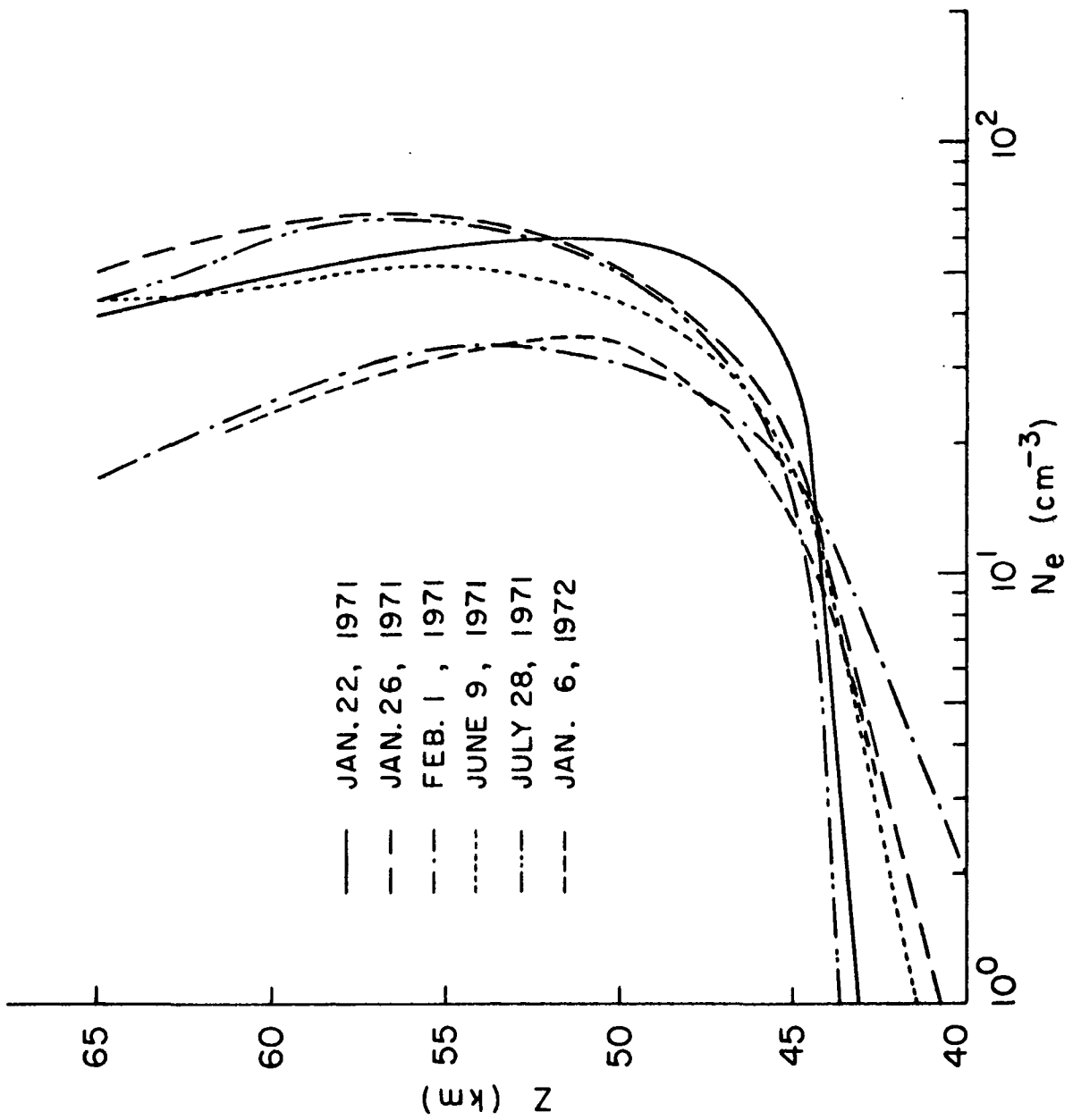
Figure 4.19. Electron Density Profiles for WSMR and WI.
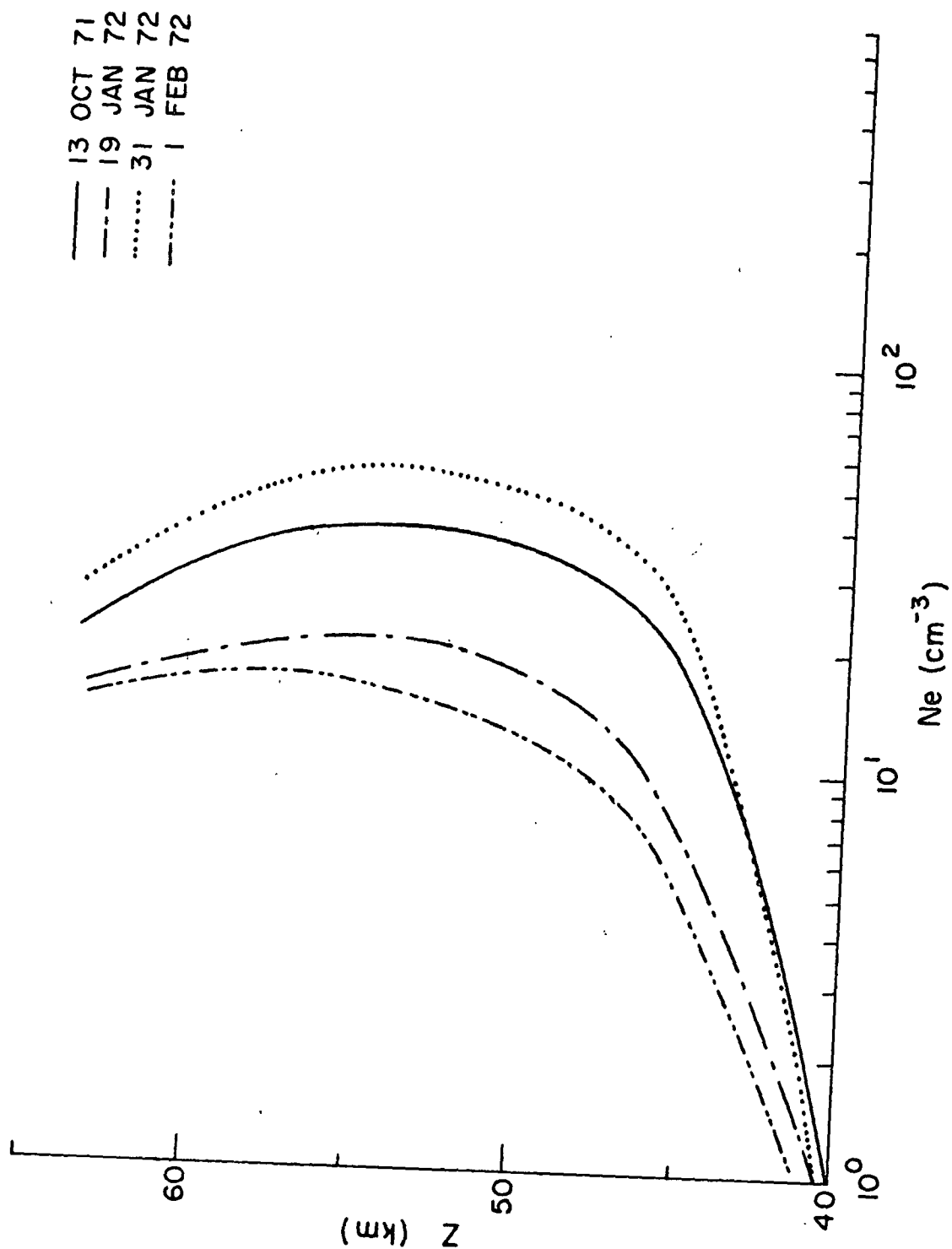
Figure 4.20. Electron Density Profiles for WSMR and WI.

Perhaps consideration of possible relative errors introduced by the data reduction procedure is more pertinent since a significant portion of the future discussion will be concerned with variations observed in the conductivity and density data. Each conductivity data point in Figures 4.3-4.8 represents several independent attempts at reducing a value from the demodulated in-flight waveform. Nominal variation limits of $\pm10\%$ were used in deciding whether or not a value was properly reduced, thus insuring that the probable relative error limits were of the same order of magnitude.

CHAPTER V

MESOSPHERIC IONIZATION

5.1 A Qualitative Discussion of the Blunt Probe Parameters

General characteristics of the blunt probe conductivity data and the deduced profiles for electron and positive ion densities will be discussed in this section. Between 30 and 40 km., the positive and negative conductivity curves (Figures 4.9-4.10) coincide, having an altitude dependence inversely proportional to neutral atmospheric density. The curves for positive and negative conductivity diverge at approximately 40 km. The steep gradient in σ_- with respect to height suggests the lowest altitude above which electrons are present. The positive conductivity curves, which are smaller in value, are essentially constant from approximately 45 km. up to their knees which fall between 60 and 65 km.

The deduced positive ion density curves in Figures 4.17-4.18 are essentially invariant with altitude below 40 km. Between 45 and 60 km., the curves for positive ion density have an altitude dependence approximately proportional to neutral air density. The turnover in positive ion density at approximately 65 km. corresponds to the knee observed in the positive conductivity profile. It should be noted that the variations in positive ion density at any given altitude reflect the corresponding variations measured in positive conductivity since positive ion mobility was assumed similar for all launches. At one time this

assumption was considered valid. Recent studies, however, concerned specifically with the variations measured in conductivity indicate that a somewhat stronger case can be made for attributing the variations in positive ion conductivity to changes in its mobility. This topic will be considered in more detail in the following chapter.

The deduced electron density profiles (Figures 4.19-4.20) have a very steep gradient with respect to height at approximately 45 km. and are essentially invariant with altitude between 50 and 65 km. To summarize, the functional behavior with respect to altitude for N_+ and N_e' may be expressed as follows:

$30 < Z$ (km.) < 40	$45 < Z$ (km.) < 60
$N_+ \simeq$ constant $\simeq N_-$	$N_+ \propto n \propto N_-$
$N_e \simeq 0$	$N_e \simeq$ constant

where n is the atmospheric neutral number density.

5.2 D-Region Ion Chemistry Models

The relatively complex chemical structure of the D-region makes modeling its processes difficult. One approach to the modeling problem is to develop comprehensive computer programs (Keneshea, 1967; Reid, 1971) which can account for many reaction rates and obtain solutions for many coupled differential equations. Although this procedure offers the potential of complete and accurate simulation, many of the reactions and corresponding

rates are at present uncertain, thus greatly reducing the
effectiveness of such models. A simpler method for
studying the D-region involves the use of effective or
lumped parameter models in which the chemical processes of
many species are accounted for by representative reaction
rates and continuity equations. Examples of this approach
are the two negative ion model of Adams and Megill (1967)
and the two positive ion model of Haug and Landmark (1970).

An intermediate approach is represented by the six ion
model of Mitra and Rowe (1972) and the twelve ion model
developed recently by Rowe (1973). These models attempt
to identify specific ions and reactions where possible and
to lump together uncertain or unknown ion species and
processes. The six ion model includes four positive ions
(NO^+, O_2^+, O_4^+, and an unknown Y^+) and two negative ions
(O_2^- and X^-). The twelve ion model includes six
additional negative ions (O_3^-, CO_3^-, NO_2^-, O_4^- CO_4^-, and
NO_3^-).

As discussed by Rowe (1973), the six ion model
(Figure 5.1) incorporates Adams and Megill's (1967) two
negative ion model and Haug and Landmark's (1970) two
positive ion model. In the six ion model, the positive ion
O_2^+ is produced primarily from the ionization of $O_2(^1\Delta_g)$
by solar ultraviolet radiation. The NO^+ ions result from
ionization of nitric oxide by Lyman-α radiation and
secondarily, by charge transfer from O_2^+. The variable Y^+
represents the terminal positive ions, thought to be mostly
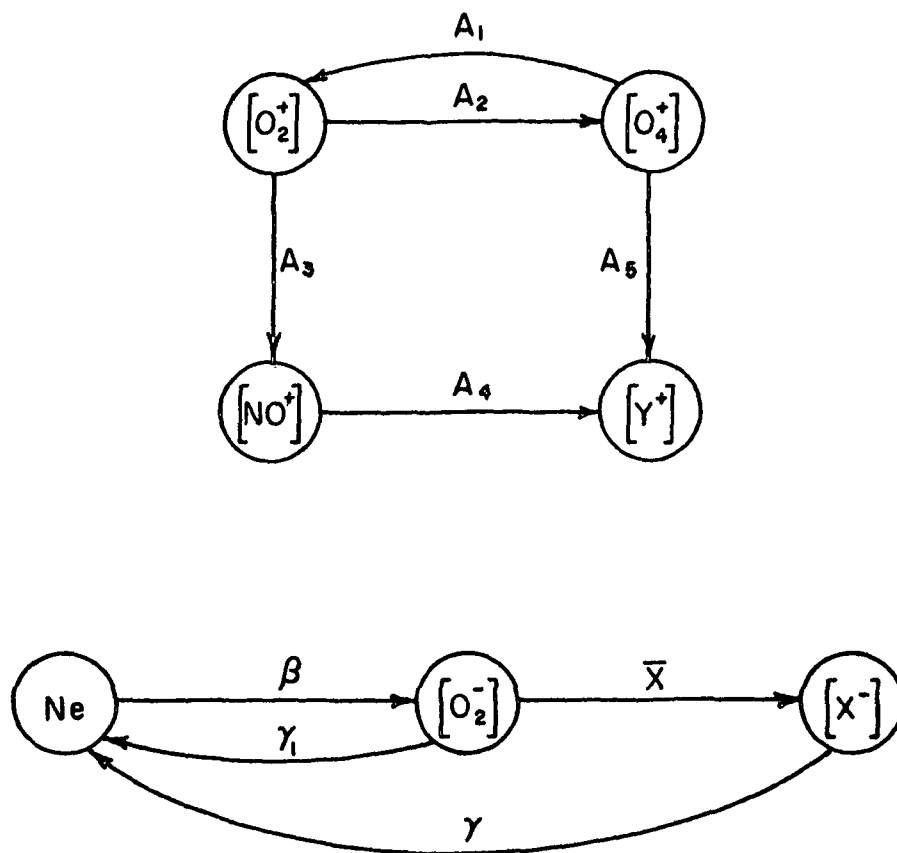
Figure 5.1.   D-Region Six Ion Chemistry Model

hydrates ($H^+ \cdot (H_2O)n$; $n = 1,2,$---) (Narcisi and Bailey, 1965; Goldberg and Aikin, 1971). The positive ion O_4^+ enters into the positive ion chemistry by virtue of its charge transfer behavior with O_2^+ and as a possible charge transfer path to the terminal Y^+ ions. Negative ions are formed by electrons attaching to O_2 at a rate β. The O_2^- ions may undergo detachment or charge transfer to eventually form a terminal ion X^-. Mutual neutralization and dissociative recombination loss processes are not shown in this figure.

For the altitude region below 85 km., ionization of $O_2(^1\Delta_g)$ by solar UV radiation to form O_2^+ is thought to be relatively insignificant (Paulsen, Huffman and Larrabee, 1972). Thus, the Mitra-Rowe model simplifies to the two positive ion - two negative ion model shown in Figure 5.2. In this model, the parameter Q represents production by ionizing radiation; N_e is the electron number density; the α_d's and α_i's are respectively the dissociative recombination and mutual neutralization coefficients; β is the rate for electron attachment to molecular oxygen; A and $\overline{X}$ represent the charge transfer rates to the terminal positive and negative ions, respectively; and the γ's represent the detachment coefficients. Physically, the variable N_{L+} represents the concentration of simple ions (eg. NO^+) which have a dissociative recombination coefficient on the order of 2-5x $10^{-7} cm^3/s$., while N_{H+} represents the number density for more complex cluster ions (hydrates) which have comparatively larger α_d values (10^{-6}-$10^{-5} cm^3/s$.).
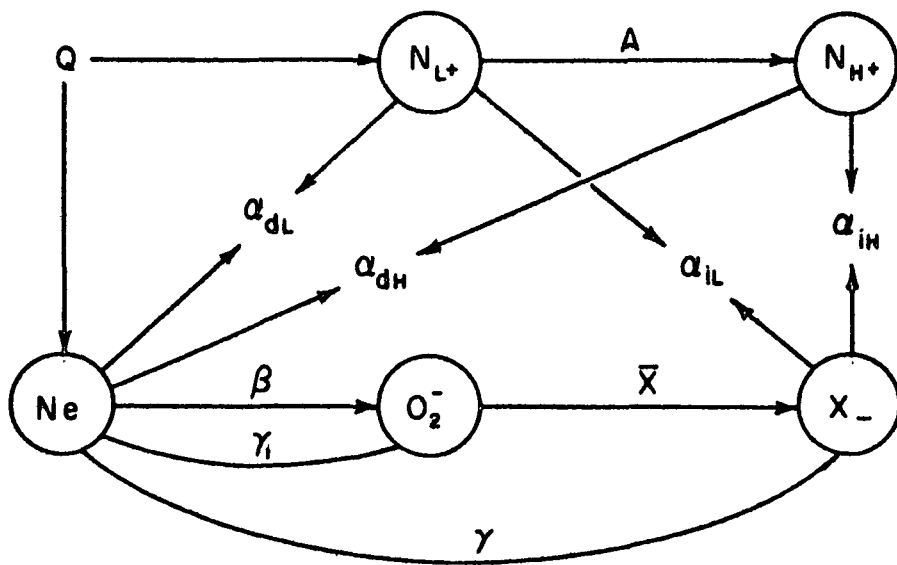
Figure 5.2.   Two Positive Ion-Two Negative Ion Model

Two simplifications of this model will now be considered for the D-region. Below 80 km., charge exchange of O_2^- to form terminal negative ions becomes sufficiently rapid such that the O_2^- density becomes quite small, thus simplifying the model to a two positive ion model with a single negative ion (Figure 5.3). Neglecting transport processes, the positive ion continuity equations for this model are

$$\frac{dN_{L+}}{dt} = Q - \alpha_{dL} N_{L+} N_e - AN_{L+} - \alpha_{iL} N_{L+} N_- \qquad (5.1)$$

$$\frac{dN_{H+}}{dt} = AN_{L+} - \alpha_{dH} N_{H+} N_e - \alpha_{iH} N_{H+} N_- \qquad (5.2)$$

where N_- is the concentration of negative ions. Assuming that the mutual neutralization loss terms for the positive ions are much smaller than their respective dissociative recombination terms, the steady state solutions for N_{L+} and N_{H+} are

$$N_{L+} = \frac{Q}{\alpha_{dL} N_e + A} \qquad (5.3)$$

$$N_{H+} = \frac{AN_{L+}}{\alpha_{dH} N_e} \qquad (5.4)$$

Using the above two equations and assuming conservation of charge, the following expression is obtained:
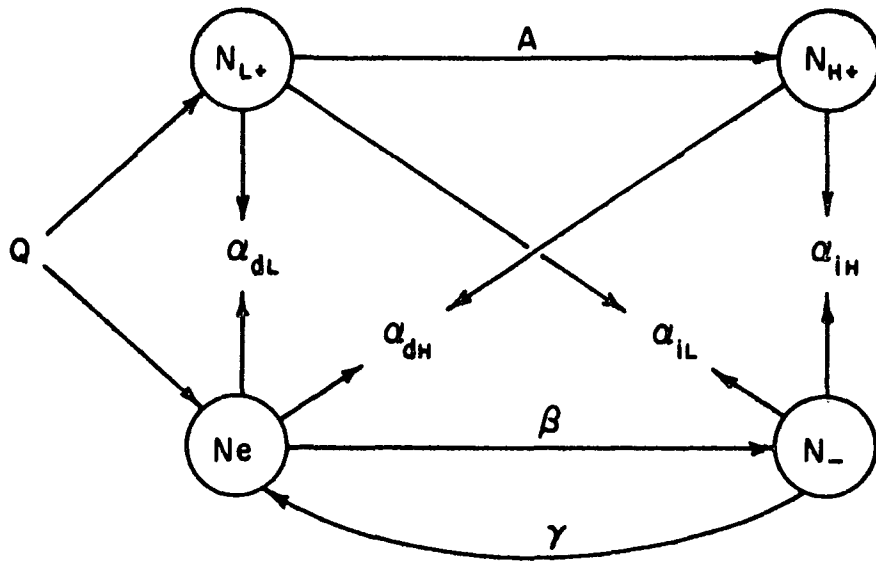
Figure 5.3.   Two Positive Ion-One Negative Ion Model

$$Q = \alpha_{dH}(1+\lambda) \left(\frac{A+\alpha_{dL}N_e}{A+\alpha_{dH}N_e} \right) (N_e)^2 \qquad \qquad (5.5)$$

where λ is the negative ion to electron concentration ratio, N_-/N_e. It is interesting to observe that under certain specific conditions, namely $\alpha_{dH} >> A/N_e >> \alpha_{dL}$, it is possible to obtain attachment-like behavior $(N_e \propto Q)$ from the above equation. In particular, equation (5.5) under these conditions reduces to the following expression:

$$Q \simeq A(1+\lambda) N_e \qquad \qquad (5.6)$$

It is believed that the two positive ion-one negative ion model is the simplest model that offers a reasonable prospect for approximately modeling the D-region under all conditions. The need for two positive ions at greatly differing recombination coefficients derives primarily from the need to explain the response of this region to disturbances such as solar flares (Mitra and Rowe, 1972). Under disturbed conditions the apparent "effective" recombination coefficient is much smaller than under steady state conditions, an effect which is explained by the two positive ion model. For nighttime and normal undisturbed daytime conditions, however, nearly all of the positive ions may be assumed to be in the terminal state N_{H+} and the need for a precursor ion N_{L+} is unnecessary. For this case, the simple one positive ion-one negative ion

model of Figure 5.4 may be employed, for which the steady state positive ion and electron continuity equations are:

$$\frac{dN_+}{dt} = Q - \alpha_d N_+ N_e - \alpha_i \ N_+ N_- \simeq 0 \qquad (5.7)$$

$$\frac{N_e}{dt} = Q - \alpha_d \ N_+ N_e + \gamma N_- - \beta N_e \simeq 0 \qquad (5.8)$$

This may be shown to be equivalent in the steady state to the two positive ion-one negative ion model if weighted averages are used for the recombination coefficients:

$$\alpha_d = \alpha_{dL} \frac{N_{L+}}{N_+} + \alpha_{dH} \frac{N_{H+}}{N_+} \qquad (5.9)$$

$$\alpha_L = \alpha_{iL} \frac{N_{L+}}{N_+} + \alpha_{iH} \frac{N_{H+}}{N_+} \qquad (5.10)$$

In the remainder of this work, the simple lumped parameter model having the coefficients α_d, α_i, β, and γ will be used. It must be reiterated that these parameters only have specific meaning in relation to the quasi-steady state daytime condition to which they are applied. It should be pointed out that the difficulties encountered in using such models in the past have derived from attempts to apply them to dynamic situations for which they are generally invalid.
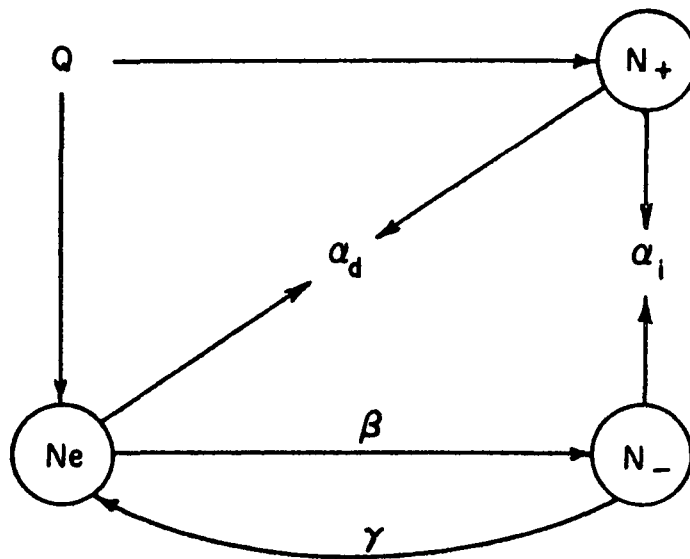
Figure 5.4.   Lumped Parameter Ion Chemistry Model

5.3 Implications of the Blunt Probe Charge Number Densities Using a Lumped Parameter Model

5.3.1 D-Region Production Rates

In the 30-80 km. altitude region, ionization from extraterrestrial radiation is derived primarily from galactic cosmic rays and solar Lyman-α radiation. The production rate for galactic cosmic rays is:

$$Q_{CR} = I_o \, n \tag{5.11}$$

where n is the neutral number density and I_o is an ionization constant dependent upon geomagnetic latitude, season, and solar activity. A value of 7.5×10^{-18} s.$^{-1}$ (Nicolet, 1972), which is consistent with the data of Neher (1967), will be used for the galactic cosmic ray ionization constant.

Above 65 km. in the D-region, ionization of nitric oxide by Lyman-α radiation is considered the principal production mechanism for positive ions. The ionization rate for this process is

$$Q_L = \sigma_i(NO) \left[NO\right] I_\infty \, e^{-\gamma} \tag{5.12}$$

where σ_i (NO) ($= 2.0 \times 10^{-18}$ cm.^{2}, Watanabe, 1954) is the ionization cross section for nitric oxide at 1216 $\overset{o}{A}$.; $\left[NO\right]$ represents the concentration of nitric oxide; I_∞ ($= 3.0 \times 10^{11}$ photons/cm.^{2}s., Aikin, Kane and Troim, 1964) is the Lyman-α flux at the top of the ionosphere; and τ is the optical depth for 1216 $\overset{o}{A}$. radiation. Assuming that Lyman-α

radiation is absorbed at higher altitudes in the atmosphere by molecular oxygen, the optical depth is

$$\tau = \sigma_a(O_2) \int_h^\infty [O_2] \sec \chi \, dz \qquad (5.13)$$

where $\sigma_a(O_2)$ $(=1.0 \times 10^{-20} cm^2$, Watanabe, 1958) and $[O_2]$ are respectively the absorption cross section and concentration for molecular oxygen and χ is the solar zenith angle. For an isothermal atmosphere, the expression for τ simplifies to the following:

$$\tau = \sigma_a(O_2) [O_2] H \sec \chi \qquad (5.14)$$

where H is the mean molecular scale height.

Curves for the total production rate Q are drawn in Figure 5.5 for different solar zenith angles typical of the blunt probe launches. Values used for n, $[O_2]$ (assumed mixed), and H were obtained from CIRA 1965. Values for $[NO]$ are representative of the measurements of Pontano and Hale (1970) and Meira (1971). In general, production by Lyman- α radiation supplants production by galactic cosmic rays at an altitude corresponding approximately to the observed turnover in positive ion density (Figures 4.17-4.18).

5.3.2 Electron Attachment

The most effective electron attachment process in the D-region is considered to be three-body attachment involving
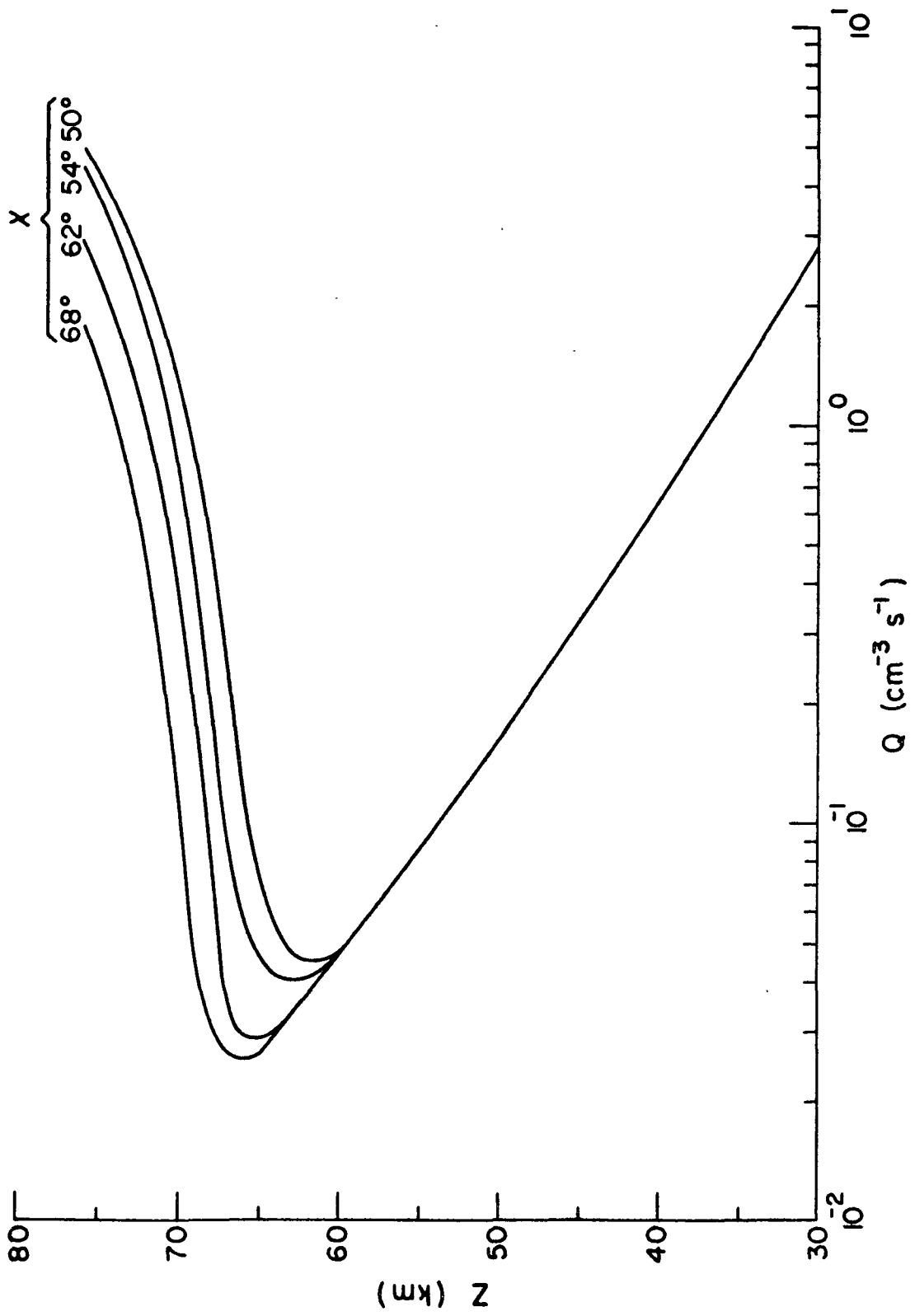
Figure 5.5.   Production Rates for Extraterrestrial Ionizing Radiation.

O_2 with either N_2 or O_2 (Whitten and Poppoff, 1971). The important reactions for this process are given below (DASA, 1967):

$$N_2 + O_2 + e \rightarrow O_2^- + N_2; \quad K = \frac{300}{T} \, 10^{-31} e^{-600/T} \, cm^6/s$$

$$O_2 + O_2 + e \rightarrow O_2^- + O_2; \quad K = 10^{-29} \, cm^6/s$$
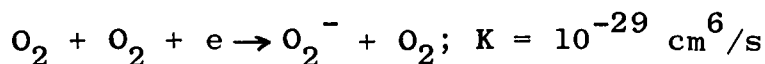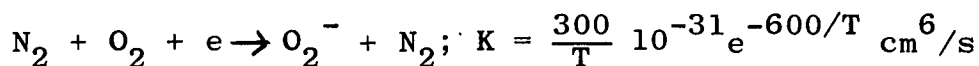
where T is the absolute temperature and $\left[N_2 \right]$ and $\left[O_2 \right]$ are the concentrations of molecular nitrogen and oxygen, respectively. The expression for ß determined from the above two reactions is

$$\beta = (\frac{300}{T}) \, 10^{-31} e^{-600/T} \left[N_2 \right] \left[O_2 \right] + 10^{-29} \left[O_2 \right]^2$$

(5.15)

Since N_2 and O_2 are both mixed constituents, the attachment coefficient is proportional to the square of neutral air density. A graph for ß using data from CIRA 1965 is drawn in Figure 5.6.

5.3.3 Positive Ions

To review briefly, the functional dependence of N_+, N_e, and Q with respect to neutral density n are:

$\underline{30 < z(km.) < 40}$

$N_+ \simeq$ constant $\simeq N_-$

$N_e \simeq 0$

$Q \simeq I_o n$ (5.16)
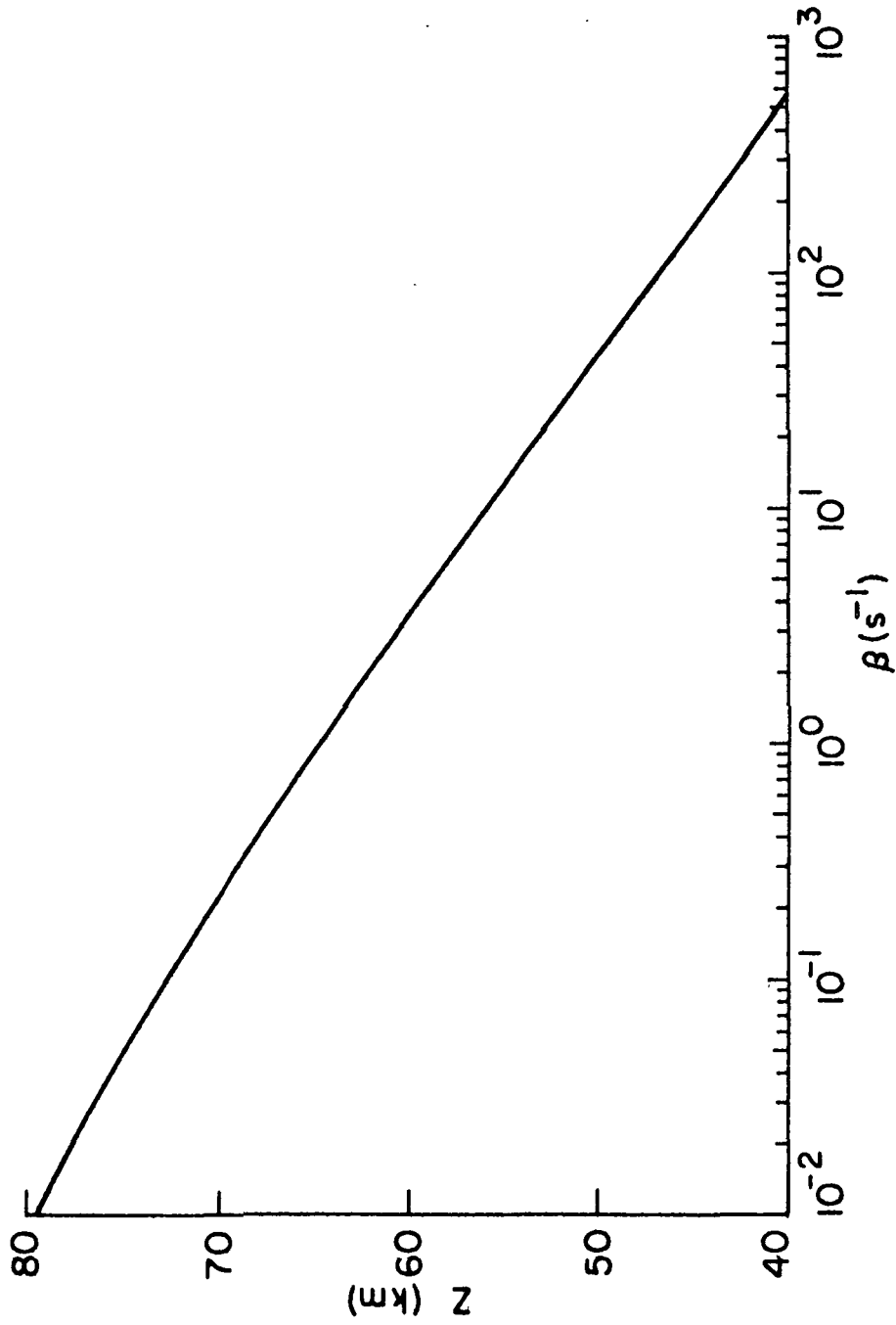
Figure 5.6. Three Body Electron Attachment Rates Involving O_2 and N_2.

$$45 < z(km.) < 60$$

$$N_+ \propto n \propto N_-$$

$$N_e \simeq \text{constant}$$

$$Q \simeq I_o n \tag{5.17}$$

Below 40 km. where the electron density is comparatively negligible, the expressions in (5.16) and the steady state solution of the positive ion continuity equation (equation (5.7)) imply that α_i is proportional to neutral atmospheric density, suggesting that the dominant positive ion loss process is probably three-body ion-ion recombination (Dalgarno, 1961). The 40-45 km. region is a transition region in which the dominant loss process for positive ions goes from three-body to two-body ion-ion recombination, as demonstrated by the curvature in the N_+ profiles. Between 45 and 60 km., the steady state positive ion continuity equation (5.7) and the expressions in (5.17) give the following relation

$$\underbrace{Q}_{\propto n} \simeq \underbrace{\alpha_d N_+ N_e}_{\propto n} + \underbrace{\alpha_i N_+ N_-}_{\propto n^2} \tag{5.18}$$

The functional form of the variable n in this equation suggests that dissociative recombination is the dominant positive ion loss process. This would place an upper limit for α_i on the order of 10^{-8} cm.^{3}/s. which is about an order of magnitude lower than the value deduced from the corrected nighttime blunt probe data (Hale, 1967).

Using the curves in Figures 4.17, 4.19 and 5.2, calculations of α_d for a two-body mutual neutralization coefficient on the order of 10^{-8} cm.^{3}/s. are plotted in Figure 5.7. The variations in α_d at a given altitude result from variations in either N_+, which are perhaps questionable, or in N_e. The calculations in Figure 5.7 imply that the dissociative recombination coefficients on days of moderate to high absorption ($\sim 10^{-6}$ cm.^{3}/s.) are approximately a factor of 3-4 smaller than the α_d values for days of low radio wave absorption. These values for the dissociative recombination coefficient are representative of the rates for hydrated ions which are considered the dominant species in this altitude region (Narcisi and Bailey, 1965; Goldberg and Aikin, 1971).

5.3.4 Electrons

For electron and positive ion density values on the order of those measured by the blunt probe, the steady state electron density as determined from equation (5.8) is controlled primarily by detachment and attachment processes:

$$N_e \simeq \frac{\gamma N_-}{\beta} \tag{5.19}$$

Values of the detachment coefficient γ for the blunt probe data of June 9, 1971 are dranw in Figure 5.8.

Assuming that attachment is a three-body process ($\propto n^2$) and that electrons are detached as follows:
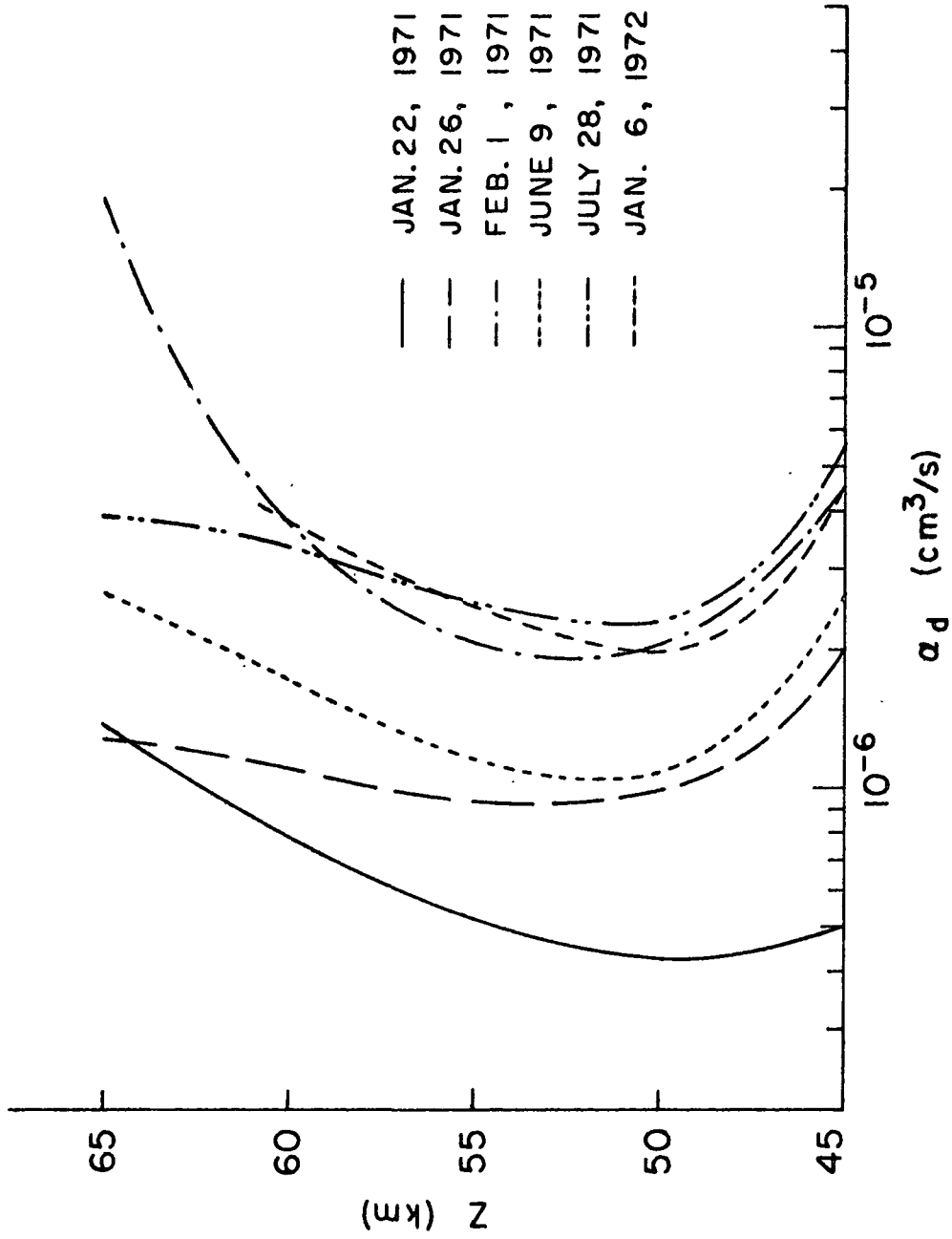
Figure 5.7. Dissociative Recombination Rates for the Blunt Probe Measurements.
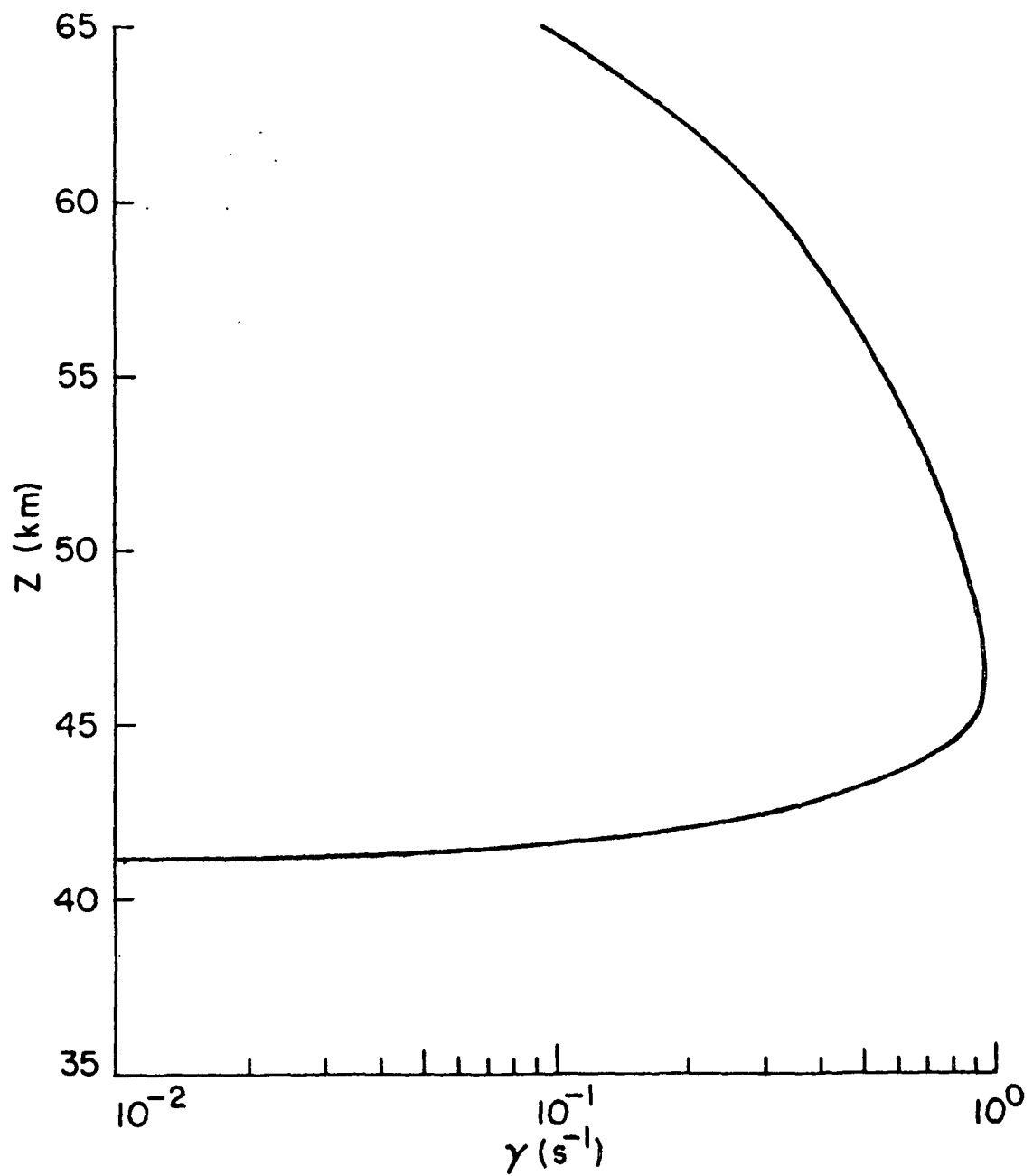
Figure 5.8.   Detachment Coefficients for the Blunt Probe
Data of June 9, 1971.

$$N_d + N_- \xrightarrow{K_d} N_d + N + e \qquad\qquad (5.20)$$

the expressions for N_e and N_- in equations (5.16) and (5.17)

suggest that the detaching species (N_d) should be mixed

from 65 km. down to 45 km. and then diminish sharply in

value between 45 and 40 km. One minor species exhibiting

these properties is $O_2(^1\Delta_g)$, an excited state of molecular

oxygen (see Figure 5.9). Since $O_2(^1\Delta_g)$ is produced by

photolysis and thus goes back to its more stable form at

night, such a detachment process also explains the absence

of electrons in the lower nighttime D-region. For the

$O_2(^1\Delta_g)$ data of Evans and Llewellyn (1970) and the

detachment coefficients determined for June 9, 1971

(Figure 5.8), sample calculations of the rate K_d are

plotted in Figure 5.9. Laboratory reaction rates for such

processes are quite limited and therefore this explanation

concerning $O_2(^1\Delta_g)$ as a possible detaching species should

be considered speculative.
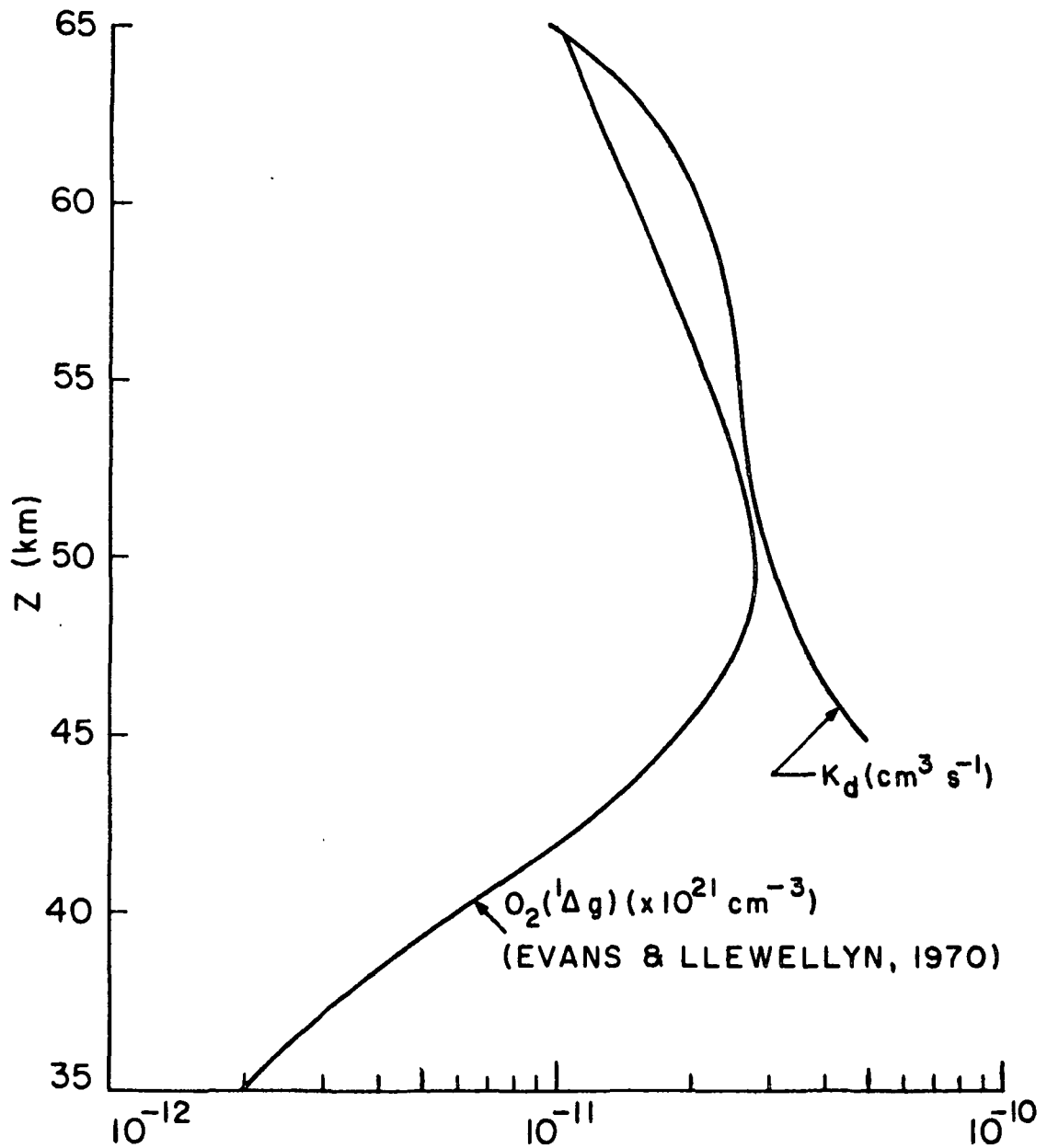
Figure 5.9.   Detachment Rates for the Blunt Probe Data of
June 9, 1971.

CHAPTER VI

VARIABILITY OF MESOSPHERIC IONIZATION

6.1 Introduction

In the previous chapter, general properties of the conductivity data and deduced density values were discussed. It was demonstrated that a simple lumped parameter model could explain the blunt probe charge density values for the undisturbed lower D-region. Implications of the data, in terms of this model under steady state conditions, were considered.

This chapter will examine the day-to-day variations measured in positive and negative conductivity. The results of a recent correlation study involving blunt probe measurements and certain atmospheric parameters are discussed. The usefulness of a lumped parameter model for explaining the variations in charge densities is demonstrated.

6.2 Correlation Studies Using Blunt Probe Parameters

As a further investigation of recently presented blunt probe results (Mitchell and Hale, 1972), Cipriano (1973) has performed a detailed correlation study using the blunt probe data, MRN temperature data (Olsen, 1972), and A3 radio wave absorption measurements. The MRN temperature data (Figures 6.1-6.2) were obtained from temperature sondes (Ballard and Rofe, 1969) flown typically within three hours of the blunt probe launches.
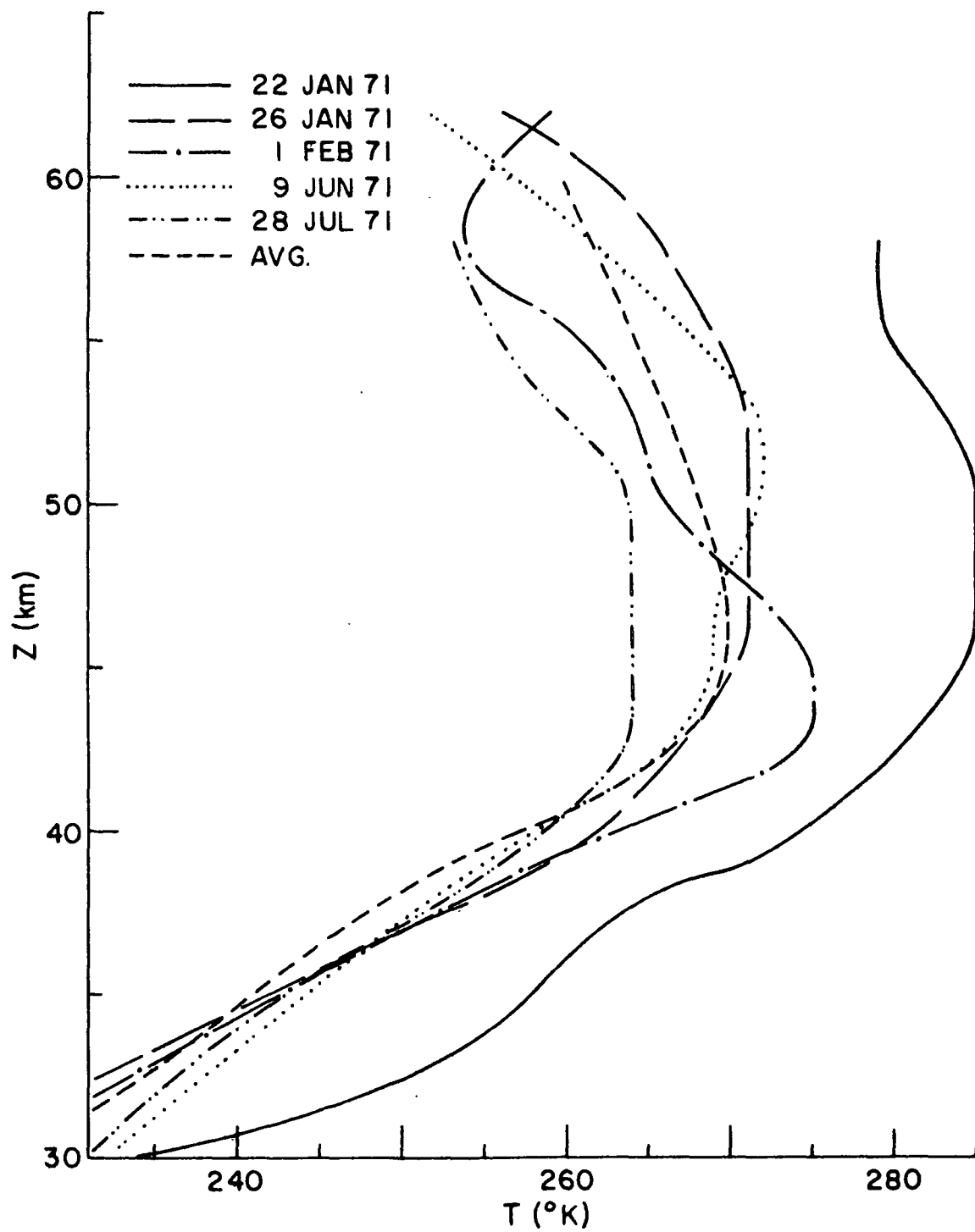
Figure 6.1. MRN Temperature Data for WSMR and WI
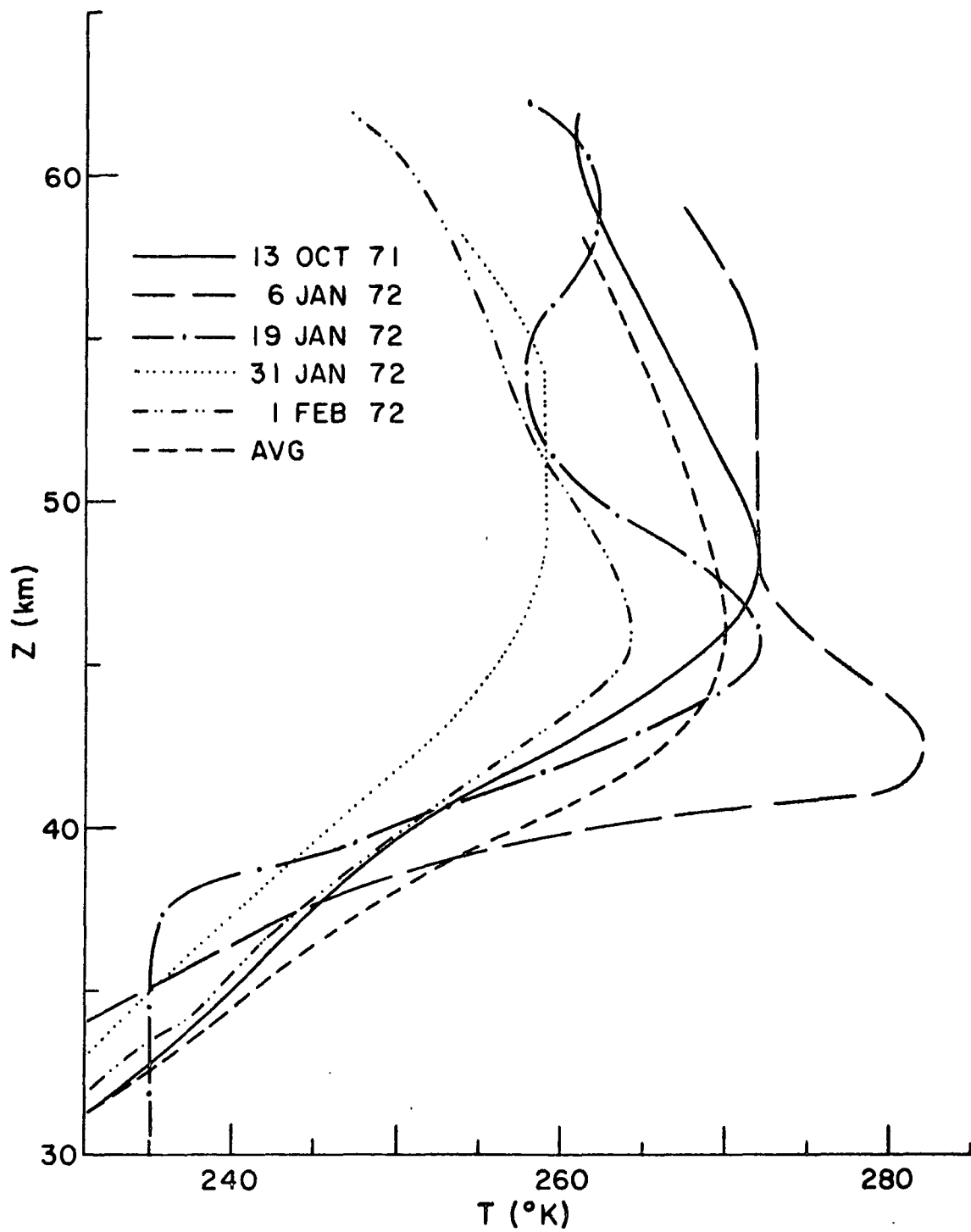
Figure 6.2. MRN Temperature Data for WSMR and WI

The results of this study show that variations in positive conductivity correlate very well with changes in temperature and rather poorly (a correlation coefficient less than 0.5) with variations in radio wave absorption and negative conductivity. A graph of positive conductivity versus temperature at 55 km. is drawn in Figure 6.3. The correlation coefficient (r) for a straight line fit was found to be 0.8 or greater for the altitude range of 34 to 58 km. (Figure 6.4). In demonstrating this linear relationship between σ_+ and T, the percentage variation in positive conductivity with respect to temperature was estimated to be $4\%/^{\circ}C.$, an order of magnitude larger than the value obtained assuming a temperature dependence for mobility as given by equation (4.9). This observation possibly suggests that the positive ions' ability to cluster is extremely temperature dependent, thus resulting in a more variable dependence for mobility on temperature than as described by equation (4.9).

Cipriano's analyses for negative conductivity have demonstrated a good correlation with radio wave absorption between 53 and 63 km. (Figure 6.5) but comparatively poor agreement with MRN temperature data. A graph showing the linear relationship between negative conductivity and noontime radio wave absorption for four different altitudes is given in Figure 6.6. The relative variation in the slopes of these straight lines is attributable to changes in electron mobility with height.
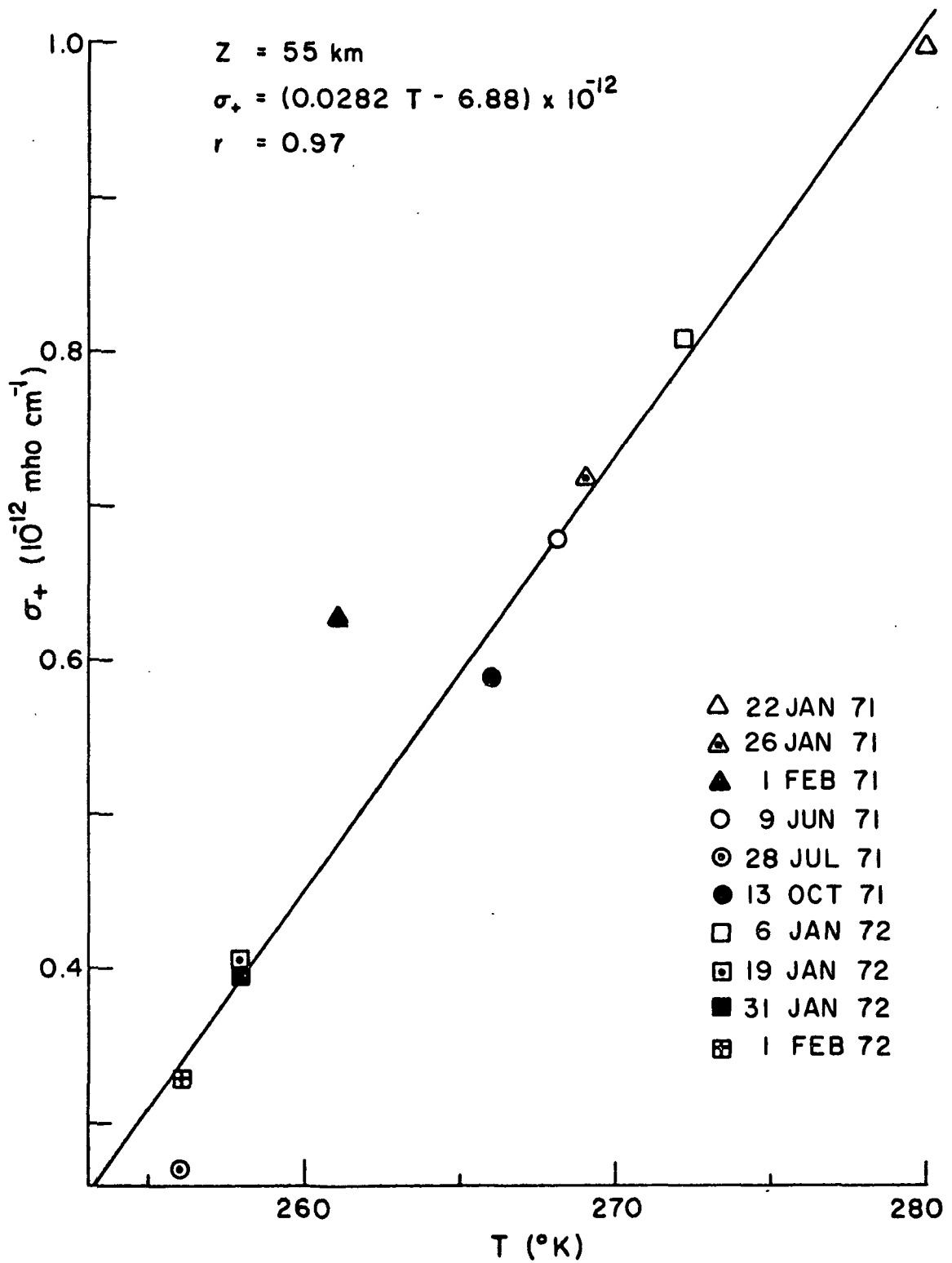
Figure 6.3. Correlation of Positive Conductivity and
Temperature for Z = 55 km.
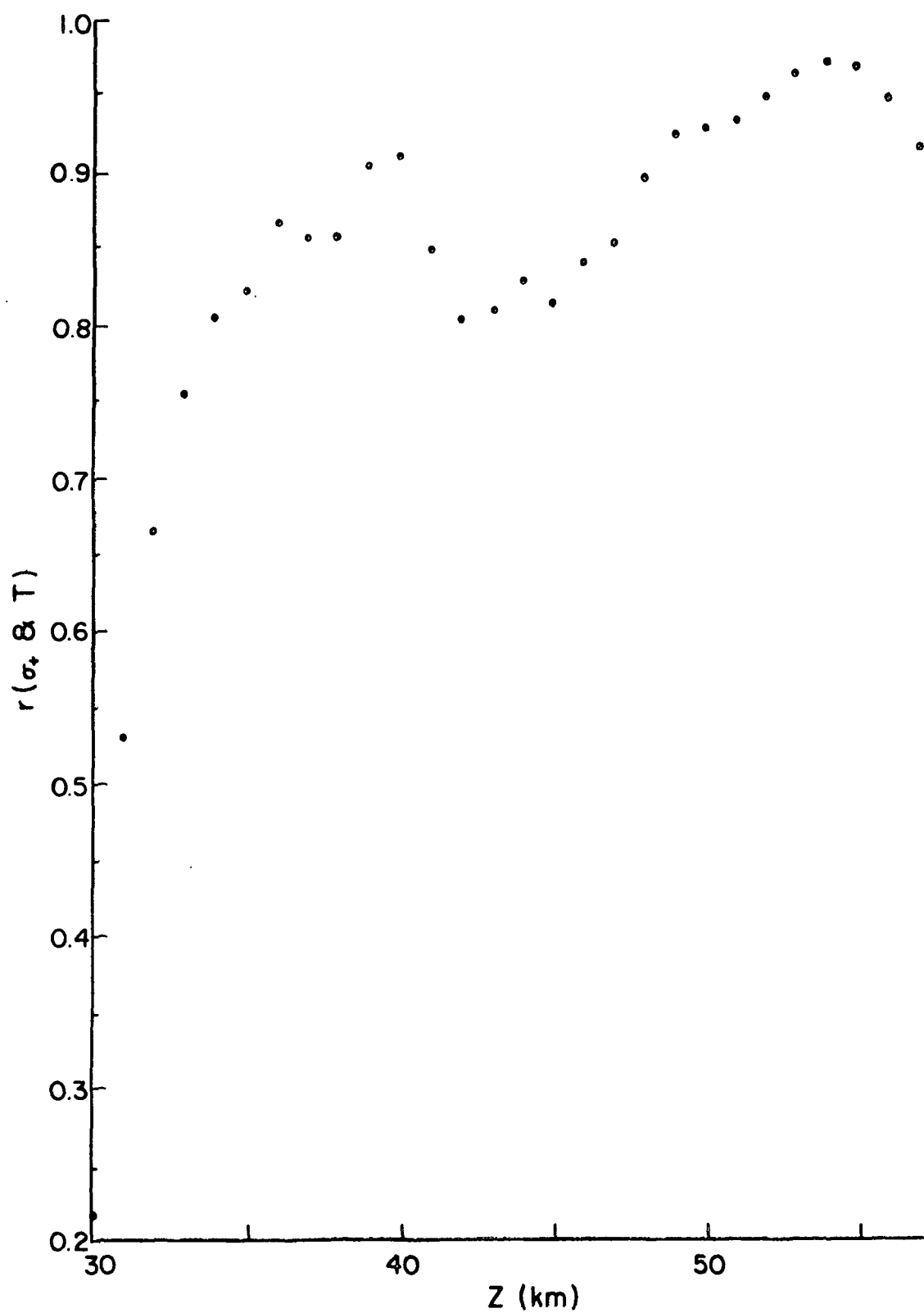
Figure 6.4.   Correlation Coefficients for Positive
Conductivity and Temperature Versus Altitude.
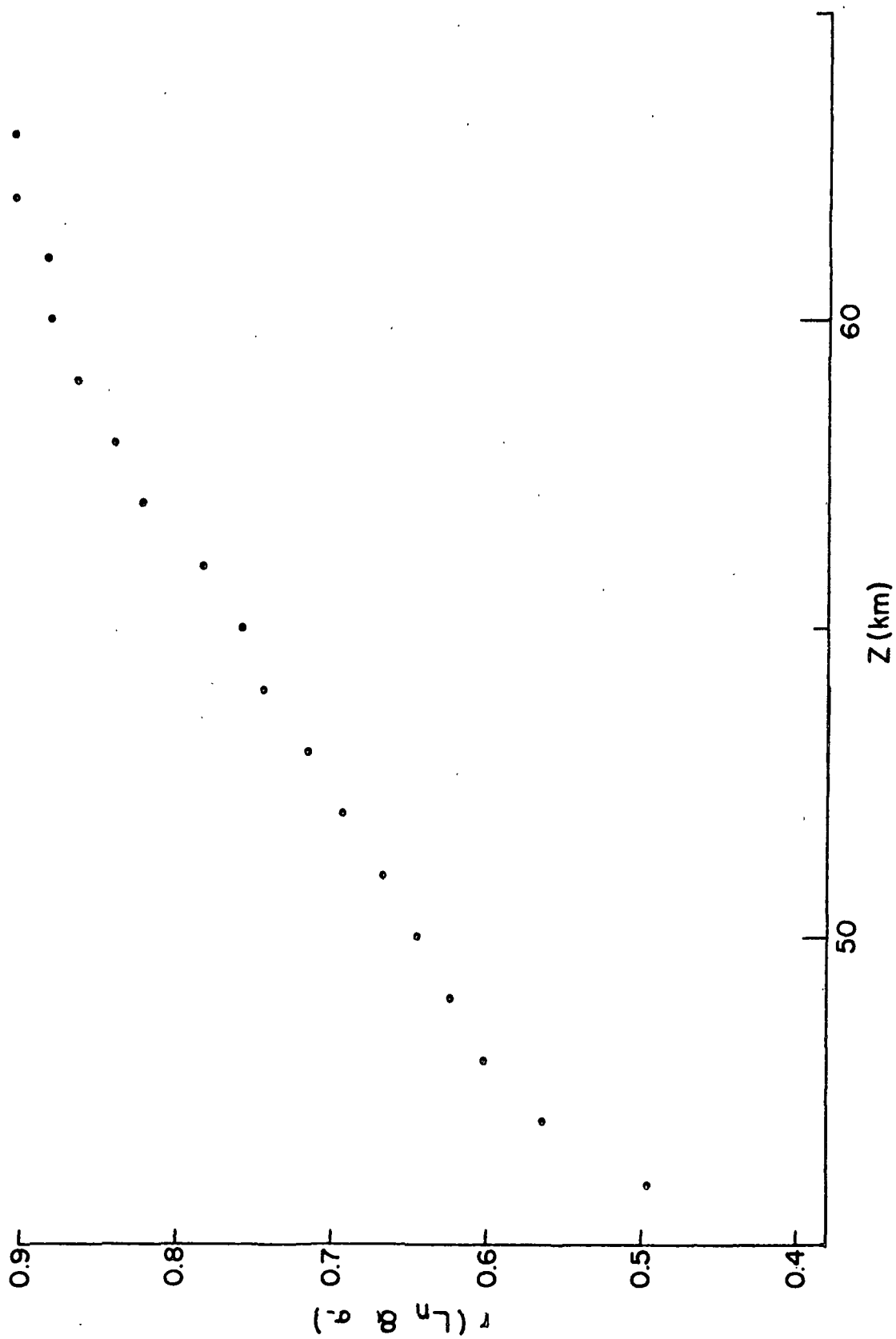
Figure 6.5. Correlation Coefficients for A3 Radio Wave Absorption and Negative Conductivity Versus Altitude.
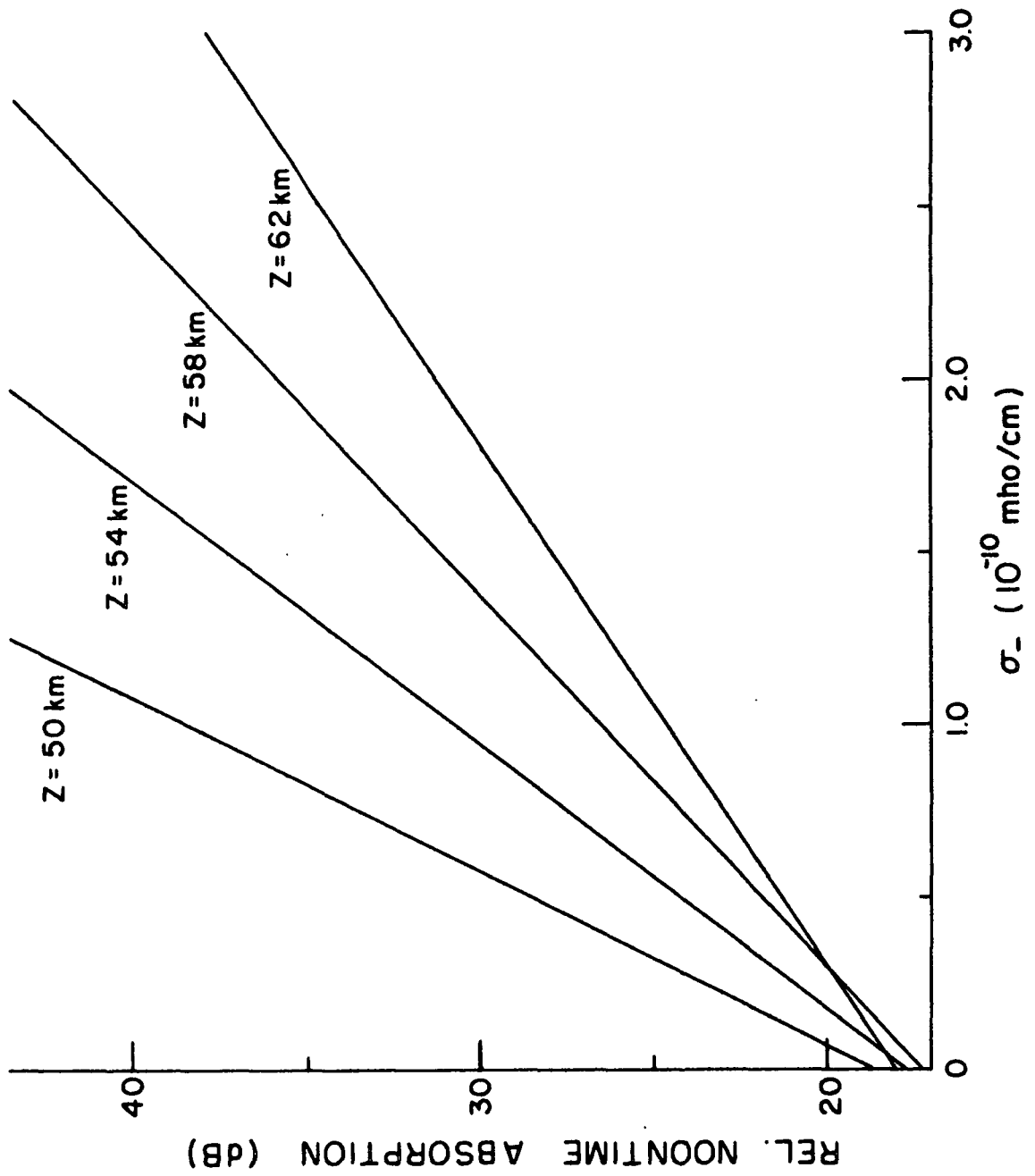
Figure 6.6. Correlation of Absorption and Negative Conductivity for Various Altitudes.

The good correlation between variations in negative conductivity from 53 to 63 km. and noontime radio wave absorption is interesting since the variations in absorption are presumably resulting from changes in electron concentration at altitudes higher than the blunt probe measurements. This would suggest that electron density variations in both altitude regions are related to a similar process, thus excluding the possibility of relating the variations in density to changes in production by ionizing radiation. In particular, this correlation does not support attributing the electron density variations to either changes in the nitric oxide concentration (Manson, 1971; Sechrist, 1967) or to changes in the flux of Lyman-α radiation (Gnanalingam, 1972). The poor correlation observed between σ_- and T makes it difficult to postulate a possible relationship between variations in electron density and temperature such as has been observed on occasion during stratospheric warmings (Sechrist, et al. 1969).

To explain the measured variations in negative conductivity, which presumably reflect changes in N_e, it is useful to consider a simple ion chemistry model such as the lumped parameter model in section 5.2.

6.3 Implications of Charge Number Density Variations when Considering a Simple Ionospheric Model

Neglecting transport processes, the steady state solutions for N_+ and N_e from equations (5.7) and (5.8) may be written exclusively in terms of coefficients of the lumped parameter model:

$$N_+ \simeq \sqrt{\frac{Q}{\alpha_d} \frac{\beta}{\gamma}} \qquad\qquad (6.1)$$

$$N_e \simeq \sqrt{\frac{Q}{\alpha_d} \frac{\gamma}{\beta}} \qquad\qquad (6.2)$$

The processes for production (Q) and attachment (β) in the lower D-region are dependent on neutral number density. Since fluctuations in number density for this altitude region are relatively insignificant (Faire, Champion and Murphy, 1972), the day-to-day variations in charge number densities will be explained by considering the parameters for dissociative recombination (α_d) and detachment (γ).

For this discussion, the blunt probe data obtained on June 9, 1971 will be assumed representative of the lower D-region and thus serve as the reference data. A summer launch is chosen as the control day since day-to-day variations in electron density, as indicated statistically by the A3 absorption data, are not as extreme during the summer as in the winter.

Between 50 and 65 km., the electron density profiles (Figure 4.19) for February 1, 1971 and January 6, 1972, days of relatively low absorption, are generally a factor of 2-3 smaller than the other four electron density curves. To explain these smaller values, equation (6.2) suggests that the detachment coefficient must become smaller or the dissociative recombination coefficient must increase. Since the N_+ profiles for these two days (Figure 4.17) are comparable in this altitude range with the reference data

(June 9, 1971), the decrease in N_e can only be explained by an increase in α_d with a corresponding decrease in γ, such that N_+ remains essentially unchanged.

To posutlate how this might possibly occur, the speculation in Chapter V concerning the role of $O_2(^1\Delta_g)$ as a principal detaching agent is considered along with the following mesospheric reaction scheme (Nicolet, 1970):

$$O_3 + h\nu \longrightarrow O_2(^1\Delta_g) + O(^1D)$$

$$O(^1D) + H_2O \rightarrow OH + OH^+$$

$$OH + O \rightarrow O_2 + H$$

$$H + O_3 \rightarrow OH + O_2 \qquad\qquad (6.3)$$
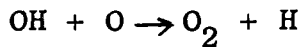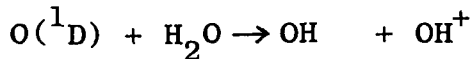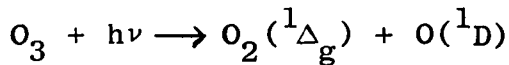
If it is initially assumed that there is an increase in the positive ions' degree of hydration, presumably from a larger concentration of water vapor, the value of α_d would become greater (Biondi, 1969). From the above reaction scheme, it is observed that an increase in H_2O would consequently destroy O_3 which is the source of $O_2(^1\Delta_g)$. Thus, for the speculated detaching species $O_2(^1\Delta_g)$, an increase in α_d results in a smaller value for γ, which is consistent with the blunt probe measurements.

Since positive conductivity is proportional to the produce of positive ion density and mobility, it is difficult

to determine whether the day-to-day variations in this measurement are caused by changes in number density or mobility. If the variations reflect changes in positive ion density, the curves in Figure 4.17 indicate that the values for January 22, 1971 and July 28, 1971, in the 45-60 km. region, differ by approximately a factor of two from the control data. Since the electron density profiles for these two days are comparatively similar to the control data, it is necessary for both the detachment and dissociative recombination coefficients to change mutually such that their ratio remains unchanged (see equations (6.1) and (6.2)). Such behavior is inconsistent with the previously discussed ion chemistry involving $O_2(^1\Delta g)$ as a possible detaching species.

Another possibility is that the variations in σ_+ result from changes in u_+. As mentioned previously, changes in u_+ are possibly explained by variations in the ions' degree of clustering, a very temperature dependent process (Kebarle, Searles, Zolla, Scarborough and Arshadi, 1967). Thus, a warming of the stratosphere and mesosphere (e.g. January 22, 1971) could possibly cause a considerable increase in positive ion mobility, thereby significantly enhancing the conductivity of this region. The general lack of correlation between variations in positive and negative conductivity lends plausibility to associating the variations in positive conductivity with changes in mobility, presumably induced by temperature, rather than positive ion density.

CHAPTER VII

CONCLUSIONS

The study of ionization processes below 65 km. is of interest because the primary ionizing radiation, galactic cosmic rays, remains relatively constant with some fluctuation caused by solar activity. Thus, large variations in ionization at these altitudes must be due to variations in the atmosphere, either meteorological or chemical. The following conclusions are drawn from the blunt probe ionization measurements made in this region:

(1) The relative constancy with altitude of σ_+ and N_e between 45 and 60 km. indicates that these quantities are not strongly related to atmospheric number density in this region.

(2) A simple lumped parameter ion chemistry model is useful for explaining the blunt probe electron and positive ion density data. Between 45 and 60 km., the altitude distribution of positive ion density and the relatively constant N_e suggest that dissociative recombination is the principle positive ion loss mechanism. The observed values of electron density require an effective detachment coefficient which increases with decreasing altitude between 65 and 50 km., approximately proportional to atmospheric number density, but cuts off sharply below 45 km.

(3)   A relatively large variation in positive ion
        conductivity with mesospheric temperature was
        observed. It is not known whether this
        conductivity variation is due to changes in ion
        density or ion mobility, but a somewhat stronger
        case can be made for the latter at this time. In
        the future, independent measurements of both
        positive ion mobility and conductivity would be
        useful for better understanding this variation.

(4)   Variations in electron density for days having
        different amounts of radio wave absorption
        persisted as low as 50 km. Such changes in the
        midlatitude D-region cannot be explained by
        precipitating energetic electrons or variations
        in nitric oxide concentration.

(5)   The good correlation between variations in
        negative conductivity in the 55-65 km. region
        and the noontime radio wave absorption measure-
        ments, which primarily indicate changes in
        electron density for heights above the blunt
        probe measurements, suggest that variations in
        both regions are caused by a similar process,
        presumably changes in electron loss.

BIBLIOGRAPHY

Adams, G. W. and L. R. Megill, Planetary Space Sci. <u>15</u>, 1111, 1967.

Aikin, A. C., J. A. Kane and J. Troim, J. Geophys. Res. <u>69</u>, 4621, 1964.

Appleton, E. V., Proc. R. Soc. <u>A162</u>, 451, 1937.

Appleton, E. V. and W. R. Piggott, J. Atmosph. Terr. Phys. <u>5</u>, 141, 1954.

Baker, D. C. and L. C. Hale, <u>Space Res. X</u>, North-Holland, Amsterdam, 208, 1970.

Ballard, H. N. and B. Rofe, <u>Stratospheric Circulation</u> (Edited by Willis L. Webb), Academic, New York, 141, 1969.

Biondi, M. A., Can. J. Chem. <u>47</u>, 1711, 1969.

Bossolasco, M. and A. Elena, C. R. Acad. Sci. <u>256</u>, 4491, 1963.

Bowhill, S. A., E. A. Mechtly, C. F. Sechrist, Jr. and L. G. Smith, <u>Space Res. VII</u> (Edited by R. L. Smith-Rose), North-Holland, Amsterdam, 246, 1967.

Budden, K. G., <u>Radio Waves in the Ionosphere</u>, Cambridge University, Cambridge, 1961.

Cipriano, J. P., M.S. Thesis in Meteorology, The Pennsylvania State University, 1973.

<u>CIRA 1965</u>, COSPAR International Reference Atmosphere, North-Holland, Amsterdam, 1965.

Cole, R. K. and E. T. Pierce, J. Geophys. Res. <u>70</u>, 2735, 1965.

Cuffin, N., Sci. Rep. No. 249, Ionosphere Research Laboratory, The Pennsylvania State University, 1965.

Dalgarno, A., Ann. Geophys. <u>17</u>, 16, 1961.

Dalgarno, A., <u>Atomic and Molecular Processes</u> (Edited by D. R. Bates), Academic, New York, 643, 1962.

DASA Reaction Rate Handbook, DASA 1948, General Electric, California, 1967.

Davies, K., Ionospheric Radio Waves, Blaisdell, Waltham, 1969.

Evans, W. J. F. and E. J. Llewellyn, Ann. Geophys. 26, 167, 1970.

Faire, A. C., K. S. W. Champion and E. A. Murphy, Paper presented at COSPAR Symposium, Madrid, 1972.

Geller, M. A. and C. F. Sechrist, Jr., J. Atmosph. Terr. Phys. 33, 1027, 1971.

Gnanalingam, S., Paper presented at Spring URSI Meeting, Washington, D.C., 1972.

Goldberg, R. A. and A. C. Aikin, J. Geophys. Res. 76, 8352, 1971.

Hale, L. C., Space Res. VII (Edited by R. L. Smith-Rose), North-Holland, Amsterdam, 140, 1967.

Hale, L. C., Solar Eclipses and the Ionosphere, Plenum Press, 81, 1970.

Hale, L. C. and D. P. Hoult, Sci. Report No. 247, Ionosphere Research Laboratory, The Pennsylvania State University, 1965.

Hale, L. C., D. P. Hoult and D. C. Baker, Space Res. VIII, North-Holland, Amsterdam, 320, 1968.

Hale, L. C., D. P. Hoult and R. G. Willis, Electron Density Profiles in Ionosphere and Exosphere (Edited by Jon Frihagen), North-Holland, Amsterdam, 108, 1966.

Hale, L. C., J. R. Mentzer and L. C. Nickell, Paper presented at COSPAR Symposium on 1969 PCA Event, Boston, 1971.

Hale, L. C., L. C. Nickell, B. Kennedy and T. A. Powell, Radio Sci. 7, 89, 1972.

Haug, A. and B. Landmark, J. Atmosph. Terr. Phys. 32, 405, 1970.

Hoult, D. P., J. Geophys. Res. 70, 3183, 1965.

ICSU, International Council of Scientific Unions, IQSY Instruction Manual No. 4 - Ionosphere, London, 1963.

Jeans, J. H., The Math Theory of Electricity and Magnetism, Cambridge University, London, 1925.

Kebarle, P., S. K. Searles, A. Zolla, J. Scarborough and M. Arshadi, J. Am. Chem. Soc. 89, 6393, 1967.

Keller, G. E., J. Geophys. Res. 73, 3483, 1968.

Keneshea, T. J., AFCRL-67-0221, Environmental Research Papers, No. 263, 1967.

Lee, M. K., Ph.D. Thesis in Electrical Engineering, The Pennsylvania State University, 1973.

Manson, A. H., J. Atmosph. Terr. Phys. 33, 715, 1971.

McDaniel, E. W., Collision Phenomena in Ionized Gases, John Wiley and Sons, New York, 1964.

Meira, L. G., J. Geophys. Res. 76, 202, 1971.

Mitchell, J. D. and L. C. Hale, Paper presented at COSPAR Symposium, Madrid, 1972, in press, Space Res. XIII, North-Holland, Amsterdam.

Mitchell, J. D., L. C. Hale, R. O. Olsen, J. Randhawa and R. Rubio, Radio Sci. 7, 175, 1972.

Mitra, A. P. and J. N. Rowe, J. Atmosph. Terr. Phys. 34, 795, 1972.

Narcisi, R. S. and A. D. Bailey, J. Geophys. Res. 70, 3687, 1965.

Neher, R. V., J. Geophys. Res. 72, 1527, 1967.

Nicolet, M., Ann. Geophys. 26, 531, 1970.

Nicolet, M., Private Communication, 1972.

Olsen, R. O., Private Communication, 1972.

Paulsen, D. E., R. E. Huffman and J. C. Larrabee, Radio Sci. 7, 51, 1972.

Pontano, B. A. and L. C. Hale, Space Res. X, 208, 1970.

Reid, G. C., Mesospheric Models and Related Experiments, Edited by G. Fiocco) Dordrecht, 1971.

Rowe, J. N., Ph.D. Thesis in Electrical Engineering, The Pennsylvania State University, 1973.

Rowe, J. N., A. J. Ferraro and H. S. Lee, Private
    Communication, 1972.

Sechrist, C. F., Jr., J. Atmosph. Terr. Phys. $\underline{29}$, 113, 1967.

Sechrist, C. F., Jr., E. A. Mechtly, J. S. Shirke and J. S.
    Theon, J. Atmosph. Terr. Phys. $\underline{31}$, 145, 1969.

Shapley, A. H. and W. J. G. Beynon, Nature, Lond. $\underline{206}$, 1242,
    1965.

Sonin, A. A., J. Geophys. Res. $\underline{72}$, 4547, 1967.

Watanabe, K., J. Chem. Phys. $\underline{22}$, 1564, 1954.

Watanabe, K., Advances in Geophysics 5, Academic, New York,
    1958.

Whitten, R. C. and I. G. Poppoff, Fundamentals of Aeronomy,
    John Wiley and Sons, New York, 1971.

York, T. M., Private Communication, 1972.

DOCUMENT CONTROL DATA - R & D

(Security classification of title, body of abstract and indexing annotation must be entered when the overall report is classified)

1 ORIGINATING ACTIVITY *(Corporate author)*	2a. REPORT SECURITY CLASSIFICATION
The Ionosphere Research Laboratory	2b. GROUP

3. REPORT TITLE

An Experimental Investigation of Mesospheric Ionization

4. DESCRIPTIVE NOTES *(Type of report and inclusive dates)*

Scientific Report

5. AUTHOR(S) *(First name, middle initial, last name)*

John D. Mitchell

6. REPORT DATE	7a. TOTAL NO. OF PAGES	7b. NO. OF REFS
June 29, 1973	110	

8a. CONTRACT OR GRANT NO. DAHCO4-68-C-0034	9a. ORIGINATOR'S REPORT NUMBER(S)
b. PROJECT NO. NASA Grant NGR 39-009-015	PSU-IRL-SCI-416
c.	9b. OTHER REPORT NO(S) *(Any other numbers that may be assigned this report)*
d.	

10. DISTRIBUTION STATEMENT

Supporting Agencies

11. SUPPLEMENTARY NOTES	12. SPONSORING MILITARY ACTIVITY
	U.S. Army Research Office National Aeronautics and Space Administration

13. ABSTRACT

Mesospheric ionization and its variability are the subject of this research. Data for this study were obtained primarily by the parachute-borne blunt probe technique conducted in coordinated rocket experiments at White Sands Missile Range, New Mexico and Wallops Island, Virginia. Electrical conductivity measurements and deduced charge density values from ten rocket launches are presented and discussed. Positive ion conductivity and electron density were found to be relatively invariant with height between 45 and 60 km. Variations in positive conductivity of a factor of two and enhancements in negative conductivity by as much as a factor of four were measured by the blunt probe.

A simple lumped parameter ion chemistry model is shown to satisfactorily explain the charge density values for the undisturbed lower D-region. Implications of the data in terms of this model are considered. The principal loss mechanism for positive ions in the 45 to 60 km. region is concluded to be dissociative recombination. Electron densities deduced from the conductivity data are explained by detachment involving a minor neutral constituent which is mixed between 65 and 45 km. and then cuts off sharply below 45 km.

A correlation study involving blunt probe measurements shows relatively good agreement between variations in positive conductivity and temperature. The good correlation between variations in negative conductivity in the 55 to 65 km. region and noontime A3 radio wave absorption, which primarily indicates changes in electron density for heights above the blunt probe measurements, suggests that variations in both regions are caused by a similar process.

DD FORM 1473 (PAGE 1)
1 NOV 65
S/N 0101-807-6811

NONE
Security Classification
A-31408